Space-division multiplexing: the next frontier in optical communication

Guifang Li,[1,2,5] Neng Bai,[1,3] Ningbo Zhao,[2,4] and Cen Xia[1]

[1]CREOL, The College of Optics & Photonics, University of Central Florida, Orlando, Florida 32816-2700, USA

[2]College of Precision Instrument and Opto-Electronic Engineering, Tianjin University, Tianjin, China

[3]Infinera Corporation, 140 Caspian Ct., Sunnyvale, California 94089, USA

[4]e-mail: nbzhao@tju.edu.cn

[5]e-mail: li@ucf.edu

Received July 23, 2014; revised October 23, 2014; accepted October 27, 2014; published December 23, 2014 (Doc. ID 217643)

Space-division multiplexing (SDM) uses multiplicity of space channels to increase capacity for optical communication. It is applicable for optical communication in both free space and guided waves. This paper focuses on SDM for fiber-optic communication using few-mode fibers or multimode fibers, in particular on the critical challenge of mode crosstalk. Multiple-input–multiple-output (MIMO) equalization methods developed for wireless communication can be applied as an electronic method to equalize mode crosstalk. Optical approaches, including differential modal group delay management, strong mode coupling, and multicore fibers, are necessary to bring the computational complexity for MIMO mode crosstalk equalization to practical levels. Progress in passive devices, such as (de)multiplexers, and active devices, such as amplifiers and switches, which are considered straightforward challenges in comparison with mode crosstalk, are reviewed. Finally, we present the prospects for SDM in optical transmission and networking.

OCIS codes: (060.0060) Fiber optics and optical communications; (060.1660) Coherent communications; (060.2320) Fiber optics amplifiers and oscillators; (060.4230) Multiplexing
http://dx.doi.org/10.1364/AOP.6.000413

Space-division multiplexing: the next frontier in optical communication

Guifang Li, Neng Bai, Ningbo Zhao, and Cen Xia

1. Introduction

Optical fiber communication is the backbone for the telecommunications infrastructure that supports the internet. Fueled by emerging bandwidth-hungry applications and the increase in computer processing power that follows Moore's law, internet traffic has sustained exponential growth in the past, and this trend is expected to continue for the foreseeable future. It is well known that the capacity of a communication channel cannot exceed the Shannon limit. In the past two decades, internet traffic demand was mainly met by wavelength-division multiplexing (WDM) technology [1], which can increase the spectral bandwidth of a fiber-optic communication channel by 2 orders of magnitude. It should be noted that the spectral bandwidth of the fiber-optic communication channel can be further increased by exploiting the low-loss transmission window of optical fiber beyond the C and L bands. However, this bandwidth expansion is limited to below 1 order of magnitude. Furthermore, lack of an integrated amplification platform makes such a system unattractive from a technical and economic perspective.

Recently, coherent detection has attracted much attention for providing capacity increase for optical fiber communication systems [2]. Coherent detection can maximize the SNR of a fiber-optic communication channel in comparison with direct detection. High SNR enables high-spectral efficiency quadrature amplitude modulation (QAM) that transmits information in both amplitude and phase of the optical signal. Digital coherent fiber-optic communication systems have recently become commercially available. Further increase in SNR can be achieved only by increasing the signal power. However, the increase in channel capacity scales logarithmically with the increase in signal power. This logarithmical channel capacity scaling ultimately cannot meet the demands of exponential traffic growth from a technical perspective as well as the perspective of power consumption per bit. In addition, fiber nonlinearity imposes an upper limit on how much power can be transmitted in a fiber. Digital coherent optical communication does make polarization multiplexing practical, providing a factor of 2 increase in channel capacity.

While it might be impossible to provide exponential growth in optical fiber communication capacity to match the exponential growth in capacity demand, multiplicative growth in optical communication capacity, for example using WDM, has satisfied traffic demand in the past. As today's WDM coherent optical communication has already taken advantage of all degrees of freedom of a light wave in a single-mode fiber (SMF), namely, frequency, polarization, amplitude, and phase, further multiplicative growth must explore new degrees of freedom that do not exist in SMFs. Similar to the multiple-input–multiple-output (MIMO) architecture in wireless communication, space is the degree of freedom that is being considered for optical fiber communication beyond WDM. Space-division

multiplexing (SDM), including mode-division multiplexing (MDM) using multimode fibers (MMFs) or few-mode fibers (FMFs) and/or core multiplexing using multicore fibers (MCFs), has attracted much attention in the last 3 to 4 years for the next multiplicative capacity growth for optical communication [3–5].

In this paper, we review recent progress in SDM. We start by introducing the concept of MDM in Section 2, followed by a description of mode coupling and its impact on MDM in Section 3. Section 4 presents electronic techniques for equalizing mode crosstalk and their computational complexities. Section 5 describes optical techniques to reduce computational complexity for mode crosstalk equalization. Passive and active components for SDM are presented in Section 6. Section 7 contains the state-of-the-art SDM transmission experiments as well as a discussion of linear and nonlinear capacity limits for MDM. SDM-compatible and mode-selective networking are discussed in Section 8. Section 9 presents conclusions and outlook for SDM.

For an introduction to the conventions for symbols used in the paper, the reader is referred to Appendix A: symbols with single overbar represent vectors, symbols with a double overbar represent matrices, and regular (bold) symbols represent quantities in the time (frequency) domain.

2. Fiber Modes for MDM

Fibers guide light using a high-index core and low-index cladding by a mechanism that can be intuitively understood as total internal reflection at the core–cladding boundary. In step-index fiber, the refractive index n_1 is uniformly distributed across the core surrounded by a cladding with refractive index n_2. The propagation constant β of any guide mode is thus bounded by $(n_1 k_0, n_2 k_0)$, where k_0 is the propagation constant of light in vacuum. In typical fiber used for optical communication, the relative index difference defined by $\Delta = (n_1 - n_2)/n_1$ is less than 10^{-2}; therefore, fiber modes are weakly guided. Under the weakly guided approximation, the vectorial modes of the fiber can be simplified using linear polarization (LP) modes. SMFs are the dominant transmission medium for fiber-optic communication systems in use today. In MDM, we explore other modes that can be supported in optical fibers.

Figure 1 schematically illustrates a step-index circular fiber with an increasing cross-sectional area. This fiber will always support the fundamental mode, the LP_{01} mode (where the subscripts describe radial and azimuthal variations) characterized by its propagation constant β_{01}, and the normalized mode profile $\psi_{01}(r,\theta)$ such that the power contained in the mode $A_{01}\psi_{01}(r,\theta)\exp\{-i[\omega t - \beta_{01} z]\}$ is $|A_{01}|^2$. When the fiber diameter is increased to a point at which the V number, $V = (2\pi/\lambda)a\sqrt{n_1^2 - n_2^2}$, of the fiber is greater than 2.405, the fiber can guide light in the next higher order mode, the LP_{11} mode, characterized by its propagation constant β_{11} and the normalized mode profile $\psi_{11}(r,\theta)$. The LP_{11} mode has a twofold degeneracy, rotated by 90°, as illustrated in Fig. 1.

Generally, for weakly guiding fibers with more modes, the transverse field of LP modes in the core is of the form [6]

$$E_y(r,\theta) = E_y(a)\frac{J_p(k_r r)}{J_p(k_r a)}\cos(p\theta), \tag{1}$$

Figure 1

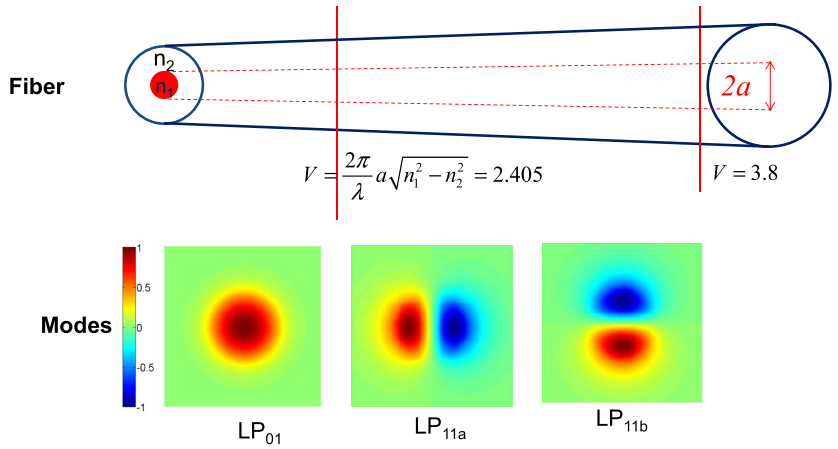

Schematic of a step-index circular fiber with an increasing cross-sectional area and profiles of supported modes along the fiber.

where a is the radius of the core, $k_r = (k^2 n_1^2 - \beta^2)^{1/2}$, and p is a non-negative integer referred to as the azimuthal mode number. For the same p value, k_r can take on discrete values, labeled by a non-negative integer q corresponding to the number of zero crossings of the field along the radial direction. The LP modes can be labeled LP_{pq}, each having twofold degeneracies in polarizations in x and y, and for $p \neq 0$, twofold degeneracies in spatial orientations separated by a rotation of $\pi/2p$. The total number of modes of the step index core fiber is approximately [6]

$$M \approx \frac{1}{2} V^2. \tag{2}$$

Orbital angular momentum (OAM) modes are linear combinations of a subset of eigenmodes of the fiber. Since any advantage that may exist for OAM modes can also be exploited using the OAM-less eigenmodes that comprise the OAM modes, we will not discuss OAM multiplexing in this paper.

By definition, modes supported by the fiber are orthonormal, i.e.,

$$\iint \psi_{rs} \cdot \psi_{pq}^* r \mathrm{d}r\mathrm{d}\theta = \delta_{pr}\delta_{qs}, \tag{3}$$

which is the basis for MDM: transmitting and receiving independent information simultaneously in each fiber mode.

Throughout this paper we will use the simplest case of two modes to illustrate important concepts and techniques for MDM. These concepts and techniques are described mathematically based on vectors and matrices. The two-mode case helps to visualize these vectors and matrices, which can be generalized to arbitrarily larger number of modes by simply increasing the dimension. MDM signals contain a superposition of modes, which can be described, in the case of a fiber containing two mode groups (total of three modes), as

$$s(t, r, \theta) = A_{01}(t)\psi_{01}(r, \theta) + A_{11}(t)\psi_{11}(r, \theta), \tag{4}$$

where $\psi_{11}(r,\theta)$ represents one of the degenerate LP_{11} modes. It follows from the orthogonality equation [Eq. (3)] that the time-domain signals modulated onto the two modes can be separated [7], for example, by coherent beating of the MDM signal with the local oscillator of the corresponding mode:

$$A_{pq}(t) = \iint s(t,r,\theta)\cdot\psi_{pq}^{*} r\mathrm{d}r\mathrm{d}\theta. \tag{5}$$

Coherent beating is one example of mode-division demultiplexing. Methods for multiplexing and demultiplexing of MDM signals will be described in Section 5.

In SMFs, the fundamental mode has two degenerate polarization states. These two polarization states have been used for polarization multiplexing. The general state of polarization-multiplexed signals can be represented using the Jones vector, consisting of the normalized complex amplitudes of the two polarizations. The Jones vector has an isomorphic correspondence with the Stokes vector, which resides in the three-dimensional real space. The state of signal with MDM, which in general encompasses both spatial and polarization modes, can be described by the *generalized Jones vector* or the *generalized Stokes vector* [8,9]. The generalized Jones vector represents the $2M$-dimensional *state of modes* (SOM) for MDM signals:

$$\bar{J} = [A_{01}^{x} \quad A_{01}^{y} \quad A_{11a}^{x} \quad A_{11a}^{y} \quad \cdots \quad A_{pq}^{x} \quad A_{pq}^{y} \quad \cdots]^{T}, \tag{6}$$

where all amplitudes are complex, the superscripts denote x or y polarizations, and T represents transpose. The factor of 2 comes from two polarizations for each of the M modes. Just as in the case of single-mode fields, the SOM can also be represented by a vector on a $(4M-2)$-dimensional manifold in the $(4M^2-1)$-dimensional real space, called generalized Stokes space [8], as will be described in detail in Section 5.3e.

3. Mode Coupling and Its Impact on MDM

The concept of MDM has been around for a very long time [7] but has not been pursued until recently. The reason is that the orthogonality of modes can be maintained in practical application for only a very short distance because of crosstalk among modes due to fiber imperfections, bending, and twisting. Mode coupling is a *fundamental* obstacle for MDM [10] and thus must be addressed first.

3.1. Mode Coupling due to Nonideal Fiber Cross Section

If the index distribution of the fiber deviates from the ideal circularly symmetric distribution, for which the degenerate modes have the same propagation constant, the modes will couple to each other. For example, the coupling coefficient for the degenerate LP_{11} mode is given by [11]

$$\kappa_{LP_{11a}\leftrightarrow b} = \frac{\omega\varepsilon_0 \int_{-\infty}^{+\infty}\int_{-\infty}^{+\infty}[n^2(x,y)-n_{\mathrm{ideal}}^2(x,y)]\vec{E}_{LP_{11},a}^{*}\vec{E}_{LP_{11},b}\mathrm{d}x\mathrm{d}y}{\int_{-\infty}^{+\infty}\int_{-\infty}^{+\infty}\hat{z}\cdot(\vec{E}_{1\ LP_{11},a}^{*}\times\vec{H}_{LP_{11},b}+\vec{E}_{LP_{11},a}\times\vec{H}_{LP_{11},b}^{*})\mathrm{d}x\mathrm{d}y}, \tag{7}$$

where n and n_{ideal} are the refractive index distributions of the actual and ideal fibers, respectively, and $\hat{z}$ is a unit vector in the z direction. The coherence length for degenerate modes is of the order of hundreds of meters for a conventional

MMF and of the order of kilometers for FMFs with two-mode groups. Because the degenerate modes couple with each other, independent data streams contained in the respective local LP_{11} degenerate modes at the transmitter will be dispersed into the local LP_{11} degenerate modes at the receiver. In other words, the signal detected in either one of the local LP_{11} modes at the receiver will contain both data streams modulated onto the two local LP_{11} degenerate modes at the transmitter. In the absence of chromatic dispersion, this crosstalk between two degenerate modes involves only one symbol, one from each mode, as they propagate together along the fiber. With chromatic dispersion, this crosstalk will involve as many symbols as the dispersive spreading of each symbol. To recover the independent data streams, the coupling/crosstalk between the degenerate modes must be undone. One may choose to transmit a single data stream in the two degenerate modes, a method called mode-group multiplexing (MGM), obviously at the expense of wasting 1 degree of freedom.

3.2. Mode Coupling due to Longitudinal Variations

In an ideal fiber, there is no coupling between nondegenerate modes. This is schematically shown in Fig. 2(a) for a two-mode fiber, where two parallel lines symbolically represent the noninteracting trajectories for the LP_{01} and LP_{11} modes. However, index distribution of real fibers will have variations along the direction of propagation. Such a variation can be caused by the fiber manufacturing process as well as by micro and macro bending of the fiber. The index perturbation can be decomposed into Fourier components in the z direction as

$$\Delta\varepsilon(x,y,z) = \int \varepsilon_0 \Delta\boldsymbol{\varepsilon}_r(x,y,K)(\cos Kz)\mathrm{d}K. \tag{8}$$

The (spatial) spectral component $\varepsilon_0\Delta\boldsymbol{\varepsilon}_r(x,y,\beta_{01}-\beta_{11})$ of the index perturbation will provide the phase-matching condition for the LP_{01} and LP_{11} modes to couple to each other, with a coupling coefficient given by

$$\kappa = \frac{(\omega/c)^2}{\beta}\iint \Delta\boldsymbol{\varepsilon}_r(x,y,\beta_{01}-\beta_{11})\psi_{01}(x,y)\psi_{11}^*(x,y)\mathrm{d}x\mathrm{d}y. \tag{9}$$

Coupling coefficients between other nondegenerate modes are expressed with appropriate substitutions of the mode profiles and spectral components of the index perturbation. Therefore, the strengths of coupling among nondegenerate modes depend on the spectrum of the index perturbation. The length scale of nondegenerate mode coupling depends on $\varepsilon_0\Delta\boldsymbol{\varepsilon}_r(x,y,\beta_{01}-\beta_{11})$, which generally is a low pass (in terms of spatial frequency) function, and therefore modes with small differences in propagation constants tend to couple strongly [12,13].

Figure 2

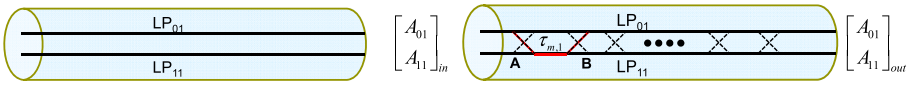

(a) (b)

Schematic of (a) an ideal two-mode fiber in which the two parallel lines represent two orthogonal modes and (b) a real fiber that has distributed crosstalk.

Since the index perturbation along the fiber is random in nature, the strengths and locations of coupling between nondegenerate modes are statistical. This random coupling along the fiber can be represented by a series of coupling events along the fiber, as shown in Fig. 2(b). In this discrete model, the interplay between mode coupling and modal dispersion is apparent. With two discrete coupling events A and B, the signal can arrive from A to B in the LP_{01} mode via two different paths: (1) the straight path in which the signal remains in the LP_{01} mode and (2) the multiple-coupled path in which the signal is coupled from the LP_{01} mode into the LP_{11} mode at the first coupling event A and is coupled from the LP_{11} mode back into the LP_{01} mode at the second coupling event B. Because of modal dispersion, the signal arriving via the multiple-coupled path will accumulate a modal group delay (MGD).

Mathematically, each coupling event between the modes can be described by a linear coupling matrix,

$$\bar{\bar{C}}_i = \begin{bmatrix} c_{11,i} & c_{12,i} \\ c_{21,i} & c_{22,i} \end{bmatrix}, \tag{10}$$

which is typically a unitary matrix of complex numbers. The independent propagation of the two nondegenerate modes between the two coupling events can be described by a linear propagation matrix,

$$\bar{\bar{\boldsymbol{P}}}_i = \begin{bmatrix} e^{j\beta_{01}L_i} & 0 \\ 0 & e^{j\beta_{11}L_i} \end{bmatrix}, \tag{11}$$

in the frequency domain in which the propagation constants are generally frequency dependent, or its inverse Fourier transform in the time domain, which is also unitary:

$$\bar{\bar{P}}_i = F^{-1}\{\bar{\bar{\boldsymbol{P}}}_i\}. \tag{12}$$

The output is related to the input by

$$\begin{bmatrix} A_{01}(t) \\ A_{11}(t) \end{bmatrix}_{\text{out}} = \bar{\bar{P}}_N * \bar{\bar{C}}_N \cdots \bar{\bar{C}}_2 * \bar{\bar{P}}_2 * \bar{\bar{C}}_1 * \bar{\bar{P}}_1 * \begin{bmatrix} A_{01}(t) \\ A_{11}(t) \end{bmatrix}_{\text{in}} = \bar{\bar{H}} * \begin{bmatrix} A_{01}(t) \\ A_{11}(t) \end{bmatrix}_{\text{in}}, \tag{13}$$

where $*$ denotes convolution.

3.3. Mode Coupling Matrix

Ignoring the effect of chromatic dispersion in each mode, the input–ouput relationship with nondegenerate mode coupling, for the case of a two-mode fiber, can be expressed as a matrix convolution:

$$\begin{bmatrix} A_{01}(t) \\ A_{11}(t) \end{bmatrix}_{\text{out}} = \begin{bmatrix} h_{11} & h_{21} \\ h_{21} & h_{22} \end{bmatrix} * \begin{bmatrix} A_{01}(t) \\ A_{11}(t) \end{bmatrix}_{\text{in}}. \tag{14}$$

Based on the mode-coupling picture in Fig. 2(b), each matrix element corresponding to an appropriate impulse response is not a simple complex number, but is of the form of a tapped-delay line filter or finite impulse response (FIR) filter. For example,

$$h_{11} = \mathcal{L}\delta(t) + \sum \varepsilon_i \delta(t - \tau_i), \qquad 0 \le \tau_i \le \tau_{\mathrm{MGD}}, \tag{15}$$

where $\mathcal{L}$ represents reduction of the amplitude of the input impulse, and the summation represents all possible combinations of the discrete coupling events along the fiber that allow the input signal in the LP_{01} mode to remain in the same mode at the receiver. ε_i and τ_i represent the strength and time delay associated with the ith coupling combination, and τ_i is no greater than the total MGD of the entire link,

$$\tau_{\mathrm{MGD}} = \Delta\tau \cdot L, \tag{16}$$

where $\Delta\tau$ is the differential modal group delay (DMGD) and L is the length of the fiber.

Even including the effect of chromatic dispersion of each mode, the form of the coupling matrix will remain the same—a matrix of tapped-delay line filters. For example, the first term in h_{11} will be of the form $\mathcal{L}\delta * h_{\mathrm{cd}}(t)$, where $h_{\mathrm{cd}}(t)$ is the impulse response of the chromatic dispersion of the LP_{01} mode of the fiber. Including chromatic dispersion, the length of the tapped-delay line filter is the summation of the MGD and chromatic dispersion spreading $\tau_{\mathrm{CD}} = D \cdot \Delta\lambda \cdot L$, where D is the chromatic dispersion parameter and $\Delta\lambda$ is the bandwidth of the signal. The coupling matrix between degenerate modes is a special case of Eq. (15) with $\tau_i = 0$. When more than two (spatial and polarization) modes are supported by the multimode fiber, the dimension of the coupling matrix will be increased so that the rank of the coupling matrix will be the same as the number of modes.

Assuming that the number of spatial modes supported by the multimode fiber is M, with polarization multiplexing the total degrees of freedom for SDM is $D_s = 2M$. The input–output relation can be expressed as

$$\overline{y(t)} = \overline{\overline{H(t)}} * \overline{x(t)}, \tag{17}$$

where the input $\overline{x(t)}$ and output $\overline{y(t)}$ are column vectors of length D_s, and the coupling matrix $\overline{\overline{H(t)}}$ is a $D_s \times D_s$ matrix of tapped-delayed line filters. Because all spatial degrees of freedom couple with each other, independent data streams contained in the respective spatial degree of freedom at the transmitter will be dispersed into all local spatial degrees of freedom along the fiber and at the receiver. To recover the independent data streams, the coupling/crosstalk among the spatial degrees of freedom must be equalized by inverting the coupling matrix.

4. MIMO Digital Signal Processing for SDM

Based on the nature of coupling among the spatial degrees of freedom, it is highly unlikely that the coupling matrix can be inverted using optical techniques. To invert the coupling matrix in the electronic domain, the signals in all spatial degrees of freedom arriving at the receiver must be coherently and synchronously detected because the coupling and propagation in the fiber is sensitive to the phase of the signals. The detected signals are first digitized and then processed using digital signal processing (DSP). Before describing methods for inverting the coupling matrix, it is useful to discuss the basic characteristics

of the $D_s \times D_s$ coupling matrix $\overline{\overline{H(t)}}$ of tapped-delayed line filters. The number of taps (also called tap length or memory) of each filter is related to the symbol rate (or baud rate) B of the SDM transmission system, the sampling rate R_s (samples/symbol), the chromatic dispersion, and the MGD of the fiber:

$$N_{\text{Tap}} = (\tau_{\text{MGD}} + \tau_{\text{CD}}) \cdot B \cdot R_s. \tag{18}$$

The total number of complex parameters in the coupling matrix is $D_s \times D_s \times N_{\text{Tap}}$.

As an example, consider a SDM system employing $D_s = 24$ degrees of spatial freedom, opearting at a symbol rate of 25 GBaud over 2000 km with $\Delta\tau = 50$ ps/km, and the total number parameters is 1,440,000 at one sample per symbol. As a further complication, since the constituent coupling and propagation matrices $\bar{\bar{C}}_i$ and $\bar{\bar{P}}_i$ are subject to environmental changes of the fiber, the coupling matrix $\overline{\overline{H(t)}}$ is random and time varying and, therefore, is also generally unknown. To undo the crosstalk among the spatial degrees of freedom, one must determine as well as invert the unknown matrix $\overline{\overline{H(t)}}$ all within a time scale much faster than the characteristic time constant for environmental changes [14]. Since the coupling matrix $\overline{\overline{H(t)}}$ is linear and well behaved, all the unknowns in $\overline{\overline{H(t)}}$ can be determined if one makes enough (more than the number of unknowns) independent measurements, using training symbols, for example. The time it takes for 24 channels to transmit 1,440,000 symbols at 25 GBaud is 2.4 μs, which is much shorter than the characteristic time scale of environment change on the order of milliseconds. Of course, actual adaptation of the multimode channel will take longer. Fortunately, many MIMO algorithms have been developed in wireless communication, which can be adopted and adapted to equalize mode crosstalk in SDM.

So far, two main linear equalization techniques have been investigated: adaptive time-domain equalization (TDE) [15,16] and frequency-domain equalization (FDE) [17,18]. In this section, we review both approaches and discuss their algorithmic complexities.

4.1. Time-Domain Equalization

4.1a. Algorithm Description

To recover transmitted signals from what is received in different mode channels at the receiver, an ideal linear equalizer can estimate an inverted channel matrix $\overline{\overline{W(t)}} = \overline{\overline{H(t)}}^{-1}$ and apply it to the received signals to recover the transmitted signal:

$$\overline{x(t)} = \overline{\overline{W(t)}} * \overline{y(t)}. \tag{19}$$

According to Eq. (19), this equalization can be intuitively implemented in the time domain. Figure 3 shows a canonical structure of an adaptive TDE for two-mode transmission.

Figure 3

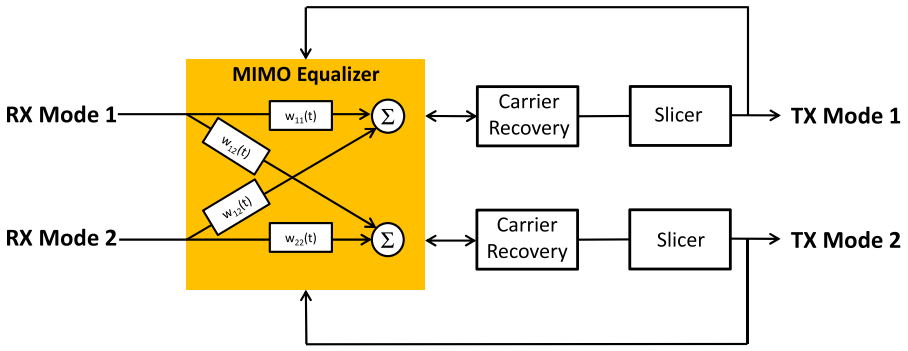

DSP structure of adaptive TDE for two-mode transmission. The MIMO equalizer has a butterfly configuration.

In the coherent receiver (RX), both in-phase (I) and quadrature (Q) components of signals from all spatial channels are detected and digitized. The electric fields of the signals $\overline{y_{1,2}(k)}$ are then reconstructed and resampled. The channel inversion process is performed by a filter matrix that contains four taped-delay line filters:

$$\begin{bmatrix} \overline{\hat{x}_1(k)} \\ \overline{\hat{x}_2(k)} \end{bmatrix} = \begin{bmatrix} \overline{w_{11}(k)} & \overline{w_{12}(k)} \\ \overline{w_{21}(k)} & \overline{w_{22}(k)} \end{bmatrix} * \begin{bmatrix} \overline{y_1(k)} \\ \overline{y_2(k)} \end{bmatrix} = \overline{\overline{W(k)}} * \begin{bmatrix} \overline{y_1(k)} \\ \overline{y_2(k)} \end{bmatrix}, \tag{20}$$

where $\bar{\hat{x}}_{1,2}(k)$ denotes equalized symbols, $\{\bar{w}_{ij}(k)\}(i,j=1,2)$ represents inverse channel filters, and the $*$ here denotes element-wise convolution. Figure 4 is a detailed block diagram of the MIMO TDE for one spatial channel.

In order to eventually recover the transmitted symbols, laser phase noises have to be estimated and mitigated. The mth symbol after carrier recovery can be written as

$$\hat{x}'_{1,2}(m) = \hat{x}_{1,2}(m)\exp(-j\hat{\phi}_{1,2}(m)), \tag{21}$$

where $\hat{\phi}_{1,2}$ denote the estimated laser phase fluctuations, which can be computed using the Viterbi–Viterbi approach [19] or the maximum likelihood estimation

Figure 4

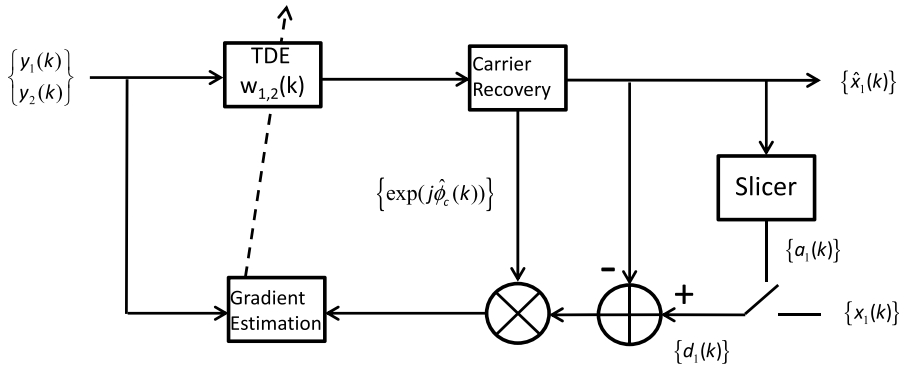

Block diagram of MIMO TDE for one spatial channel.

method [20]. The estimation of filter coefficients generally can be acquired using the blind or data-aided (DA) approach. The blind estimation approach can determine the filter coefficients by using information of the receiving signal itself. However, blind equalization normally exhibits slower convergence rate, worse performance for low SNR, and more instability compared to DA equalization [21]. In this paper, we focus on DA estimation methods in which a known training sequence is inserted in the preamble of each data frame. Because of the high data rates used in optical fiber communication, the least-mean-square (LMS) method is a standard method to estimate the filter coefficients using the following iterative algorithm:

$$\overline{w_{ij}^{(m)}} = \overline{w_{ij}^{(m-1)}} + \mu \varepsilon_i^{(m)} \overline{y_j^*(k)} \Big|_{m-\lfloor \frac{N_f}{2} \rfloor + 1}^{m+\lfloor \frac{N_f}{2} \rfloor}, \tag{22}$$

where $\lfloor \rfloor$ denotes floor operation and

$$\overline{y_j^*(k)} \Big|_{m-\lfloor \frac{N_f}{2} \rfloor + 1}^{m+\lfloor \frac{N_f}{2} \rfloor}$$

represents a block of signal necessary for accurate phase estimation:

$$\left[y_i^* \left(m - \lfloor \frac{N_f}{2} \rfloor + 1 \right), \quad y_i^* \left(m - \lfloor \frac{N_f}{2} \rfloor + 2 \right), \ldots y_i^* \left(m + \lfloor \frac{N_f}{2} \rfloor \right) \right].$$

The error signals represent the difference between the training symbol $d_{1,2}(k)$ and the recovered symbol multiplied by the laser phase noise and are calculated as

$$\varepsilon_{(1,2)}(m) = (d_{1,2}(m) - \hat{x}'_{1,2}(m)) \exp(j\hat{\phi}_{1,2}(m)), \tag{23}$$

where m is the symbol index label and μ denotes the convergence step size. In practical implementations, μ has to be optimized as a result of the trade-offs among speed of convergence, stability, and misadjustment of the adaptive process. It is noted that the phase noise is multiplied in Eq. (23). By doing so, phase fluctuations of $y_{1,2}^*(k)$ can be canceled in Eq. (22) and laser phase noise will not corrupt channels estimation and inversion.

After successful channel estimation using DA mode [$d_{1,2}(m) = x_{1,2}(m)$], the MIMO equalizer operates in the decision-directed (DD) mode with $d_{1,2}(m) = a_{1,2}(m)$, where $a_{1,2}$ are symbols after hard decision to receive useful information as well as continuously update the channel matrix.

4.1b. Algorithm Complexity

The complexity of TDE using an FIR filter matrix adapted by the LMS algorithm can be measured by the number of complex multiplications per symbol per mode. The number of taps in each filter, ignoring chromatic dispersion, is given by

$$N_{\text{Tap}} = R_s \Delta\tau LB. \tag{24}$$

To obtain every output symbol per mode, we need $D_s N_{\mathrm{Tap}}$ multiplications. Updating the filter coefficients requires $D_s \Delta\tau LB$ multiplications. Therefore, the complexity for TDE without carrier recovery can be expressed as

$$C_{\mathrm{TDE}} = D_s(R_s + 1)\Delta\tau LB. \tag{25}$$

The complexity of TDE scales linearly with the MGD of the link, the number of modes, and the symbol rate.

Even though it is theoretically possible to invert the MIMO channel matrix of multimode fibers, the computational load required can be staggering. As an example, for a 2000 km 30-mode MDM system, in comparison to a SMF system, the capacity could be increased by a factor of 30, and the DSP complexity is increased by a factor of 1 million in comparison to dispersion equalization for SMF transmission. Therefore, DSP complexity is a critical challenge, which determines the feasibility of MDM. In the next subsection, we present FDE, an electronic approach to tackle the DSP complexity challenge. Optical methods to reduce DSP complexity will be presented in Section 5.

4.2. Frequency-Domain Equalization

4.2a. Algorithm Description

Adaptive FDE for MDM transmission was first reported in [22]. To reduce the complexity of equalization algorithms, FDE can be implemented using multiplications rather than convolution, as in the case of TDE, by inserting (inverse) fast Fourier transform (FFT) [IFFT] into Fig. 4. This is shown in Fig. 5, where the filter coefficients are frequency-domain values. However, both the received signal and the error are in the time domain, as the latter are obtained by subtracting the received signal from desired symbols. To adjust the FDE coefficients, the error is transformed back into the frequency domain.

In real-time implementations, the received signals are parallelized and processed in blocks to facilitate FFTs/IFFTs. The overlap-and-save method is normally used to compute convolutions between received signals and the equalizer. The received signal is partitioned into overlapping blocks $\overline{y}_{i,b} = \overline{y_i(k)}\Big|_{bN_B - N_f + 1}^{(b+1)N_B - 1}$, where i and b are the mode and block indices, respectively. The length of overlap block $N_{\mathrm{FFT}} = N_f + N_B - 1 = 2^N$ is chosen as an integer

Figure 5

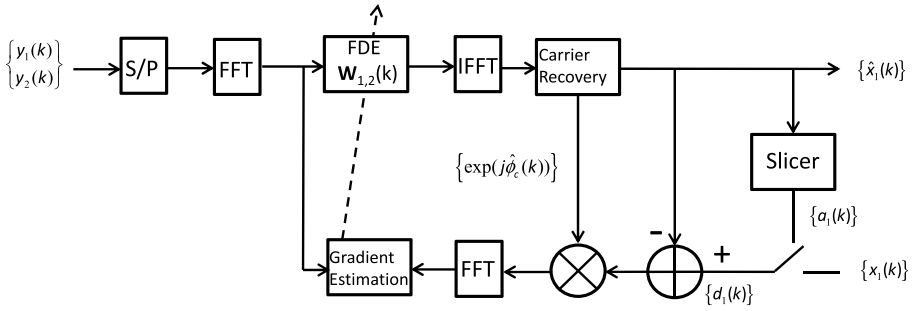

Block diagram of MIMO FDE for one mode channel.

power of 2. A circular convolution is computed by taking the FFT of the signal block, multiplying it with the equalizer block, and then taking the IFFT. The last N_B samples of circular convolution are the same as the linear convolution and therefore are saved as equalized symbols.

For adaptive FDE, error blocks can be computed in the same way as for TDE in the time domain [Eq. (23)]. Frequency-domain LMS is used to iteratively calculate equalizer coefficients as follows:

$$\overline{\boldsymbol{W}_{ij}^{(b)}} = \overline{\boldsymbol{W}_{ij}^{(b-1)}} + \mu \bar{\boldsymbol{E}}_{i,b} \otimes \bar{\boldsymbol{Y}}_{j,b}^{*}, \tag{26}$$

where $\bar{\boldsymbol{E}}_{i,b}$ represents the bth error block for the ith mode, $\bar{\boldsymbol{Y}}_{i,b}^{*}$ denotes the conjugate of the signal block, and $\otimes$ symbolizes element-wise multiplication. Although FDE updates in the duration of a block, the error signal is permitted to vary at the symbol rate, which determines the effective updating rate. Consequently, FDE has tracking performance similar to that of TDE [23]. To reduce convergence speed, the recursive least-mean-square (RLS) algorithm can be used [24].

4.2b. Algorithm Complexity

For adaptive FDE, it is most common to use a block length of twice the equalizer length. By using even and odd subequalizers, an equivalent half-symbol-spacing FIR filter can be realized in the frequency domain [25]. To obtain $N_{\mathrm{Tap}}/2$ output symbols per mode per block, we need $D_s N_{\mathrm{Tap}}$ multiplications. Updating both even and odd equalizers requires additional $D_s N_{\mathrm{Tap}}$ multiplications, also. The total number of FFT/IFFT per mode is $4 + 2D_s$ containing two FFT for the input, a FFT/IFFT pair in the updating loop, and $2D_s$ FFT/IFFT for executing the gradient constraint in the gradient estimation block [23]. FFT is assumed to be implemented by the radix-2 algorithm requiring $N \log(N)/2$ complex multiplications to execute FFT of N complex numbers. Thus, the complexity for the proposed FDE can be expressed as

$$C_{\mathrm{FDE}} = (4 + 2D_s)\log_2(R_s \Delta\tau LB) + 4D_s. \tag{27}$$

To compare the algorithmic complexity of FDE and TDE, Fig. 6 shows the complexity as a function of the number of taps.

It can be seen that FDE reduces the complexity significantly from TDE. For long-haul MDM transmission, the advantage of FDE is even more prominent since the required filter tap length is high.

To further reduce the complexity of adaptive FDE at the receiver side, a cyclic prefix can also be used [26]. This brings about a comparison between coherent SDM systems using single-carrier or multicarrier modulation. Multicarrier modulation is typically implemented using orthogonal frequency-division multiplexing (OFDM) [27–30]. One main difference in DSP structure between OFDM and adaptive FDE is that OFDM requires IFFT at the transmitter side. However, the complexity of DSP on the receiver side is reduced. For adaptive FDE, the error calculation is done in the time domain, which requires an IFFT/FFT pair. To enable fast adaptation and low excess error, additional FFTs are needed to enforce time-domain gradient constraints. The other difference is that OFDM uses a cyclic prefix to combat modal dispersion. The length of the cyclic

Figure 6

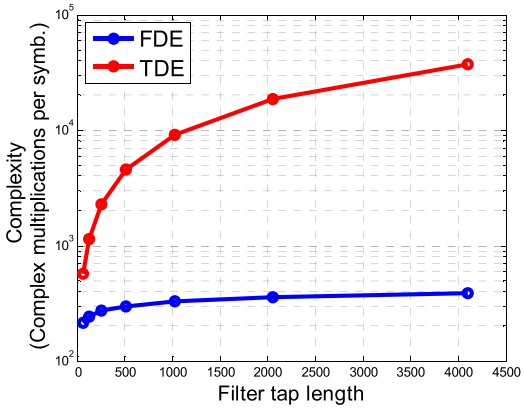

Number of multiplications per symbol versus filter tap length for TDE and FDE. FDE can significantly reduce the computational complexity.

prefix has to be at least equal to the MGD spread of the link. A drawback of this approach is a reduction of throughput efficiency. To maximize the throughput of the system, the FFT size should be sufficiently large to increase the cyclic prefix efficiency parameter:

$$\eta_{\mathrm{CP}} = \frac{N_{\mathrm{FFT}}}{N_{\mathrm{FFT}} + N_{\mathrm{CP}}},$$

where N_{CP} is the length of cyclic prefix. Then, the FFT block size N_{FFT} for OFDM would be much bigger than that for FDE. However, FFT block size directly translates into DSP circuit size. Additionally, in long-haul systems, multicarrier modulation is more prone to fiber nonlinearity than single-carrier modulation. Single-carrier modulation has been used in all commercial systems to date.

4.3. Experimental Results

MDM experiments using adaptive TDE [15,31] and adaptive FDE [32] have been experimentally demonstrated. Reference [32] also includes a comparison between TDE and FDE. In the experiment reported in [32], six channels of 28 Gbaud QPSK data were multiplexed into six SDM channels of a 50 km FMF (three spatial modes each contain dual polarization). The baseband electrical signals in the six SDM channels were sampled and digitized using three synchronized sampling oscilloscopes with a sampling rate of 40 GSa/s and 16 GHz bandwidth. A total of 490,000 symbols per spatial/polarization mode are evaluated to estimate bit error ratio (BER). For fair comparison between TDE and FDE, equalizer memory lengths, initial tap coefficients, and the training step size were set to the same values. The DMGD of the FMF is 63 ps/km. The total link MGD of 3.15 ns corresponds to 88 symbols. An equalizer length of 256 per MIMO tributary was chosen, corresponding to a memory length of 128 symbols. This is sufficient to undo the channel crosstalk but is shorter than the minimum decorrelation delay between the six spatial/polarization modes to avoid spurious convergence.

Figure 7

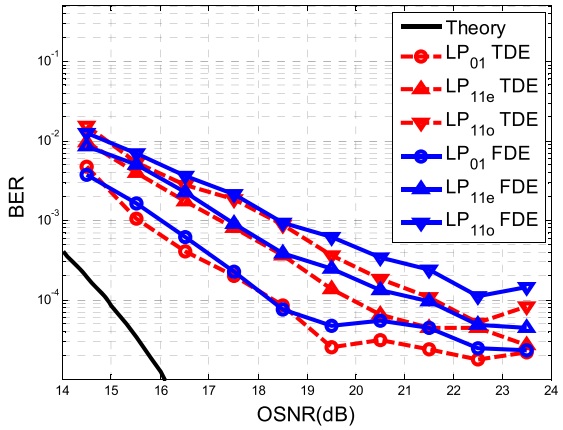

BER versus OSNR for MDM transmission. The results of using TDE and FDE for MIMO equalization are compared.

Figure 7 shows BER versus OSNR using both TDE and FDE where the black curve represents the theoretical limit as a reference. The BER shown for each spatial mode is the average of the two orthogonal polarizations. We observe similar BER performance for both FDE and TDE. On the other hand, at an equalizer length of 256, the FDE approach reduces algorithmic complexity by a factor of 8.5 compared with the TDE.

5. SDM Fibers to Simplify MIMO Equalization

As discussed in Section 4, the DSP complexity for an MDM system is proportional to the MGD of the FMF link. Therefore, it is critical to design and fabricate an FMF with the proper modal dispersion properties. There are a number of approaches in the optical domain that can reduce the computational load for SDM MIMO signal processing. They include the following:

- Fibers with small DMGD: the total MGD is proportional to the DMGD when fiber modes are weakly coupled.
- Fibers with positive and negative DMGD: they can be concatenated to achieve overall reduced MGD.
- Strongly coupled MMF: when fiber modes strongly couple to each other, the MGD can be reduced significantly.
- Multicore fibers: they can also reduce computational load by making the channel matrix sparse.

Characteristics of these fibers are discussed in the following subsections.

5.1. Reducing DMGD

In general, modal dispersion is determined by the overlap between the index profile of the fiber and the transverse mode profile. Currently, two types of index profile are proposed to achieve flexible modal dispersion control for MMFs. The first is the trench-assisted multistep index profile [33], shown in Fig. 8(a). By adjusting the index difference between the two core layers ($\Delta_d = \Delta_1 - \Delta_2$), the DMGD can be tuned from positive to negative. The second is the trench-assisted

graded index (GI) profile [34,35], shown in Fig. 8(b). Both techniques utilize the inner cladding trench to improve confinement and thus the loss of high-order modes and to tune modal dispersion of high-order modes.

The index profile of a GI core is normally described as

$$n(r) = \begin{cases} n_1[1-2\Delta(r/a)^{\alpha_n}]^{1/2} & (r \le a) \\ n_2 & (r > a) \end{cases}, \tag{28}$$

where α_n is the power coefficient of the GI profile, which is around 2 for most GI fiber used in data-communications applications. When a GI fiber supporting a great number of guided modes is considered, under the weakly guide assumption, the Wentzel–Kramers–Brillouin (WKB) approximation can be used to simplify the calculation of the propagation constants [36]:

$$\beta_m = n_1 k_0[1-2\Delta(m/\sqrt{M})^{2\alpha_n/(\alpha_n+2)}]^{1/2}. \tag{29}$$

Here, m is the degenerate mode number $m = 2q + p + 1$ and the total number of modes M is given by

$$M \approx \frac{\alpha_n}{\alpha_n + 2}(n_1 k_0 a)^2 \Delta. \tag{30}$$

For larger m, more combinations of p and q lead to the same m, which means higher degeneracy. The advantage of multimode GI fiber is a theoretically low MGD spread. The group delay of LP_{pq} can be expressed as [37]

$$\tau_{pq} = \frac{n_1}{c}\left[1 + \Delta\left(\frac{\alpha_n - 2}{\alpha_n + 2}\right)\left(\frac{m}{\sqrt{N}}\right)^{2\alpha_n/(\alpha_n+2)} + \frac{\Delta^2}{2}\left(\frac{3\alpha_n - 2}{\alpha_n + 2}\right)\left(\frac{m}{\sqrt{N}}\right)^{4\alpha_n/(\alpha_n+2)} + O(\Delta^3)\right]. \tag{31}$$

For $\alpha_n = 2$, DMGD $\Delta\tau$ vanish to the first order of Δ.

For few-mode GI fiber, the WKB approximation is no longer accurate. However, the GI profile of Fig. 8(b) can still reduce the MGD in comparison with the step-index design [38–42]. Figure 9(a) shows the DMGD at 1550 nm of the two-mode GI fiber of Fig. 8(b), with $a_1 = 8$ μm, $a_2 = 9.875$ μm, $\Delta_1 = 0.45\%$, and $\Delta_1 = -0.395\%$. It is observed that DMGD vanishes at $\alpha_n = 2.13$. Of course, this is true only at one particular wavelength. Nevertheless, a GI two-mode fiber with a 27 ps/km DMGD across the C band, which is two orders of magnitude

Figure 8

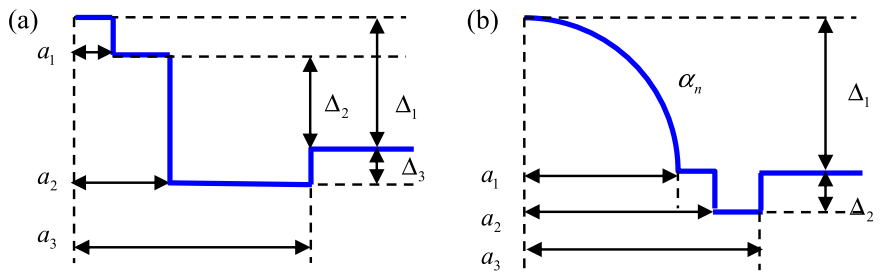

FMF index profiles for reducing DMGD: (a) multi-step index and (b) GI.

Figure 9

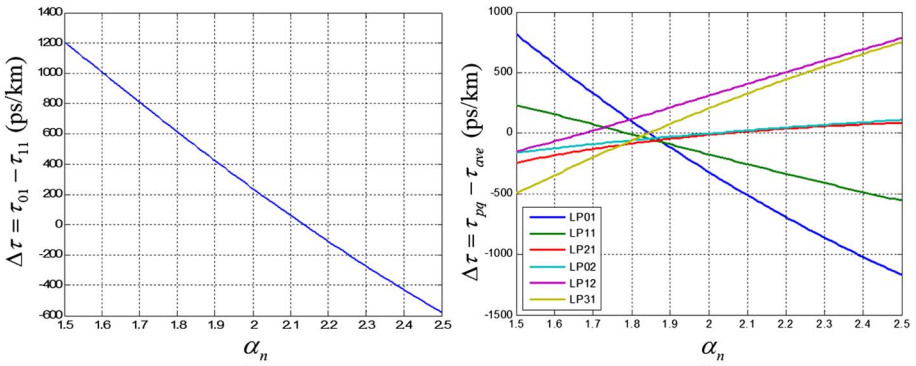

(a) DMGD of a two-mode GI fiber, showing net zero DMGD at $\alpha_n = 2.13$. (b) MGD as a function of for a six-mode-group GI fiber; at $\alpha_n = 1.8$, DMGD is only 200 ps/km.

smaller than typical step-index two-mode fibers, has been fabricated and used in recent transmission experiments [35]. In addition, this technique can be scaled to fibers with more modes. Figure 9(b) shows the MGD of a six-mode-group GI FMF [Fig. 8(b)] with $a_1 = 16$ μm, $a_2 = 9.875$ μm, $\Delta_1 = 0.45\%$, and $\Delta_1 = -0.395\%$ (referenced to the average MGD) at 1550 nm. The DMGD (between the fast and the slowest modes) is only 200 ps/km, achieved at $\alpha_n = 1.8$.

5.2. DMGD Compensation

Although DMGD can be significantly reduced using proper index profiles, due to sensitivity to index variation in the preform, most prototype FMFs have either positive or negative DMGD. Moreover, for more than four propagating mode groups, optimal DMGD is very sensitive to fabrication tolerances [40].

Figure 10

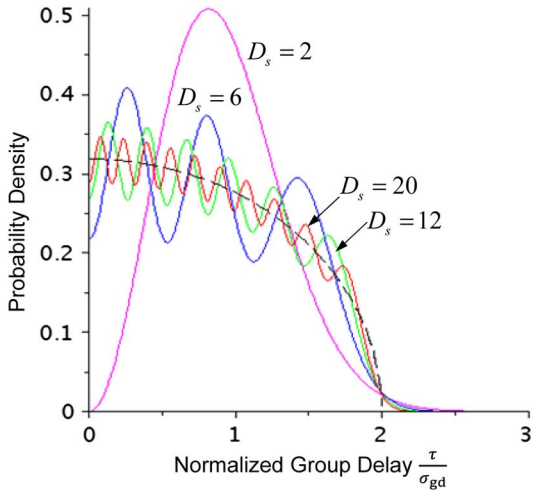

Probability density function of normalized group delay for strongly coupled multimode fibers, which approaches the semicircle distribution for a large number of modes. Courtesy of K.-P. Ho and J. M. Kahn.

An alternative approach is DMGD compensation in which two types of fiber with opposite signs of DMGD are concatenated [33,43]. For example, the two-mode fibers shown in Fig. 9(a) with $\alpha_n = 2.079$ and $\alpha_n = 2.196$ have group delays that are exactly the same in magnitude but opposite in sign. Assuming there is no mode crosstalk/coupling in each fiber and at the splice point, a concatenation of two of these fibers of *equal* length, which we shall call a DMGD compensation period, will result in net zero MGD. This is similar to optical chromatic dispersion compensation. Both modes must travel on these two fibers with *equal* length. This key requirement would not be satisfied, however, if there is mode crosstalk. The cross-coupled signal will not propagate on these two types of fiber with equal length. For transmission links consisting of multiple DMGD compensation periods, the total MGD will heavily depend on crosstalk [44]. For ease of explanation, we consider crosstalk analogous to scattering. If the system has only single scattering, DMGD compensation fails only within the compensation period where this single scattering occurs, and DMGD is compensated for all the other compensation periods. Thus, with single-scattering-type crosstalk, the maximum MGD [also called channel impulse response spread (CIRS)] of the entire link will be no larger than the worst MGD of one compensation period with mode coupling. In this case, CIRS will reduce as the length of the compensation period is reduced or as the number of periods of DMGD compensation is increased [45]. If multiple-scattering-type crosstalk also exists in the system, then the maximum MGD of the entire link will be no longer than the worst MGD of the number of compensation periods, equal to the order of scattering. DMGD-compensated fiber that can guide four LP modes has been demonstrated [10], although it might be difficult to scale to more mode groups. Therefore, DMGD compensation may be effective only for MDM transmission over short lengths and/or using a small number of modes.

5.3. Strong Mode Coupling

Another method of reducing the complexity of mode crosstalk equalization is to increase mode crosstalk, which is somewhat counterintuitive. A simple physical explanation is as follows: when modes strongly couple to each other, every independent data stream has equal probability to travel on the fast or slow modes, increasing the chances that all data streams will have similar amounts of delay. The theory behind this is quite elegant and is summarized here.

5.3a. Principal Modes

Without mode coupling, two modes, LP_{01} and LP_{11}, in a fiber will propagate independently with propagation constants β_{01} and β_{11} and group velocities $v_{g01} = 1/\beta'_{01}$ and $v_{g11} = 1/\beta'_{11}$. Consider the case of coupling between the LP_{01} and LP_{11} modes, whether intentionally introduced or due to fiber imperfections. The coupled-mode equation for the amplitude of these two waves is given by

$$\frac{\partial}{\partial z}\begin{bmatrix} \boldsymbol{A}_{01} \\ \boldsymbol{A}_{11} \end{bmatrix} = i\begin{bmatrix} \beta_{01} & \kappa \\ \kappa^* & \beta_{11} \end{bmatrix}\begin{bmatrix} \boldsymbol{A}_{01} \\ \boldsymbol{A}_{11} \end{bmatrix}, \tag{32}$$

where losses have been neglected. The propagation and coupling of the two modes are linear processes, and, as such, in the frequency domain, the mode amplitude vector can be expressed as

$$\bar{A}(\omega,z)=\begin{bmatrix}A_{01}(\omega,z)\\A_{11}(\omega,z)\end{bmatrix}=a_0(\omega,z)e^{i\Phi(\omega,z)}\bar{\bar{J}}(\omega,z),\tag{33}$$

where $a_0(\omega,z)$ and $\Phi(\omega,z)$ are the amplitude and phase of the field and $\bar{J}(\omega,z)$ is the generalized Jones vector representing the state of modes (SOM). The mode amplitude vectors at the input and output are related by a complex transfer matrix in the form

$$\bar{A}(\omega,z)=\bar{\bar{H}}(\omega,z)\bar{A}(\omega,0).\tag{34}$$

Being lossless, the transfer matrix is unitary:

$$\bar{\bar{H}}(\omega,z)=\begin{bmatrix}h_1(\omega,z) & h_2(\omega,z)\\ -h_2^*(\omega,z) & h_1^*(\omega,z)\end{bmatrix},\tag{35}$$

with

$$|h_1|^2+|h_2|^2=1.\tag{36}$$

Since the transfer matrix $\bar{\bar{H}}(\omega,z)$ is, in general, frequency dependent for an *arbitrary but fixed* input state of modes or generalized Jones vector, the output generalized Jones vector will vary with the frequency of the input wave. To see this frequency dependence, we follow [46]. Taking the derivative of Eqs. (33) and (34) with respect to frequency yields

$$\frac{\partial\bar{A}(\omega,z)}{\partial\omega}=\left[\frac{1}{a_0}a_0'+i\Phi'\right]\bar{A}(\omega,z)+a_o e^{i\Phi}\frac{d\bar{J}(\omega,z)}{d\omega},\tag{37}$$

$$\frac{\partial\bar{A}(\omega,z)}{\partial\omega}=\frac{\partial\bar{\bar{H}}(\omega,z)}{\partial\omega}\bar{A}(\omega,0),\tag{38}$$

where $'$ denotes derivative with respect to frequency. Combining Eqs. (37) and (38), using Eqs. (33) and (35), leads to

$$a_0e^{i\Phi}\frac{d\bar{\bar{J}}}{d\omega}=[\bar{\bar{H}}'-i\tau\bar{\bar{H}}]\bar{A}(\omega,0),\tag{39}$$

where

$$\tau=\Phi'-i\frac{1}{a_0}a_0'.\tag{40}$$

The rate of change of SOM with respect to frequency at the output will vanish if the right-hand side of Eq. (39) is zero:

$$[\bar{\bar{H}}'-i\tau\bar{\bar{H}}]\bar{A}(\omega,0)=0\quad\text{or}\quad[i\bar{\bar{H}}^{+}\bar{\bar{H}}'+\tau]\bar{A}(\omega,0)=0.\tag{41}$$

Since τ is group delay Φ' [for lossless transmission $(a_0'=0)$], which is the eigenvalue of $i\bar{\bar{H}}^{+}\bar{\bar{H}}'$,

$$i\bar{\bar{H}}^{\dagger}\frac{\partial\bar{\bar{H}}}{\partial\omega}\quad\text{or}\quad -i\frac{\partial\bar{\bar{H}}^{\dagger}}{\partial\omega}\bar{\bar{H}}\tag{42}$$

is called the *group delay operator*. The eigenvalues can be found readily by setting the determinant to zero. With the help of Eq. (36) and $(\boldsymbol{h}_1\boldsymbol{h}_1^* + \boldsymbol{h}_2\boldsymbol{h}_2^*)' = \boldsymbol{h}_1'\boldsymbol{h}_1^* + \boldsymbol{h}_1\boldsymbol{h}_1^{*\prime} + \boldsymbol{h}_2'\boldsymbol{h}_2^* + \boldsymbol{h}_2\boldsymbol{h}_2^{*\prime} = 0$, we arrived at

$$\tau_\pm = \pm\sqrt{|\boldsymbol{h}_1'|^2 + |\boldsymbol{h}_2'|^2} \tag{43}$$

and the corresponding eigenvectors

$$\bar{\bar{\boldsymbol{J}}}_\pm(\omega, 0) = e^{j\rho}\begin{bmatrix} \frac{\boldsymbol{h}_2' - j\tau_\pm \boldsymbol{h}_2}{\Delta_\pm} \\ -\frac{\boldsymbol{h}_1' - j\tau_\pm \boldsymbol{h}_1}{\Delta_\pm} \end{bmatrix}, \tag{44}$$

where ρ is an arbitrary phase and $\Delta_\pm = \sqrt{2\tau_\pm(\tau_\pm - \mathrm{Im}[\boldsymbol{h}_1^*\boldsymbol{h}_1' + \boldsymbol{h}_1^*\boldsymbol{h}_2'])}$. The eigenvectors are superpositions of the modes of the uncoupled fiber and are called the *principal modes* [47]. The MGD between these two principal modes is

$$\tau_{\mathrm{MGD}} = \tau_+ - \tau_- = 2\sqrt{|\boldsymbol{h}_1'|^2 + |\boldsymbol{h}_2'|^2}. \tag{45}$$

5.3b. Reduction of DMGD

Given the mode-coupling evolution described by the coupled-mode equations [Eq. (32)], the evolution of the transfer matrix $\bar{\bar{\boldsymbol{H}}}(\omega, z)$ can be obtained analytically. Taking the derivative of Eq. (34) with respective to z and recasting it in the form of Eq. (32), ignoring a common phase factor $\exp[\mathrm{i}(\beta_{01} + \beta_{11})z/2]$ for all the elements, we obtain

$$\frac{\partial \boldsymbol{h}_1}{\partial z} = i\frac{\Delta\beta}{2}\boldsymbol{h}_1 - i\kappa\boldsymbol{h}_2^*, \tag{46a}$$

$$\frac{\partial \boldsymbol{h}_2}{\partial z} = i\frac{\Delta\beta}{2}\boldsymbol{h}_2 + i\kappa\boldsymbol{h}_1^*, \tag{46b}$$

where $\Delta\beta = \beta_{01} - \beta_{11}$. For the case of constant coupling, the solution with boundary condition $\boldsymbol{h}_1(\omega, 0) = 1$ and $\boldsymbol{h}_2(\omega, 0) = 0$ is given by

$$\boldsymbol{h}_1 = \frac{i\Delta\beta}{\sqrt{\Delta\beta^2 + 4\kappa^2}}\sin\left(\frac{z}{2}\sqrt{\Delta\beta^2 + 4\kappa^2}\right) + \cos\left(\frac{z}{2}\sqrt{\Delta\beta^2 + 4\kappa^2}\right), \tag{47a}$$

$$\boldsymbol{h}_2 = 2i\frac{\kappa}{\sqrt{\Delta\beta^2 + 4\kappa^2}}\sin\left(\frac{z}{2}\sqrt{\Delta\beta^2 + 4\kappa^2}\right). \tag{47b}$$

As a result, for large propagation distances when the modes are fully coupled, the group delay is given by

$$\tau_{\mathrm{MGD}} = 2\sqrt{|\boldsymbol{h}_1'|^2 + |\boldsymbol{h}_2'|^2} = \sqrt{\frac{\Delta\beta^2}{\Delta\beta^2 + 4\kappa^2}}|\Delta\beta' z|. \tag{48}$$

It is noted that DMGD of the principal modes is smaller than that of the uncoupled modes $|\Delta\beta' z|$ by a factor $\sqrt{\Delta\beta^2/(\Delta\beta^2 + 4\kappa^2)}$. The larger the coupling coefficient, the larger the reduction factor. This phenomenon has been known in GI multimode fibers, and was shown by simulation in [48]. This is the first

reason that strong mode coupling is beneficial. This conclusion can be intuitively understood as follows, even though the derivation is valid only within the framework of coupled-mode equations. The MGD between the eigenmodes represents the largest possible spread of signals in the time domain. With coupling, the systems support principal modes, each of which is a superposition of the two eigenmodes and thus cannot spread faster than the eigenmodes themselves in the time domain.

5.3c. Scaling of Average MGD with Fiber Length

In real fibers, the coupling coefficient is random, and therefore the group delay of the principal modes is also random. We seek to find the variance

$$\langle|\tau_{\mathrm{MGD}}|^2\rangle = 4\langle|\boldsymbol{h}_1'|^2 + |\boldsymbol{h}_2'|^2\rangle. \tag{49}$$

Following [49], by defining $\eta_{1,2} = \boldsymbol{h}_{1,2}\exp(-i\Delta\beta z)$, the differential equation ([Eq. (46)] for $\boldsymbol{h}_1$ and $\boldsymbol{h}_2$ can be simplified into

$$\frac{\partial\eta_1(\omega,z)}{\partial z} = -i\kappa(z)\eta_2^*(\omega,z)\exp(-i\Delta\beta z), \tag{50a}$$

$$\frac{\partial\eta_2(\omega,z)}{\partial z} = i\kappa(z)\eta_1^*(\omega,z)\exp(-i\Delta\beta z). \tag{50b}$$

By taking the derivative with respective to z of Eq. (49) twice and making use of Eq. (50) as well as $\eta_1'\eta_1^* + \eta_1\eta_1^{*\prime} + \eta_2'\eta_2^* + \eta_2\eta_2^{*\prime} = 0$, we obtain

$$\frac{d\langle|\tau_{\mathrm{MGD}}|^2\rangle}{dz} = 4i\Delta\beta'\langle\eta_1\eta_1'^* + \eta_2\eta_2'^*\rangle + 2\Delta\beta'^2 z, \tag{51a}$$

$$\frac{d^2\langle|\tau_{\mathrm{MGD}}|^2\rangle}{dz^2} = -4\Delta\beta'\exp(i\Delta\beta z)\langle\kappa^*(\eta_1\eta_2' - \eta_1'\eta_2\rangle + \text{c.c.} + 2\Delta\beta'^2. \tag{51b}$$

We assume that $\kappa(z)$ is a stationary random processing with an autocorrelation function

$$R(\xi) = \langle\kappa^*(z)\kappa(z-\xi)\rangle, \tag{52a}$$

with a correlation length of z_0 such that $R(\xi) = 0$ for $|\xi| > z_0$. As a result,

$$\frac{d^2\langle|\tau_{\mathrm{MGD}}|^2\rangle}{dz^2} = -2r_\tau\frac{d\langle|\tau_{\mathrm{MGD}}|^2\rangle}{dz} + 2\Delta\beta'^2, \tag{52b}$$

where

$$r_\tau = \int_{-\infty}^{\infty} R(\xi)\exp(-i\Delta\beta\xi)\mathrm{d}\xi. \tag{53}$$

The solution is given by

$$\langle|\tau_{\mathrm{MGD}}|^2\rangle = \frac{\Delta\beta'^2}{2r_\tau^2}[\exp(-2r_\tau z) - 1 + 2r_\tau z]. \tag{54}$$

In the limit of low mode coupling, $\lim_{r_\tau z\to 0}\langle|\Delta\tau|^2\rangle = \Delta\beta'^2 z^2$. However, in the limit of strong mode coupling,

$$\lim_{r_\tau z \gg 1} \langle |\tau_{\mathrm{MGD}}|^2 \rangle = \frac{\Delta\beta'^2 z}{r_\tau}. \tag{55}$$

Therefore in the limit of strong crosstalk, the MGD accumulates with the square root of the propagation distance. This phenomenon has been known since the 1980s [50]. This is the second reason that strong mode coupling is beneficial [26].

5.3d. Statistical Distribution of MGD

The above results are very useful to find the average values of MGD. But we must also find the high-order statistics so as to quantify the probability of achieving this average system performance. The complex transfer matrix, generalized for higher dimensions, can be decomposed using singular value decomposition (SVD) into a product of three matrices:

$$\bar{\bar{\boldsymbol{H}}}(\omega) = \bar{\bar{\boldsymbol{V}}}(\omega)\bar{\bar{\Lambda}}(\omega)\bar{\bar{\boldsymbol{U}}}^{\dagger}(\omega), \tag{56}$$

where $\bar{\bar{\Lambda}}(\omega)$ is a diagonal matrix of singular values of matrix $\bar{\bar{\boldsymbol{H}}}(\omega)$, and $\bar{\bar{\boldsymbol{V}}}(\omega)$ and $\bar{\bar{\boldsymbol{U}}}(\omega)$ are the left-singular and right-singular unitary matrices, which are dependent on frequency. If all singular values are nondegenerate, then SVD is unique. Assuming transmission losses of all fiber modes are compensated (the same), the complex transfer matrix $\bar{\bar{\boldsymbol{H}}}(\omega)$ is unitary (except for a constant factor). There exists a special decomposition, similar to SVD,

$$\bar{\bar{\boldsymbol{H}}}(\omega) = \bar{\bar{\boldsymbol{V}}} \cdot \bar{\bar{\Lambda}}(\omega) \cdot \bar{\bar{\boldsymbol{U}}}^{\dagger}, \tag{57}$$

such that $\bar{\bar{\boldsymbol{U}}}$ and $\bar{\bar{\boldsymbol{V}}}$ are independent of frequency to the first order. The column vectors $\bar{\boldsymbol{u}}_m$ of $\bar{\bar{\boldsymbol{U}}}$, representing the input principal modes of $\bar{\bar{\boldsymbol{H}}}(\omega)$, are the eigenvector of the group delay operator [Eq. (42)]

$$\bar{\bar{\boldsymbol{G}}}(\omega) = -i\frac{d\bar{\bar{\boldsymbol{H}}}^{\dagger}(\omega)}{d\omega} \cdot \bar{\bar{\boldsymbol{H}}}(\omega) \tag{58}$$

corresponding to an eigenvalue of τ_m. The column vectors $\bar{v}_m$ of $\bar{\bar{\boldsymbol{V}}}$, representing the output principal modes of $\bar{\bar{\boldsymbol{H}}}(\omega)$, are the eigenvector of the group delay operator corresponding to the same eigenvalue of τ_m, and

$$\bar{\bar{\Lambda}}(\omega) = \mathrm{diag}\{e^{-i\omega\tau_1}, \ldots, e^{-i\omega\tau_M}\}. \tag{59}$$

Fiber of any length can be described using the above model. We summarize the analysis in [51–54] in determining the statistics of MGD in the strongly coupled regime. Because mode coupling is random, the transfer matrix $\bar{\bar{\boldsymbol{H}}}(\omega)$ and thus the principal MGDs are also random. It is important to understand the statistics of MGD spread and its scaling law with propagation distance, since this determines the memory length of MIMO equalizations. It should be noted that mode coupling along the fiber is a random process with a certain correlation length. For propagation within the correlation length, the principal modes are correlated and the principal MGD increases linearly with propagation distance. We divide the fiber into K sections with length slightly greater than the correlation length, but much smaller than the total transmission distance. Each section is represented by a transfer matrix $\bar{\bar{\boldsymbol{H}}}_k(\omega)$:

$$\bar{\bar{\boldsymbol{H}}}_k(\omega) = \bar{\bar{\boldsymbol{V}}}_k \cdot \bar{\bar{\Lambda}}_k(\omega) \cdot \bar{\bar{\boldsymbol{U}}}_k{}^{\dagger}. \tag{60}$$

The matrix $\bar{\bar{\Lambda}}_k(\omega)$ and the input and output unitary matrices $\bar{\bar{\boldsymbol{U}}}_k$ and $\bar{\bar{\boldsymbol{V}}}_k$ are uncorrelated and statistically independent from section to section. Nevertheless, because the randomness is statistically identical from section to section, the statistics of group delay is the same for all sections. The overall transfer matrix is given by

$$\bar{\bar{\boldsymbol{H}}}(\omega) = \bar{\bar{\boldsymbol{H}}}_K(\omega) \cdot \bar{\bar{\boldsymbol{H}}}_{K-1}(\omega) \cdots \bar{\bar{\boldsymbol{H}}}_2(\omega) \cdot \bar{\bar{\boldsymbol{H}}}_1(\omega). \tag{61}$$

The corresponding group delay operator is given by

$$\begin{aligned}\bar{\bar{\boldsymbol{G}}} = -i\frac{d\bar{\bar{\boldsymbol{H}}}_1{}^{\dagger}}{d\omega} \cdot \bar{\bar{\boldsymbol{H}}}_1 + \bar{\bar{\boldsymbol{H}}}_1{}^{\dagger} \cdot \left(-i\frac{d\bar{\bar{\boldsymbol{H}}}_2{}^{\dagger}}{d\omega} \cdot \bar{\bar{\boldsymbol{H}}}_2\right) \cdot \bar{\bar{\boldsymbol{H}}}_1 + \bar{\bar{\boldsymbol{H}}}_1{}^{\dagger} \cdot \bar{\bar{\boldsymbol{H}}}_2{}^{\dagger} \\ \cdot \left(-i\frac{d\bar{\bar{\boldsymbol{H}}}_3{}^{\dagger}}{d\omega} \cdot \bar{\bar{\boldsymbol{H}}}_3\right) \cdot \bar{\bar{\boldsymbol{H}}}_2 \cdot \bar{\bar{\boldsymbol{H}}}_1 + \ldots.\end{aligned} \tag{62}$$

It can be seen that the resulting group delay operator is a summation of K random matrices. Therefore, the matrix elements of $\bar{\bar{\boldsymbol{G}}}$ are identically distributed Gaussian random variables for sufficiently large K in accordance with the central limit theorem. For the first matrix, $-i\frac{d\bar{\bar{\boldsymbol{H}}}_1{}^{\dagger}}{d\omega} \cdot \bar{\bar{\boldsymbol{H}}}_1 = \bar{\bar{\boldsymbol{U}}}_1 \mathrm{diag}\{\bar{\tau}_1\} \bar{\bar{\boldsymbol{U}}}_1{}^{\dagger}$, each element (i,j) has a variance $\frac{\sigma_\tau^2 D_s}{(D_s+1)(D_s+\delta_{ij}-1)}$. In fact, all the matrices are uncorrelated but statistically identical to the first matrix. Therefore, each element of $\bar{\bar{\boldsymbol{G}}}$ has a variance $\frac{K\sigma_\tau^2 D_s}{(D_s+1)(D_s+\delta_{ij}-1)}$. The group delay variance associated with $\bar{\bar{\boldsymbol{G}}}$ is then given by

$$\sigma_{gd}^2 = \frac{1}{D_s}\sum_m \langle \tau_m^2 \rangle = \frac{1}{D_s}\langle tr[\bar{\bar{\boldsymbol{G}}} \cdot \bar{\bar{\boldsymbol{G}}}^{\dagger}] \rangle = K\sigma_\tau^2. \tag{63}$$

The probability density function (pdf), as shown in Fig. 10, of the eigenvalue distribution for $\bar{\bar{\boldsymbol{G}}}$, which is a zero-trace Gaussian unitary ensemble [55], is

$$p_D(\tau) = \sqrt{\frac{D_s^2-1}{2\sigma_{gd}^2 D_s}} \cdot f_D\left(\sqrt{\frac{D_s^2-1}{2\sigma_{gd}^2 D_s}}\tau\right), \tag{64a}$$

where

$$f_D(x) = \frac{\exp(-D_s x^2/(D_s-1))}{\sqrt{\pi D_s(D_s-1)}} \times \sum_{m=0}^{D_s-1} \frac{1}{2^m m!} H_m^2\left(\frac{-t}{2\sqrt{D_s-1}}\right), \tag{64b}$$

where t^k should be replaced algebraically by the Hermite polynomial $H_k\left(\frac{D_s x}{\sqrt{D_s-1}}\right)$ in the evaluation of the summation in Eq. (64b). In the limit of a very large number of modes, the pdf approaches the well-known Wigner semicircle distribution with radius $\sqrt{2D_s}$.

Although an analytical expression is not available for the pdf of group delay spread (difference between the largest and smallest principal MGD), the

analytical expression for the pdf of group delay distribution, Eq. (64), can be used to numerically compute the statistics of the group delay spread. In the limit of a large number of modes, both the minimum and maximum group delays are given by two independent Tracy–Widom distributions [56]. The complementary cumulative probability function (cCPF) of group delay spread τ_{MGD} calculated based on the Tracy–Widom distribution is shown in Fig. 11.

Using the same random matrix approach, the mode-dependent loss (MDL) can also be studied. If $\bar{\bar{\boldsymbol{H}}}(\omega, z)$ is the transfer matrix for forward propagation, $\bar{\bar{\boldsymbol{H}}}^{\dagger}(\omega, z)$ then represents the transfer matrix backward from z to 0. Therefore, the eigenvectors of $\bar{\bar{\boldsymbol{H}}}^{\dagger}(\omega, z)\bar{\bar{\boldsymbol{H}}}(\omega, z)$ represent field distributions that are unchanged through round-trip propagation with the exception of a linear scaling factor, which corresponds the loss of the fiber. Therefore,

$$\bar{\bar{\boldsymbol{L}}} = \bar{\bar{\boldsymbol{H}}}^{\dagger}(\omega, z)\bar{\bar{\boldsymbol{H}}}(\omega, z) \tag{65}$$

can be defined as the *loss operator* [57,58], which is also a multiplication of two matrices, like the group delay operator. When decomposed as multiplication of transfer matrices from uncorrelated segments, $\bar{\bar{\boldsymbol{L}}}$ is also a Gaussian random matrix. Therefore, as expected, MDL also follows the same statistical distribution [Eq. (64)]. Let the eigenvalues of $\bar{\bar{\boldsymbol{L}}}$ be $\lambda_i = e^{-g_i}$. For systems with small MDL, the statistics of g_i are exactly the same as Eq. (64) for the MGD τ_i [58]. Moreover, MDL not only reduces but also scales with the square root of propagation distance with strong mode coupling. This is the third reason that strong mode coupling is beneficial [58,59]. The Stokes space formalism has been shown to provide a convenient description of MDL and its impact on system performance [60].

5.3e. Stokes-Space Description of MGD

The evolution of the transfer matrix $\bar{\bar{\boldsymbol{H}}}(\omega, z)$ in the direction of propagation, given by Eq. (46) for the case of two-mode coupling, can be generalized as

Figure 11

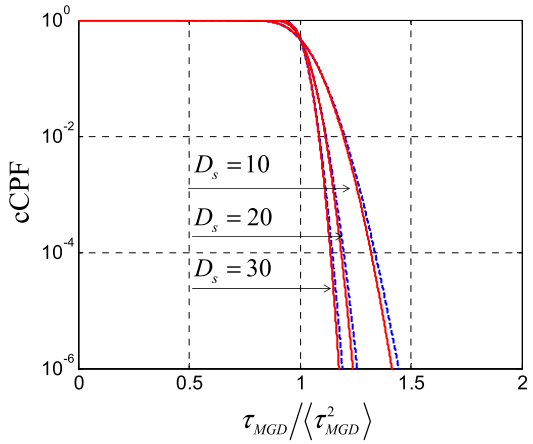

Complementary cumulative probability function (cCPF) of group delay spread τ_{MGD} for strongly coupled multimode fibers calculated using the Tracy–Widom approximation of random matrix theory (dotted lines) and the chi distribution in the Stokes space approach (solid lines).

$$\frac{\partial \bar{\bar{\boldsymbol{H}}}(\omega,z)}{\partial z} = i\bar{\bar{\boldsymbol{B}}}(\omega,z)\bar{\bar{\boldsymbol{H}}}(\omega,z). \tag{66}$$

Similarly, the frequency evolution can be generalized from Eq. (41) as

$$\frac{\partial \bar{\bar{\boldsymbol{H}}}(\omega,z)}{\partial \omega} = i\bar{\bar{\boldsymbol{T}}}(\omega,z)\bar{\bar{\boldsymbol{H}}}(\omega,z). \tag{67}$$

The Stokes space analysis of MGD presented here is a summary of [8,9]. When propagation losses are the same for all modes (no MDL), $\bar{\bar{\boldsymbol{H}}}(\omega,z)$, $\bar{\bar{\boldsymbol{B}}}(\omega,z)$ and $\bar{\bar{\boldsymbol{T}}}(\omega,z)$ are Hermitian matrices, which can be expanded as a superposition of a basis set consisting of the identity matrix and $4M^2-1$ zero-trace matrices satisfying the trace-orthogonal condition:

$$\frac{1}{2M} Tr\{\bar{\bar{\boldsymbol{\sigma}}}_i \cdot \bar{\bar{\boldsymbol{\sigma}}}_j\} = \delta_{ij}. \tag{68}$$

All matrices in the inner product space defined by Eq. (68) can be expanded using the basis set as

$$\bar{\bar{\boldsymbol{H}}}(\omega,z) = \frac{1}{2M}(\eta_0 \boldsymbol{I} + \bar{\eta}\cdot\underline{\underline{\boldsymbol{\sigma}}}), \tag{69a}$$

$$\bar{\bar{\boldsymbol{B}}}(\omega,z) = \frac{1}{2M}(\beta_0 \boldsymbol{I} + \bar{\beta}\cdot\underline{\underline{\boldsymbol{\sigma}}}), \tag{69b}$$

$$\bar{\bar{\boldsymbol{T}}}(\omega,z) = \frac{1}{2M}(\tau_0 \boldsymbol{I} + \bar{\tau}\cdot\underline{\underline{\boldsymbol{\sigma}}}), \tag{69c}$$

where $\underline{\underline{\boldsymbol{\sigma}}}$ is a vector of matrices $\bar{\bar{\boldsymbol{\sigma}}}_j$ and the dot product is defined as $\bar{\eta}\cdot\underline{\underline{\boldsymbol{\sigma}}} = \sum \eta_j \bar{\bar{\boldsymbol{\sigma}}}_j$. This is the generalization of polarization-mode dispersion ($M=1$) in which the basis set consists of the identity matrix and the three Pauli matrices [61]. Vectors $\bar{\eta}, \bar{\beta}, \bar{\tau}$ are called generalized Stokes vectors residing in the $(4M^2-1)$-dimensional space, which is referred to as the generalized Stokes space. By using the Stokes expansion, Eqs. (66) and (67) can be written as

$$\frac{\partial \bar{\bar{\boldsymbol{H}}}(\omega,z)}{\partial z} = \frac{i}{2M}(\beta_0 \boldsymbol{I} + \bar{\beta}\cdot\underline{\underline{\boldsymbol{\sigma}}})\cdot\bar{\bar{\boldsymbol{H}}}(\omega,z), \tag{70}$$

$$\frac{\partial \bar{\bar{\boldsymbol{H}}}(\omega,z)}{\partial \omega} = \frac{i}{2M}(\tau_0 \boldsymbol{I} + \bar{\tau}\cdot\underline{\underline{\boldsymbol{\sigma}}})\cdot\bar{\bar{\boldsymbol{H}}}(\omega,z). \tag{71}$$

Therefore, the group delay operator can be expressed as (z dependence dropped for simplicity)

$$\bar{\bar{\boldsymbol{G}}}(\omega) = -i\bar{\bar{\boldsymbol{H}}}^{\dagger}(\omega)\cdot\frac{d\bar{\bar{\boldsymbol{H}}}(\omega)}{d\omega} = \bar{\bar{\boldsymbol{H}}}^{\dagger}(\omega)\cdot\frac{1}{2M}(\tau_0 \boldsymbol{I} + \bar{\tau}\cdot\underline{\underline{\boldsymbol{\sigma}}})\cdot\bar{\bar{\boldsymbol{H}}}(\omega). \tag{72}$$

The vector $\bar{\tau}$ represents the expansion coefficients of the group delay operator, apart from a rotation by $\bar{\bar{\boldsymbol{H}}}(\omega,z)$, which does not change the length of $\bar{\tau}$, and

$$|\bar{\tau}|^2 = \frac{1}{2M} Tr\{[\bar{\tau}\cdot\underline{\underline{\boldsymbol{\sigma}}}]^2\} \tag{73}$$

can be used to characterize MGDs. The vector $\bar{\tau}$ can therefore be called the modal dispersion (MD) vector or *MD vector*, which is the generalization of the polarization-mode dispersion (PMD) vector.

From Eq. (70), it can be easily shown that for a fiber with infinitesimal length Δz, the transfer matrix is given by

$$\Delta\bar{\bar{\boldsymbol{H}}}(\omega, z) = \boldsymbol{I} + \frac{i}{2M}(\bar{\beta}\cdot\underline{\underline{\boldsymbol{\sigma}}})\Delta z. \tag{74}$$

Taking the derivative of Eq. (74) with respect to frequency yields

$$\frac{\partial\Delta\bar{\bar{\boldsymbol{H}}}(\omega, z)}{\partial\omega} = \frac{i}{2M}\left(\frac{\partial\bar{\beta}}{\partial\omega}\cdot\underline{\underline{\boldsymbol{\sigma}}}\right)\Delta z, \tag{75}$$

signifying that the MD vector of this infinitesimal length of fiber is

$$\Delta\bar{\tau} = \frac{\partial\bar{\beta}}{\partial\omega}\Delta z, \tag{76}$$

rotated by the matrix $\Delta\bar{\bar{\boldsymbol{H}}}(\omega, z)$. Therefore, the evolution of the MD vector is given by

$$\bar{\tau}(L) = \int_0^L \bar{\bar{\boldsymbol{R}}}(L, z)\cdot\frac{\partial\bar{\beta}}{\partial\omega}\mathrm{d}z, \tag{77}$$

where $\bar{\bar{\boldsymbol{R}}}(L, z)$ is the rotation matrix for the fiber extending from z to L. In real fibers, transfer matrix $\bar{\bar{\boldsymbol{H}}}(\omega, z)$ and MD vector $\bar{\tau}$ vary randomly along z. If we divide the fiber into pieces that are slightly longer than the correlation length but much shorter than the total fiber length, the evolution of the MD vector is a $(4M^2-1)$-dimensional random walk. Therefore, it is Gaussian distributed and its length $|\bar{\tau}|$ obeys a chi distribution with $4M^2-1$ degrees of freedom and the mean-squared length scales with propagation distance as $\langle|\bar{\tau}|^2\rangle = \zeta^2 z$, where $\langle\partial\bar{\beta}(z)/\partial\omega\cdot\partial\bar{\beta}(z')/\partial\omega\rangle = \zeta^2\delta(z-z\prime)$. Although length $|\bar{\tau}|$ cannot be directly translated into group delay spread in higher dimensions except for the simplest case of $M=1$ for PMD, it is still indicative of modal dispersion. The square-root scaling of MGD with length derived here by using the Stokes space model is the same as those obtained using the random matrix formulation in Section 5.3c.

The statistics of the MD vector spread is also not available analytically. It was found numerically that the group delay spread τ_{MGD} also follows the chi distribution [8], which agrees very well with those obtained from random matrix theory, as shown in Fig. 11 for comparison.

5.3f. Methods to Introduce Strong Mode Coupling

Mode coupling can exist randomly in fibers due to manufacturing imperfections as well as bending and twisting of the fibers. The strength of such random coupling may not be strong enough to realize the desired scaling of MGD spreading and MDL. Therefore, strong mode coupling may have to be introduced intentionally. Offset splicing [62,63] and grating couplers [64] have been suggested as means of introducing strong mode coupling. However, both methods will also introduce excess loss, especially implemented in a distributed fashion.

Supermode fibers have been shown to exhibit sublinear scaling of MGD with propagation distance [65]. To understand the possible reason for this, we will describe some details of the supermode fiber.

Consider a supermode fiber with three identical single-mode cores [Fig. 12(a_2)] each of radius a; the index difference between the core and cladding is Δ and core-to-core pitch is d. The interaction between the modes of the three individual cores can be described by the following coupled-mode equation [66,67]:

$$\frac{d}{dz}\begin{bmatrix} A_1 \\ A_2 \\ A_3 \end{bmatrix} = i\bar{\bar{M}}\begin{bmatrix} A_1 \\ A_2 \\ A_3 \end{bmatrix} = i\begin{bmatrix} \beta_0 & \kappa & \kappa \\ \kappa & \beta_0 & \kappa \\ \kappa & \kappa & \beta_0 \end{bmatrix}\begin{bmatrix} A_1 \\ A_2 \\ A_3 \end{bmatrix}, \tag{78}$$

where A_i is the complex amplitude of the electrical field of the ith core, β_0 is the propagation constant of the fundamental mode in the isolated core, and κ is the coupling coefficient between cores. Since $\bar{\bar{\bar{M}}}$ is Hermitian for a lossless system, it can be diagonalized by a unitary matrix such that $\bar{\bar{Q}}^{-1}\bar{\bar{M}}\,\bar{\bar{Q}} = \bar{\bar{\Lambda}}$, where $\bar{\bar{\Lambda}}$ is a diagonal matrix and the diagonal elements $\Lambda_{11} = \beta_0 + 2\kappa$ and $\Lambda_{22} = \Lambda_{33} = \beta_0 - \kappa$ are the propagation constants of the three supermodes so that supermode amplitudes $\bar{B} = \bar{\bar{\bar{Q}}}^{-1}\bar{A}$ evolve as $d\bar{B}/dz = i\bar{\bar{\Lambda}}\,\bar{B}$.

Figure 12 illustrates the mode profiles of the three supermodes. Since they are superpositions of the modes of individual cores, their intensity profiles are strongly correlated. Therefore, if the index distribution in the fiber cross section deviates from ideal uniform distribution, the modes will couple to each other, as shown in Eq. (78).

In some sense, the supermode fiber can be considered another way of designing FMFs. There are some immediate advantages of using the supermode structure, as well. First, since the transformation matrix from the uncoupled modes to the supermodes is unitary, coupling from the isolated cores to the supermode fiber is lossless and therefore must be without MDL. Second, the effective areas of these supermodes are larger than the corresponding step-index FMFs for the same bending loss [67]. Another advantage is that the supermode structure allows more degrees of freedom to provide the desired propagation characteristics. The supermode fiber can tune the effective index difference and DMGD by changing the geometrical parameters and the indices of the core and cladding. Both low DMGD and strong crosstalk are beneficial for MIMO processing.

5.4. Multicore Fiber

Another technique to reduce computation load for mode crosstalk equalization is actually to "divide and conquer." Take, for example, an SDM system with six

Figure 12

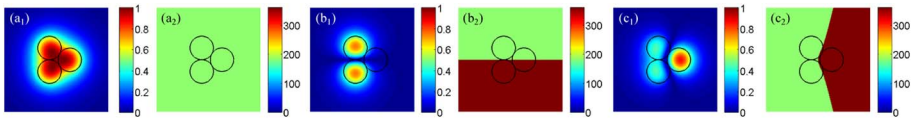

Amplitude (x1) and phase (x2) of mode profiles of supermodes in a three-core supermode fiber: (a) the fundamental supermode, and (b) and (c) the degenerate pair of supermodes.

channels. If it is implemented as a mode-division multiplexed system using a six-mode FMF, the crosstalk matrix has 36 entries. In contrast, if the six channels are divided into two cores of three modes each, then the crosstalk matrix has 18 entries. SDM using few-mode multicore fibers (FM-MCFs) reduces the DSP computation complexity by a factor equal to the number of cores. For a 10-core fiber, DSP complexity can reduce by a factor of 10. Even though MCFs have applications in data communications with core multiplexing [68–71], one of the primary reasons that MCFs will be useful in long-haul SDM is to reduce DSP complexity [72,73]. The reasons are (1) single-mode MCFs do not have a clear and significant advantage over SMF bundles, and (2) to ensure low crosstalk and large effective area [74–76] within a cladding diameter of 250 μm restricted by the mechanical properties of silica, the number of cores within an MCF is limited to about 20.

Based on the reasons above, the key performance metric for MCF in SDM is core-to-core crosstalk. The mechanism of core-to-core crosstalk is resonant tunneling, such as what occurs in directional couplers. Therefore, intuitively, one might expect that an effective way to suppress crosstalk is to destroy the resonance condition, i.e., the phase-matching condition, using heterogeneous MCF in which the diameters of cores are different from each other. It turned out that many heterogeneous MCFs fabricated had crosstalk levels much higher than theoretical predictions, while homogeneous MCFs had crosstalk levels lower than theoretical predictions. The reason is that heterogeneous MCFs have the lowest crosstalk when they are perfectly straight. As soon as the MCFs are bent or twisted, the phase-matching condition is improved. What happens in homogeneous MCFs is exactly the opposite; any bending or twisting would destroy the phase-matching condition. Since bending and twisting cannot be avoided in real fibers, homogeneous MCFs appear to be a better candidate for low core-to-core crosstalk.

Crosstalk performance of MCFs must therefore consider the effects of fiber bending and twisting. Bend-induced index perturbation can be of the order of 10^{-6}–10^{-3}. This provides the sufficient condition for bends to create or break the phase-matching condition for either heterogeneous or homogeneous MCFs. A fiber with bending alone can be equivalently viewed as a straight one with a skewed index profile induced by the bend. Fiber twist along the propagation direction, in addition, causes a periodic change of bend orientation. The effect of twisting on an already bent fiber can be modeled as if the fiber cross section rotates at the speed of twist [77,78]. Therefore bend- and twist-induced fiber indices can use the equivalent index model described by

$$n_{eq}(r, \theta, R_b) = n \cdot \left(1 + \frac{r \cos \theta}{R_b}\right), \tag{79}$$

where n is the original index without bend and twist, r is the distance from the center of the MCF to the core of interest, and $\theta = \chi z$ is the orientation of the core with respect to the bend axis due to twisting with twist rate χ. Each core is assumed to be adequately small so that the index profile of any core is still uniform under bending and twisting.

Because bending and twisting are random processes, the calculation of MCF crosstalk is quite involved. We start from the reduced coupled-mode theory with symmetric mode-coupling coefficients [79]:

$$\frac{d\boldsymbol{A}_p}{dz} = -j\sum_{q\neq p} K_{pq}\boldsymbol{A}_q(z)\exp(-j\Delta\beta'_{pq}z)f(z), \tag{80}$$

where p, q represent two different core p and q, K_{pq} is the average value of coupling coefficients κ_{pq} and, κ_{qp} which are symmetric in MCFs with the same loss $\kappa_{pq} = \kappa_{qp}$, and $\Delta\beta'_{pq}$ is the difference between the effective propagation constants of core p and q with the effects of bending and twisting:

$$\Delta\beta'_{pq} = \beta_p - \beta_q + \frac{|\beta_p\vec{r}_p - \beta_q\vec{r}_q|}{R_b}\cos(\chi z + \theta_{pq}). \tag{81}$$

Using the equivalent-index model described by Eq. (79), $\beta_{p,q}$ and $\vec{r}_{p,q}$ are the propagation constants and position vectors of core p and q of the straight fiber, $\theta_{pq} = \measuredangle(\beta_p\vec{r}_p - \beta_q\vec{r}_q)$ at $z = 0$ [79], and $f(z)$ is a function describing random fluctuation of bending and twisting in the longitudinal direction. Accordingly, the average crosstalk increment in power within a small segment $[z_1, z_2]$ can be written as

$$\begin{aligned}\Delta X_{pq} = \left\langle\left|\frac{\Delta A_p}{A_q}\right|^2\right\rangle &= K_{pq}^2\int_{z_1}^{z_2}\int_{z_1}^{z_2}\exp[-j\Delta\beta'_{pq}(z-z')]\cdot\langle f(z)\cdot f^*(z')\rangle \mathrm{d}z\mathrm{d}z' \\ &= K_{pq}^2\int_{z_1}^{z_2}\int_{z_1-z'}^{z_2-z'}\exp[-j\Delta\beta'_{pq}\xi]\cdot\langle f(z'+\xi)\cdot f^*(z')\rangle \mathrm{d}\xi\mathrm{d}z'.\end{aligned} \tag{82}$$

Since $f(z)$ can be considered a stationary random process, it has an autocorrelation function $R(\xi) = \langle f(z'+\xi)\cdot f^*(z')\rangle$ where $R(0) = 1$. Once $R(\xi)$ is substituted into Eq. (82), a simpler form yields according to the Wiener–Khinchin theorem

$$\Delta X_{pq} = K_{pq}^2\int_{z_1}^{z_2}\mathrm{d}z'\int_{-\infty}^{+\infty}\exp[-j\Delta\beta'_{pq}\xi]\cdot R(\xi)\mathrm{d}\xi = K_{pq}^2\cdot\Delta z\cdot S(\Delta\beta'_{pq}), \tag{83}$$

where $S(\Delta\beta'_{pq})$ represents the power spectral density of f. It is found that the exponential autocorrelation function $R(\xi) = \exp(-|\xi|/l_c)$, where l_c is the correlation length, can satisfactorily describe the randomness of MCF bending and twisting. Therefore, using the expression for $\Delta\beta'_{pq}$ in Eq. (81), the local power coupling coefficient $h_{pq}(z) = \Delta X_{pq}/\Delta z$ can be derived as

$$h_{pq}(z) = \frac{2K_{pq}^2 l_c}{1 + \Delta\beta'^2_{pq}(z)\cdot l_c^2}, \tag{84}$$

which is applicable to both homogeneous and heterogeneous MCFs. The average power coupling coefficient $\langle h_{pq}\rangle$ can thus be obtained. Following [80], by averaging Eq. (84) over a twist pitch, using the expression for $\Delta\beta'_{pq}$ in Eq. (81),

$$\langle h_{pq}\rangle = \frac{\gamma}{2\pi}\int_0^{2\pi/\gamma} h_{pq}(z)\mathrm{d}z = 2K_{pq}^2 l_c\left[\frac{1}{\sqrt{a_+(b+\sqrt{a_+a_-})}} + \frac{1}{\sqrt{a_-(b+\sqrt{a_+a_-})}}\right], \tag{85}$$

which is independent of the twist rate, and

$$a_{\pm} = 1 + l_c^2[(\beta_p - \beta_q) \pm |\beta_p \vec{r}_p - \beta_q \vec{r}_q|/R_b]^2, \tag{86a}$$

$$b = 1 + l_c^2(\beta_p - \beta_q) - l_c^2[|\beta_p \vec{r}_p - \beta_q \vec{r}_q|/R_b]^2. \tag{86b}$$

Consequently, according to coupled-power theory, the crosstalk after propagation length L can be easily obtained as

$$XT_{pq} = \tanh(\langle h_{pq} \rangle L), \tag{87}$$

which can be simplified as $XT_{pq} \approx \langle h_{pq} \rangle L$ for low-level crosstalk.

For homogenous MCFs where all the cores are designed to be identical, $\beta_p = \beta_q = \beta$, crosstalk between two adjacent cores can be further simplified according to Eqs. (79) and (85)–(87) as

$$XT = 2K_{pq}^2 l_c \frac{1}{\sqrt{1 + l_c^2[\beta|\vec{r}_p - \vec{r}_q|/R_b]^2}} L. \tag{88}$$

In the limit of very small bending radius or large bending curvature,

$$XT = 2\frac{K_{pq}^2 R_b}{\beta \Lambda} L, \tag{89}$$

where Λ is the distance between two adjacent cores (i.e., core pitch). From Eq. (89), we arrive at the following conclusions for homogeneous MCFs. First, crosstalk accumulation is linear with respect to fiber length and bending radius. Second, crosstalk suppression requires increased core pitch, which unfortunately decreases the core density, and/or reduced coupling coefficient between adjacent cores. Methods for reducing the coupling coefficients include trench-assisted [81,82] and hole-assisted structures [83,84], as shown in Figs. 13(a) and 13(b). A low-crosstalk FM-MCF was first reported in [72,85,86]. Recent progress in FM-MCFs include both fibers themselves [84,87–90] and SDM transmission using these fibers [91]. Crosstalk in MCF can be measured using multichannel optical time-domain reflectometer [92].

Crosstalk of heterogeneous MCFs at a certain bending radius can be calculated accurately using Eqs. (85)–(87) [82]. The local power coupling coefficient [Eq. (85)] is inversely proportional to the square of the effective propagation constant difference, which reduces to zero at a specific bending radius. Therefore, crosstalk in heterogeneous MCFs first rises with bending curvature, reaches a peak at certain bending curvature or radius R_{pk}, then drops rapidly with bending curvature. This value of R_{pk} can be calculated from Eq. (85) using Eq. (1), corresponding to zero effective propagation constant difference:

$$R_{pk} = \frac{|\beta_p \vec{r}_p - \beta_q \vec{r}_q|}{(\beta_p - \beta_q)} \approx \frac{n_{\text{eff}} \Lambda}{\Delta n_{\text{eff}}}, \tag{90}$$

where n_{eff} and Δn_{eff} are the effective index of one core and the effective index difference between two cores, respectively. Therefore, a practical way of managing crosstalk in heterogeneous MCFs is to reduce R_{pk} so that the bending radius in real fibers is always greater than R_{pk} [93,94]. From

Eq. (90), $R_{pk} = 50$ mm can be obtained by a large Δn_{eff} of about 0.001 as well as a decreased core pitch <40 μm.

5.5. Experimental Characterization of MGD

A multimode fiber is inherently a multipath channel, and once modes are superimposed, a multimode fiber becomes an interferometric device. Mode beating resulting from such interference, which is an obstacle for MDM, can be exploited to characterize properties of FMFs, including mode profiles and modal dispersion.

Let us use a two-mode (group) fiber of length L as an example. If both modes are excited at the beginning so that the input field is

$$E(x,y,0,t) = [A_{01}\psi_{01}(x,y) + A_{11}\psi_{11}(x,y)]e^{-i\omega t}, \tag{91}$$

the output field at the end of the fiber is given by

$$E(x,y,z=L,t) = [A_{01}\psi_{01}(x,y)e^{i\beta_{01}L} + A_{11}\psi_{11}(x,y)e^{i\beta_{11}L}]e^{-i\omega t}, \tag{92}$$

and the output intensity is given by

$$I(x,y,z=L,\omega) = I_{01}|\psi_{01}(x,y)|^2 + I_{11}|\psi_{11}(x,y)|^2 + 2\,\mathrm{Re}\{A_{01}A_{11}^*\psi_{01}(x,y)\psi_{11}^*(x,y)e^{i[\beta_{11}(\omega)-\beta_{01}(\omega)]L}\}. \tag{93}$$

The input and output powers, being integral of the intensity and by virtue of the orthogonality of modes, are conserved. Nevertheless, the output intensity at any point on the fiber transverse plane contains the inference of the two modes. Furthermore, this interference is frequency dependent, even if the input intensity is frequency independent [95]:

$$I(x,y,z=L,\omega+\Omega) = I_{01}|\psi_{01}(x,y)|^2 + I_{11}|\psi_{11}(x,y)|^2 + 2\,\mathrm{Re}\{A_{01}A_{11}^*\psi_{01}(x,y)\psi_{11}^*(x,y)e^{i[\beta_{11}(\omega)-\beta_{01}(\omega)]L}e^{i(\beta'_{11}-\beta'_{01})\Omega L}\}, \tag{94}$$

which can be simplified as

Figure 13

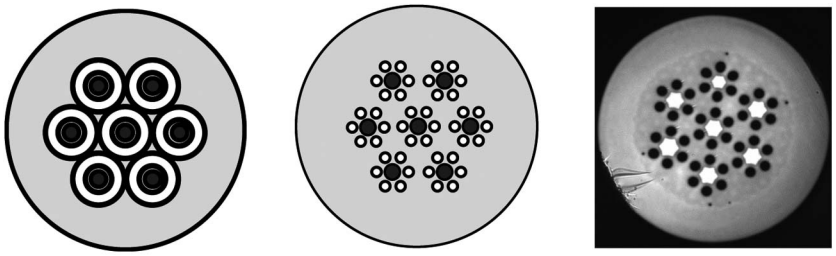

(a) (b) (c)

Schematic cross sections of (a) trench- and (b) hole-assisted MCFs, and (c) the cross section of a hole-assisted FM-MCF reported in [72]. Reprinted from C. Xia *et al.*, IEEE Photon. Technol. Lett. **24**, 1914–1917 (2012).

$$I(x,y,z=L,\omega+\Omega) = I_{01}|\psi_{01}(x,y)|^2 + I_{11}|\psi_{11}(x,y)|^2 + 2\,\mathrm{Re}\{A_{01}A_{11}^{*}\psi_{01}(x,y)\psi_{11}^{*}(x,y)\}\cos(\Delta\phi_{11})\cos(\Omega\cdot\Delta\tau_{11}), \tag{95}$$

where $\Omega \ll \omega$, $\Delta\phi_{11}$ is the differential phase and $\Delta\tau_{11} = \beta'_{11}L - \beta'_{01}L$ is the MGD between these two modes. Therefore, by measuring the oscillation period of the output spectrum at a fixed point (x,y), the MGD can be obtained. In practice, the intensity contained at a fixed point is low, so it is better to integrate over a fractional area of the fiber cross section. This is typically done by connecting with a SMF at the end of the FMF under test. The input fiber contains the amplified spontaneous emission (ASE) source and is offset from the FMF to excite both modes. The output SMF also is offset to collect both modes.

For fibers with more than two modes, the number of beat tones increases quadratically with the number of modes, making it impossible to uniquely determine the DMGDs between the modes. However, it is possible to slightly modify the input condition to reduce the number of significant beat tones. This can be accomplished by exciting one of the modes to be much stronger than all other modes at the input. By doing so, the interference between the dominant mode and weaker modes eclipses the interference among weaker modes. Assuming LP_{01} is the dominant mode, the output intensity is given by

$$I(x,y,z=L,\omega+\Omega) = I_{01}|\psi_{01}(x,y)|^2 + \sum_{m,n} 2\,\mathrm{Re}\{A_{01}A_{mn}^{*}\psi_{01}(x,y)\psi_{mn}^{*}(x,y)\} \times \cos(\Delta\phi_{mn})\cos(\Omega\cdot\Delta\tau_{mn}), \tag{96}$$

where beating among nondominant modes can be safely neglected. Taking the Fourier transform of the intensity spectrum at a fixed point (x,y), the peaks will be found at $\Delta\tau_{mn}$, revealing the MGDs referenced to the dominant mode. The spectral resolution of the interference pattern determines the maximum group delay that can be measured, and the bandwidth of the interference pattern determines the resolution of the group delay measurement.

A more powerful characterization method, S^2 imaging, can be obtained if the output intensity is resolved both spectrally, as discussed above, and spatially [96–98]. Such a measurement can be done using an ASE source to excite the required modal content and scanning the output spectrum using an optical spectrum analyzer (OSA) point by point in the transverse plane at the output. Alternatively, one can use a tunable laser to excite the required modal content and use a CCD to acquire images of output intensity as the laser wavelength is tuned, as shown in Fig. 14(a) [99]. Because OSAs have a large dynamic range but laser tuning is faster than point-to-point image scanning, the former is more accurate and the latter is faster. This spatially and spectrally resolved measurement will not only characterize the MGD, as shown in Fig. 14(b), but also the complex mode profile. The spatially varying amplitude of the DC component of Eq. (96) yields $|\psi_{01}(x,y)|^2$, and, by virtue of the fact that the mode field is all in phase, the mode profile of $\psi_{01}(x,y)$ can be obtained independent of all other modes, as shown in Fig. 14(b). The spatially varying amplitude of each component at $\Delta\tau_{mm}$ yields $\psi_{01}(x,y)\psi_{mn}^{*}(x,y)$, and with $\psi_{01}(x,y)$ already determined, the mode profile $\psi_{mn}(x,y)$ can be obtained.

Figure 14

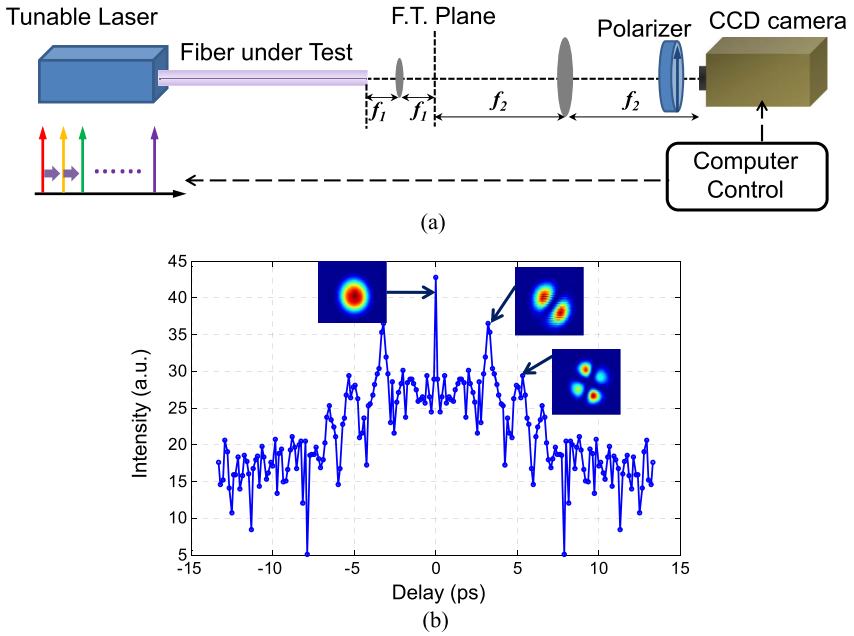

(a) Schematic of S^2 imaging using a tunable laser and a CCD camera. (b) Representative modal delay versus spectral intensity and the corresponding mode profile at the spectral peaks.

Before moving on to the next section on components, it is worth noting that all of the optical techniques for reducing mode equalization DSP complexity, except DMDG compensation, can be combined. Reducing DMDG, strong mode coupling, and MCF all have the potential to reduce DSP complexity by 1 order of magnitude or more. The combination of these optical techniques and FDE should solve the critical challenge of mode crosstalk for SDM.

6. Components for SDM

SDM will need a class of passive and active devices that are analogous to their counterparts in WDM. They include fiber input/output [100–103], connection [104–106], and mode conversion [107–109], as well as what we will focus on in this paper, mode (de)multiplexers and SDM amplifiers.

6.1. Passive Components: Mode (de)Multiplexers

Mode-division multiplexers are key components required for MDM. Mode conversion in combination with passive combining, as shown in Fig. 15, was used in early-stage MDM experiments.

Mode conversion can be achieved using fixed phase plates [110], tunable spatial light modulators, or liquid crystal on silicon (LCoS) panels [110,111]. Phase plates are thin glass plates with prescribed spatial distributions of refractive index or thickness, capable of transforming an LP_{01} mode to higher order modes. As shown in Fig. 15, a signal beam is first collimated using a lens, and then passes through the phase plate. The phase structure of the phase plate matches the spatial phase distribution of the desired mode profile. Because the fiber mode

profile is similar to its Fourier transform, the phase plate can be placed at either the image plane or the Fourier plane of the lens system [112]. The disadvantage of the conversion-plus-combination type of multiplexers is that multiplexing loss will be inevitably high because of passive combining loss (dashed arrows). The theoretical minimal insertion loss of a three-mode multiplexer in Fig. 15 is 5.5 dB with optimized splitting ratios for the beam splitters.

In what follows, we describe low-loss mode (de)multiplexers, and they fall into two categories based on the mechanism of (de)multiplexers. The first category is based on matching the transverse field profile of excitation to that of the fiber modes, into which the conversion-plus-combination falls, although not with low loss. The second category is based on matching the longitudinal propagation constant of the excitation to that of the fiber mode. The metric for all passive components including (de)multiplexers is insertion loss (IL) and MDL [113]:

$$\mathrm{IL} = \left(\frac{1}{N}\sum_{n=1}^{N}|\lambda_n|^2\right), \tag{97a}$$

$$\mathrm{MDL} = \frac{\max\{|\lambda_n|^2\}}{\min\{|\lambda_n|^2\}}, \tag{97b}$$

where $\{\lambda_n\}$ are singular values of input–output coupling matrix $\bar{\bar{C}}_S$, which can be obtained by SVD.

Another potential method is the use of holograms [114–116]. The holographic method is theoretically possible [117,118] but hard to implement because volume holographic materials at the telecommunication wavelengths are not currently available and phase-only holograms suffer from losses and crosstalk.

6.1a. (de)Multiplexers Based on Matching Transverse Mode Profiles

The first category is based on matching the transverse field profile of excitation to that of the fiber modes.

Spot-Based (de)Multiplexer

Unlike the conversion-plus-combination type of multiplexer, which maps each SMF directly to each spatial mode, the spot-based multiplexer sparsely matches the complex profile of each mode to a group of SMFs. The spot-based

Figure 15

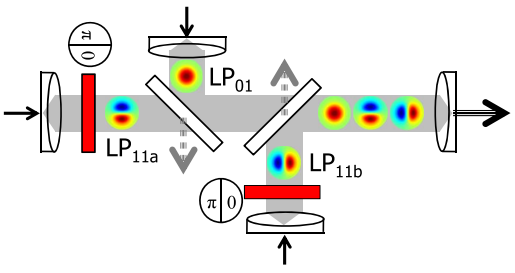

Mode-division multiplexer based on mode conversion in combination with passive combining. A demultiplexer is simply a multiplexer in reverse.

(de)multiplexer improves the insertion loss by avoiding the passive combining loss of beam splitters [119]. From simply dimensionality or degrees of freedom considerations, the minimum number of fibers needed for a spot-based multiplexer equals the number of fiber modes. Take the case of a FMF supporting two mode groups with three spatial modes, for example: three SMFs are imaged onto the facet of the FMF. The FMF mode profiles can be sparsely synthesized using three SMFs, as shown in Fig. 16. Conversely, if the FMF modes were sparsely sampled, the output in the three SMFs will be as shown in Fig. 16. Fiber arrangements for multiplexing more LP modes can be found in [113].

Mathematically, the coupler can be represented by a matrix transformation, $\bar{\bar{C}}_S$, between the field amplitudes, $\bar{A}_S$, in the SMF spots and the field amplitudes, $\bar{A}_{\mathrm{LP}}$, of the LP mode as

$$\bar{A}_{\mathrm{LP}} = \bar{\bar{C}}_S \cdot \bar{A}_S. \tag{98}$$

Each element $c_{k,l}$ of $\bar{\bar{C}}_S$ can be obtained by evaluating the overlap integral

$$c_{k,l} = \iint s_l(x,y)\psi^*_{pq}(x,y)\mathrm{d}x\mathrm{d}y, \tag{99}$$

where $s_l(x,y)$ and $\psi^*_{pq}(x,y)$ are normalized complex optical fields of the lth spot and the LP mode in the FMF. Because the sparsely synthesized field profiles are not exactly matched to those of the LP modes, the spot-based multiplexer will have insertion losses, although much smaller than the conversion-plus-combination multiplexer. With appropriately chosen beam diameter and separation, the insertion loss of a three-mode spot multiplexer can be as low as 2 dB, a 3.5 dB improvement over a conversion-plus-combination multiplexer. Because some modes (e.g., LP_{01}) are better matched other modes (e.g., LP_{11b}), the insertion losses will be mode dependent.

Photonic Lantern

The photonic lantern (PL) is the integrated-optics embodiment of the spot coupler [120,121]. The difference between the spot-based (de)multiplexer and the PL is the addition of an adiabatic transition region, necessarily formed in the guided-wave platform, between the SMFs (spots) and the FMF [121–123]. The mismatch between the transverse fields synthesized by sparse spots and the mode profiles of the FMF is eliminated by bridging the differences slowly in the adiabatic transition region. When the transition region is adiabatic, the transverse field is first almost losslessly transformed into supermodes of a three-coupled-core fiber and then into the mode profile of the FMF, as shown in Fig 17.

The PL thus has the potential of lossless multiplexing and low MDL. Ideally, the symmetric three-mode PL has a coupling matrix given by

$$\bar{\bar{C}} = \begin{bmatrix} 1/\sqrt{3} & 1/\sqrt{3} & 1/\sqrt{3} \\ \sqrt{2/3} & -1/\sqrt{6} & -1/\sqrt{6} \\ 0 & 1/\sqrt{2} & -1/\sqrt{2} \end{bmatrix}, \tag{100}$$

which is unitary.

PLs can be symmetric, mode-group-selective, and mode-selective. The input fibers for a symmetric PL multiplexer are identical, and thus signals in the input fibers resonantly couple to each other in the adiabatic taper region so that one

Figure 16

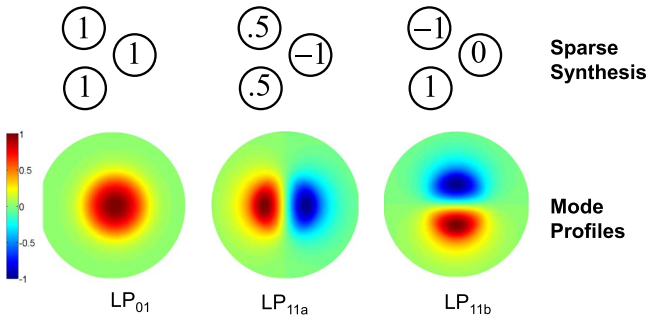

Schematic representation of sparse synthesis of modes in a two-mode group fiber using three SMFs or spots.

input signal is coupled to more than one mode group of the output FMF. It is possible to make the PLs mode(-group)-selective; that is, each fiber excites only one mode (group), which can be accomplished using dissimilar input fibers [124,125]. When symmetric PL (de)multiplexers are used, MIMO signal processing for SDM is necessary. Conversely, mode(-group)-selective PL (de)multiplexers can be used in certain SDM systems to reduce the complexity of or eliminate the need for MIMO signal processing.

6.1b. (de)Multiplexing Based on Matching Propagation Constants

The second category of mode multiplexing technique is based on longitudinal propagation constant matching of modes. It is well known that fiber-based directional couplers can couple the fundamental mode of a SMF to a high-order mode of a MMF if the propagation constants of the two modes are substantially the same [126–128]. This coupling process can be almost lossless and by repeated coupling to high-order modes, all mode orders can be excited in a MMF to carry information. However, most high-order modes are degenerate, and that independent excitation of degenerate modes is a challenge using fiber-based directional couplers. One proposed way of realizing independent excitation of degenerate modes using fiber-based directional couplers is to make the multimode fiber elliptical rather than circular [129,130]. However, elliptical fibers are not compatible with the circular MMFs used for optical transmission. Here, we present a method for multiplexing and demultiplexing degenerate modes using structured directional coupler pairs composed of only circular fibers [131,132].

The configuration of the structured directional coupler is illustrated Fig. 18(a). For simplicity, we assume the fibers are step-index fibers. The multimode fiber has core and cladding radii of a_1 and r_1, respectively. The two SMFs have core and cladding radii of a_2 (a_3) and r_2 (r_3), respectively, and length of L_2 (L_3). The orientations of the fibers are such that the angle subtended by the lines from the center of the MMF to the centers of the SMFs is φ. We use the multiplexing of the lowest order degenerate LP_{11a} (vertically oriented) and LP_{11b} (horizontally oriented) modes as an example. Multiplexing of higher order degenerate modes will be similar. If we assume that propagation constants of the LP_{11a} and LP_{11b} modes and that of the fundamental mode of each of the SMFs are the same and SMF 2 is vertically above the MMF, the coupled-wave equations for the amplitudes of the four modes are given by

Figure 17

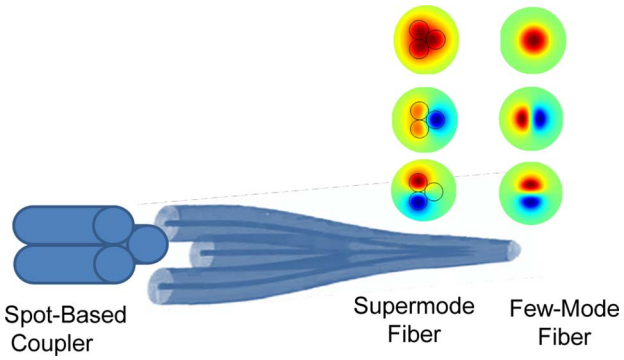

Schematic of the PL. The spot coupler of Fig. 15 is connected to the FMF via an adiabatic transition region, rather than using imaging optics. Supermodes are formed in the middle of the transition region.

$$\frac{d}{dz}\begin{bmatrix} A_2 \\ A_{11a} \\ A_{11b} \\ A_3 \end{bmatrix} = -j\begin{bmatrix} \beta & \kappa & 0 & 0 \\ \kappa & \beta & 0 & \kappa\cdot\cos\varphi \\ 0 & 0 & \beta & \kappa\cdot\sin\varphi \\ 0 & \kappa\cdot\cos\varphi & \kappa\cdot\sin\varphi & \beta \end{bmatrix}\begin{bmatrix} A_2 \\ A_{11a} \\ A_{11b} \\ A_3 \end{bmatrix}, \tag{101}$$

where $\kappa = \omega\varepsilon_0 \int_{-\infty}^{+\infty}\int_{-\infty}^{+\infty}(N^2 - N_2^2)\vec{E}_{11a}^{*}\vec{E}_2 \mathrm{d}x\mathrm{d}y / \int_{-\infty}^{+\infty}\int_{-\infty}^{+\infty}\hat{z}(\vec{E}_{11a}^{*}\times H_2 + \vec{E}_{11a}\times\vec{H}_2^{*})\mathrm{d}x\mathrm{d}y$ are the coupling coefficients in which N, N_2 are the total refractive index distributions of both MMF and SMF 2 or 3 and the indices of SMF 2 or 3 only, respectively, and $\hat{z}$ is the unit vector in the z direction. Since the length of these couplers is usually of the order a few centimeters, the degenerate modes LP_{11a} and LP_{11b} should have negligible coupling with each other and hence preserve their orientations. We have also assumed that because of the extended core-to-core distance, waves in the two SMFs do not couple to each other. The angular dependence of the coupling coefficients in Eq. (101) come from the selection rule due to the overlapping integral between the modes in the two fibers. The propagation constant is only the necessary condition for coupling; nonzero overlapping ensures energy exchange between modes in the two fibers. The degenerate modes LP_{11a} and LP_{11b} are orthogonal to each other and have a 180° rotational symmetry. As a result, for the special case of $\varphi = 90°$, $\kappa\cos\varphi = 0$. In this case, the SMFs are positioned in a way such that SMF 2 couples only to LP_{11a} and SMF 3 couples only to the LP_{11b}. Therefore, the signals in the two SMFs connected to two independent single-mode transmitters will be coupled to the two degenerate modes LP_{11a} and LP_{11b}. In the most ideal case, this coupling will be lossless and without crosstalk. It is not necessary for coupling regions between fiber 1 and fibers 2 and 3 to be lined up in the direction of propagation. As long as the separation between the two coupling regions is small so that the mode LP_{11a} in fiber 1 excited by fiber 2 has not rotated due to fiber imperfections, bending, twisting, and so on, fiber 3 can be translated (forward or backward) along the propagation direction to excite the other degenerate mode LP_{11b}, provided that its angular position with respect to fiber 2 is unchanged. Figure 18(b) shows the evolution of the magnitude of the field at several distances in the coupling reason for in-phase, out-of-phase, and quadrature excitation, clearly demonstrating the ability to generate any state of the modes within the LP_{11} group.

Figure 18

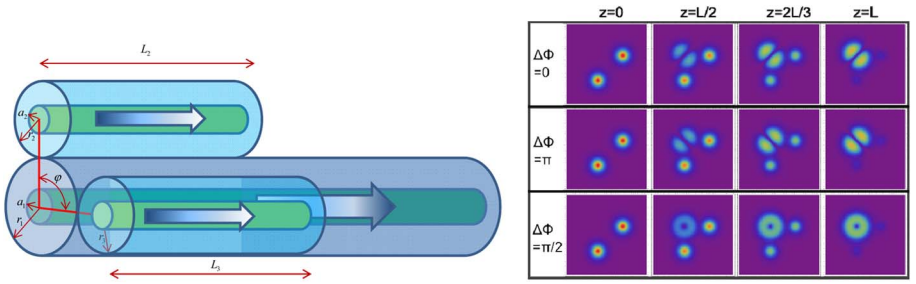

(a) (b)

(a) Example of a structured directional coupler for degenerate mode multiplexing. The larger fiber is a MMF, and two small fibers are SMFs. Fiber 1 is a MMF, and fibers 2 and 3 are SMFs. (b) Evolution of the magnitude of the field at several distances in the coupling region for in-phase, out-of-phase, and quadrature excitation [131]. Copyright 2013, Optical Society of America.

Generally, for higher-order degenerate modes LP_{mna} and LP_{mnb}, they are orthogonal and have a $(180/m)°$ rotational symmetry. When $\varphi = (90/m)°$, single-mode core 2 couples only to LP_{mna} and single-mode core 3 couples only to LP_{mnb}. This is also the case when $\varphi = 90° \pm (90/m)°$, $\varphi = 180° \pm (180/m)°$, and $\varphi = 270° \pm (270/m)°$. Using the structured directional coupler pairs (for degenerate modes) and regular directional couplers (for other modes) in cascade, MDMs, in which all the modes that are supported by the MMF can be excited from the SMFs, can be realized. Since light propagation satisfies reciprocity, the structured directional coupler pair can also be used as a mode-division demultiplexer into degenerate mode basis sets defined by the orientation of the SMFs.

Mode (de)multiplexers using symmetric directional couplers (both fibers are identical FMFs) are possible, although it cannot in general be lossless because the phase-matching condition is satisfied for all the modes [133]. These losses can be reduced by exploiting different evanescent rates of modes [134].

6.2. Active Components: Few-Mode and Multicore Fiber Amplifiers

In optical fiber communication systems, amplifiers are essential to compensate the loss of the transmission link. The technology breakthrough in erbium-doped fiber amplifiers (EDFAs) was the key enabler for WDM. For SDM systems, an integrated, broadband, and energy-efficient amplifier is highly desirable for long-distance SDM transmission. Here we discuss few-mode EDFAs, Raman amplifiers, and bulk amplifiers. Details of few-mode parametric amplifiers can be found [135,136].

6.2a. Few-Mode EDFA

A compatible amplification solution for MDM transmission in FMF is few-mode EDFA (FM-EDFA). The previous study on FM-EDFA focused on high-power laser/amplifiers [137] in which only the fundamental mode is amplified and high-order modes are suppressed. For an FM-EDFA used in MDM, signals contained in all modes must be amplified simultaneously. Each mode must receive sufficient gain to compensate its loss. In this subsection, a theoretical model for

FM-EDFA and different techniques to control/equalize mode-dependent gain (MDG) are summarized.

Theoretical Model

A schematic diagram of an FM-EDFA is shown in Fig. 19. The amplifier consists of forward and backward pumps with pump mode content controllers. The signal and pumps are combined using dichroic mirrors and a piece of few-mode erbium-doped fiber (FM-EDF). The pump modal content controllers convert pump beams from the fundamental mode to a set of desired modes and combine multimode signal beams into the FM-EDF. The theory of multimode EDFA was first explored by Desurvire [138] and then investigated numerically in [139]. In this theoretical model, the following assumptions are made: (i) the electronic transition in the Er ions responsible for amplification is assumed to be a two-level system, (ii) the fiber guiding structure and doping concentration are assumed to be homogeneous longitudinally, and (iii) the EDF is assumed to be weakly guided and the fiber modes are approximated as LP modes. The assumptions have been validated by matching numerical and experimental results in [140,141]. The operation of an FM-EDFA is described by a set of rate equations and propagation equations involving multiple transverse modes for the pump and signal:

$$\frac{dN_2(r,\phi,z)}{dt} = \sum_k \frac{P_k(z)\Gamma_k(r,\phi)\sigma_{ak}}{h\nu_k} N_1(r,\phi,z) - \sum_k \frac{P_k(z)\Gamma_k(r,\phi)\sigma_{ek}}{h\nu_k} N_2(r,\phi,z) - \frac{N_2(r,\phi,z)}{\tau_s}, \tag{102}$$

$$N_0(r,\phi) = N_1(r,\phi,z) + N_2(r,\phi,z), \tag{103}$$

where $N_0(r,\phi)$ is total doping density, and $N_1(r,\phi,z)$ and $N_2(r,\phi,z)$ are the Er ion densities in the ground state and the excited state, respectively. Each optical beam propagating in a different mode, at a different wavelength, and in a different direction is assigned a unique index k: $P_k(z)$ denotes the power of the kth beam whose normalized mode intensity profile is $\Gamma_k(r,\phi)$, ν_k represents optical frequency of the kth beam, the corresponding absorption and emission cross sections of erbium ions at ν_k are denoted as σ_{ak} and σ_{ek}, and τ_s denotes the spontaneous lifetime of the excited state. The propagation equation for the kth beam is

$$\frac{dP_k(z)}{dz} = u_k\sigma_{ek}[P_k(z) + 2\ h\nu_k\Delta\nu_k]\int_0^{2\pi}\int_0^a \Gamma_k(r,\phi)N_2(r,\phi,z)r\mathrm{d}r\mathrm{d}\phi - u_k\sigma_{ak}P_k(z)\int_0^{2\pi}\int_0^a \Gamma_k(r,\phi)N_1(r,\phi,z)r\mathrm{d}r\mathrm{d}\phi - u_k\alpha P_k(z), \tag{104}$$

where $u_k = 1 (u_k = -1)$ denotes the forward (backward) direction of kth beam, and α represents the intrinsic loss coefficient of the EDF. Equations (101)–(104) can be solved numerically by using the standard fourth-order Runge–Kutta method given initial conditions for the pump and signal power [138]. Gain and noise figures for each mode can subsequently be derived.

Modal Gain Equalization

According to Eq. (104), the power evolution of a signal mode depends on the degree of spatial overlap between the signal intensity profile $\Gamma_k(r,\phi)$ and $N_1(r,\phi,z)$, $N_2(r,\phi,z)$, which in turn depends on the pump intensity profile

Figure 19

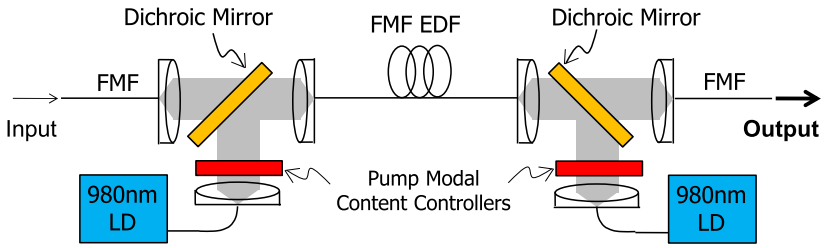

Schematic diagram of an FM-EDFA consisting of multimode input, forward and backward multimode pumps, and FM-EDF as the amplification module.

and the spatial doping profile of the Er ions. Consequently, two approaches have been proposed to control or equalize the modal gain. First is pump mode control, in which a reconfigurable multimode pump can achieve a tunable modal content. Second is doping profile control, in which a proper doping profile and refractive index profile for the EDF is designed and fabricated so that even when the pump contains only the fundamental mode, all signal modes still receive equal gain.

The pump-mode-control method is based on the principle that a signal whose mode intensity profile has better spatial overlap with that of the pump receives higher gain. In [142], this method was verified by simulations of an FM-EDF that can guide two mode groups at the signal wavelength and four mode groups at the pump wavelength. The signal and pump intensity profiles are plotted in Fig. 20(a). By solving Eqs. (101)–(104), the modal gain of each mode can be computed for various pump configurations. Figures 20(b) and 20(c) show the gain versus pump power contained only in LP_{01} and LP_{21}, respectively. When the LP_{01} pump mode is used, the LP_{01} signal mode receives higher gain due to better match with the pump intensity profile, as shown in Fig. 20(a). Conversely, pumping in LP_{21} mode results in higher gain for the LP_{11} signal mode. To fully control modal gains for both the LP_{01} and LP_{11} mode, both LP_{01} and LP_{21} pump modes can be used. This technique has been verified in experiment in [140,143], which showed that high-order mode pumps can decrease the modal gain difference between the LP_{01} and LP_{11} signal modes.

The doping-profile-control approach focuses on tailoring the Er ion concentration profile and/or refractive index profile to equalize the modal gain, using only the fundamental pump mode. References [140,144] propose and analyze the ring

Figure 20

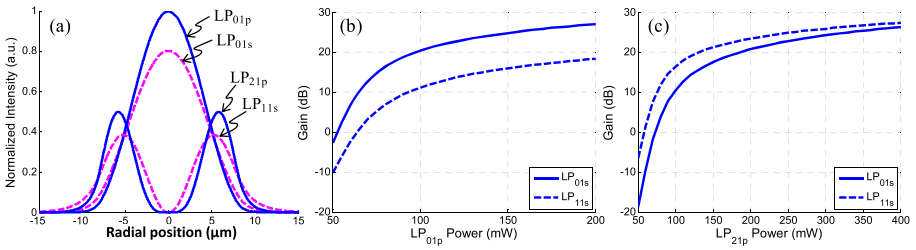

(a) Normalized signal and pump intensity profiles along the radial direction, and modal gains as functions of pump power when the pump is entirely confined in (b) LP_{01p} and (c) LP_{21p}.

doping profile for a two-mode EDFA. By tuning the thickness of the doping layer and the pump power, mode-dependent gain can be controlled. Moreover, the refractive index profile can also be designed to have a ring shape, which helps to lower differential modal gain [144]. Nevertheless, it requires careful optimization to avoid significant mismatch of the signal mode profiles in the EDF and in the transmission fiber, which results in higher splice losses. Recently, an FM-EDFA that can amplify more than four nondegenerate mode groups has been demonstrated [145–147] using the doping profile-control method.

However, the doping-profile-control method may become increasingly difficult for amplification beyond four mode groups. Furthermore, dynamic modal gain control can be achieved only by using the pump-mode-control method. So in practice, both pump-mode control and doping-profile control will be required to equalize MDG for fibers having large numbers (>4) of mode groups [148]. The effect of mode beating on the performance of FM-EDFAs [149] and transverse mode competition [139] have also been analyzed. A cladding-pumped FM-EDFA has also been experimentally demonstrated [150].

6.2b. Few-Mode Distributed Raman Amplifier

Another important type of few-mode amplifier is the distributed Raman amplifier (DRA) [151]. Raman gain arises from the transfer of power from the pump beam to the signal beam mediated by optical phonons. Compared to the EDFA, the DRA has some fundamental advantages, such as broad bandwidth, gain flatness, and a low noise figure. On the other hand, the DRA requires high pump power and long fiber length. In an FM-DRA, powers are transferred from multiple pump beams at different modes to multiple signal modes. Under the undepleted pump approximation, the evolution of signal power is given by

$$\frac{P_{s,m}(z)}{P_{s,m}(0)} = \exp[-\alpha_s z + G_m^{+}(1 - e^{-\alpha_p z}) + G_m^{-}(e^{\alpha_p z} - 1)], \tag{105}$$

where $P_{s,m}$ is the power in signal mode m, and α_s and α_p are the absorption coefficients at the signal and pump wavelengths, respectively. The coefficients $G_m^{\pm}$ describe the mode-dependent exponential gain due to the copropagated pump (+) and counterpropagated pump (−), which can be expressed as

$$G_m^{+} = \frac{\gamma_R}{\alpha_P} \sum_n f_{n,m} P_{p,n}^{+}(0), \tag{106a}$$

$$G_m^{-} = \frac{\gamma_R}{\alpha_P} \sum_n f_{n,m} P_{p,n}^{-}(L), \tag{106b}$$

where γ_R is related to the cross section of spontaneous Raman scattering, $P_{p,n}^{+}(0)$ denotes nth copropagated pump mode power at $z = 0$, while $P_{p,n}^{-}(L)$ represents the nth counterpropagated pump mode at $z = L$, where L is the span length. $f_{n,m}$ denotes the overlap integral between the normalized intensity profiles of the nth signal and the mth pump:

$$f_{n,m} = \int_{-}^{+} \int_{\infty}^{\infty} \Gamma_{s,m}(x,y)\Gamma_{p,n}(x,y)\mathrm{d}x\mathrm{d}y. \tag{107}$$

According to Eq. (106), the modal gain of a DRA is proportional to $f_{n,m}$ and pump powers. Therefore, the aforementioned pump-mode-control approach can also be applied to an FM-DRA. In [152], an equalized 8 dB Raman gain for two mode groups was achieved by using only an LP_{11} pump due to similar overlap with the two signal mode groups. In [151], an FM-DRA is further analyzed in the framework of vector modes, which can assess the spatial distribution and polarization properties of modes simultaneously. By tuning the mode content of the multimode pump carefully, a residual MDG of 0.13 dB can be obtained for each 10 dB of Raman gain. A general theoretical framework for the analysis of forward and backward Raman amplification in SDM fibers, taking into account the effect of random coupling and modal dispersion in degenerate mode groups, has been presented in [153].

6.2c. Multicore EDFA

For SDM systems using MCF, amplifiers are also required for long-haul transmission. There are two pumping schemes for multicore EDFAs (MC-EDFAs): (i) a core pump in which pump beams propagate in each core [154–157] and (ii) a cladding pump in which a multimode pump beam propagates in the cores as well as the common cladding [158]. For both schemes, to combine signals from different cores of MCF and pump(s), proper couplers, such as tapered fiber bundle (TFB) couplers or free-space couplers [157], are used. TFBs are designed so that the pitch and core dimension at the taper end match with those of the MC-EDF. For the core-pump scheme, ideally, each core can be seen as an independent amplified channel. Hence, core-pump MC-EDFAs can achieve high gain (> 20 dB), a low noise figure (< 5 dB), and efficiencies similar to single-mode EDFAs. In comparison with the core-pump scheme, cladding-pumped MC-EDFAs are less power efficient and have a higher noise figure, as the intensity overlap between the signal and pump beams is low. However, the advantage of a cladding pump is that multimode laser diodes can be used. They can achieve high output power in a cost-effective manner in comparison with the single-mode pump diodes. Moreover, multimode laser diodes used for the cladding pump have higher electrical-to-optical power conversion efficiency and in most cases do not require any thermoelectric cooling, which is expected to improve the energy efficiency [159].

In a weakly coupled MCF transmission system, low core-to-core crosstalk is required for the MC-EDFAs. To minimize crosstalk and insertion loss, careful matching between TFB and MC-EDF is desired. Currently, crosstalk levels of < -40 dB and < -30 dB can be achieved for core-pump [154,160] and cladding-pump MC-EDFAs [158], respectively.

6.2d. Bulk Amplifier

Although SDM amplifiers are straightforwardly realized in fibers, their complexity increases linearly as the number of degrees of freedom grows. In [161], an imaging amplifier is proposed for MCF. This technique involves both imaging and amplification. The facet of the input multicore or multimode fiber is imaged to the facet of the output fiber of the same type after passing through a bulk amplifying region. This exploits the parallelism in bulk optics to provide extra degrees of freedom, which is necessary for multicore or multimode amplification.

Figure 21 shows the schematic of an imaging amplifier. The output beam of the MCF (MMF) passes through imaging system 1 (IS 1) to focus at the center region of the gain medium and then couples back to output MCF (MMF) via IS 2. In [161], the amplification medium is chosen to be Er–Yb codoped phosphate glass because of its high pump absorption. Since the bulk amplifier is normally much shorter (a few centimeters) than the fiber amplifier (meters), the doping concentration is orders of magnitude higher than the fiber amplifiers. Simulation results show that the imaging amplifier can achieve an ~20 dB gain per core when the input power for an individual core is 6 mW with an optical power conversion efficiency (OPCE) of 32.5%. The advantage of the imaging amplifier is that it has no limit on the number of cores or modes for MCF or MMF. The disadvantage may be relatively low OPCE. However, for an SDM system that has larger input signal power, which is the case when the number of cores/modes is large, the OPCE of the imaging amplifier is higher.

7. SDM Transmission System

7.1. State-of-the-Art SDM Transmission Experiments

To date, three types of SDM transmission experiments have been demonstrated: (i) core-multiplexed transmission over MCF, (ii) MDM transmission over single-core FMF, and (iii) core multiplexed MDM transmission over FM-MCF. Table 1 is a summary of SDM transmission experiments so far. The highest capacity (1.01 Pb/s) of core-multiplexed transmission is demonstrated by Takara *et al.* [187] in a 52 km single span of 12-core MCF. In the other experiment by Igarashi *et al.* [188], the reach is extended to 7326 km and net total capacity is 140.7 Tb/s, leading to a record capacity–distance product of 1030.8 Pb/s × km.

Recent developments on FMF fabrication and FM-EDFAs have enabled demonstration of long-distance MDM transmission. Long-haul transmission using FMF with inline amplification via parallel single-mode EDFAs was first demonstrated in [189] with maximum transmission distance of 4200 km. Enabled by an FM-EDFA with modal gain equalization, the first loop experiment with an inline FM-EDFA was demonstrated [190]. Figure 22 shows an FMF loop experiment setup demonstrated by Ip *et al.* [191].

WDM signals consisting of 146 wavelength channels each carrying 19 GBaud QPSK data signals at 25 GHz spacing were generated and transmitted using two polarizations and three spatial modes (LP_{01}, LP_{11a}, and LP_{11b}). The recirculating loop was constructing with a 50 km FMF, a ring-doped FM-EDF, and a free-space loop switch. The FM-EDFA was carefully designed and tuned to cancel

Figure 21

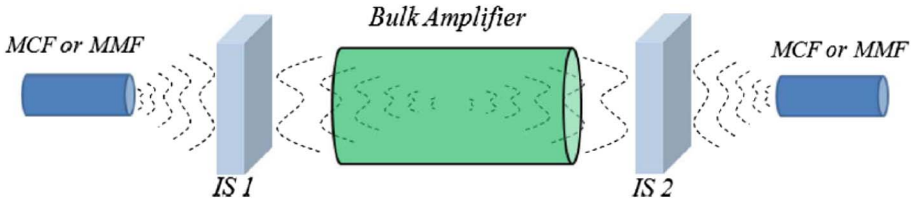

Conceptual schematic of an imaging amplifier (IS, imaging system).

Table 1. Summary of SDM Transmission Experiments

Year	Ref	Fiber Type	# Core× Mode	Distance (km)	Span Length (km)	Date Rate (Gbps/mode/core/λ)	WDM Channels/ core/mode	Net Spectral Efficiency (bit/s/Hz)	Net Total Capacity (Tb/s)	Capacity-Distance Product (Pb/s × km)
2014	[162]	MCF	7 × 1	7326	45.5	120	201	4	140.7	1030.8
2013	[163]	MCF	12 × 1	1500	50	92	748	36.8	344	516
2012	[187]	MCF	12 × 1	52	52	456	222	91.4	1012.32	52.64
2012	[164]	MCF	7 × 1	6160	55	128	40	14.44	28.88	177.87
2012	[165]	MCF	7 × 1	845	76.8	603	8	42.2	33.77	28.53
2013	[166]	MCF	19 × 1 × 1	10.1	10.1	172	100	30.5	305	3.08
2012	[189]	WC-MCF[a]	3 × 1	4200	60	80	5	3.84	0.96	4.03
2011	[167]	MCF	7 × 1	2688	76.8	128	10	15.02	7.51	20.19
2011	[168]	MCF	7 × 1	76.8	76.8	1120	1	NA	7.84	0.6
2011	[169]	WC-MCF[a]	3 × 1	1200	60	80	1	NA	0.22	0.27
2011	[170]	MCF	7 × 1	76.8	76.8	107	160	14	112	8.6
2011	[171]	MCF	7 × 1	76.8	76.8	107	80	14	56	4.3
2011	[172]	MCF	7 × 1	16.8	16.8	172	97	11.25	109.14	1.83
2014	[192]	FM-MCF	12 × 3	40	40	105	20	247.9	55.08	2.2
2012	[173]	SM-FM-MCF	12 × 1 + 2 × 3	3	3	1050	385/354	109	1050	3.15
2014	[174]	OM4	1 × 6	17	17	120	32			
2013	[191]	FMF	1 × 3	500	50	76	146	7.3	26.63	13.32
2013	[175]	FM	1 × 6	177	59	160	32	30.72	24.58	4.35
2013	[176]	PBG-FMF	1 × 3	0.31	0.31		96	12	57.6	0.02
2012	[177]	FMF	1 × 6	130	65	80	8	7.68	3.07	0.4
2012	[178]	FMF	1 × 3	119	119	256	96	12	57.6	6.85
2012	[179]	FMF	1 × 3	209	209	80	5	4.42	1.1	0.23
2012	[180]	FMF	1 × 3	1200	30	80	1	NA	0.19	0.23
2012	[181]	FMF	1 × 3	85	85	112	1	NA	0.31	0.03
2012	[35]	FMF	1 × 3	96	96	80	1	NA	0.22	0.02
2011	[182]	FMF	1 × 5	40	40	112	1	1	0.52	0.02
2011	[183]	FMF	1 × 3	50	50	112	88	6.19	27.23	1.36
2011	[15]	FMF	1 × 3	33	33	112	6	6.19	1.86	0.06
2011	[184]	FMF	1 × 3	10	10	56	1	NA	0.15	0.002
2011	[185]	FMF	1 × 2	40	40	112	1	NA	0.21	0.01
2011	[186]	FMF	1 × 2	4.5	4.5	107	1	5.4	0.2	0.001

[a] WC-MCF stands for weakly coupled MCF.

Figure 22

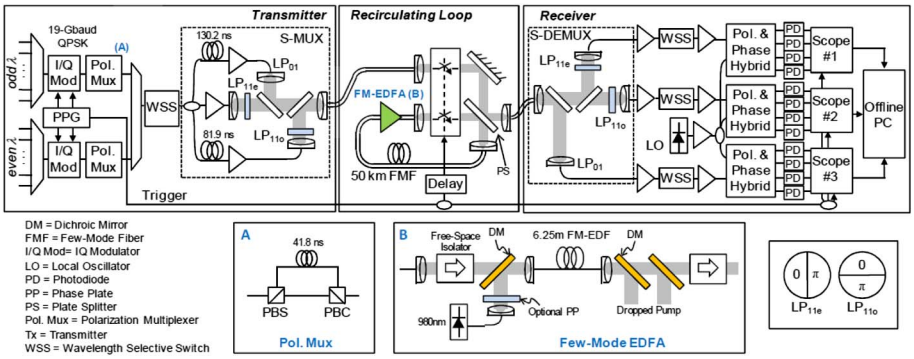

Experimental setup of a $146\lambda \times 6 \times 19$ Gbaud WDM–MDM transmission over a fiber recirculating loop [191]. Courtesy of E. Ip. Copyright 2013, Optical Society of America.

the MDL per round trip. A total capacity of 26.63 Tb/s was demonstrated through a 10×50 km FMF loop.

To further increase the capacity, core multiplexed MDM transmission has been proposed. Recently, a 12 core × 3 mode transmission via 40 km FM-MCF was demonstrated with the highest spectral efficiency (247.9 b/s/Hz) to date [192].

7.2. Capacity Limits for MDM

The capacity of a communication channel cannot exceed the Shannon limit,

$$C = W \log_2(1 + S/N), \tag{108}$$

where W is the spectral bandwidth of the channel and S/N is the SNR. In the ideal case when all available modes are used for multiplexing and loss of each mode is compensated by optical amplifiers, a D_s-channel MDM system has a capacity of

$$C = D_s \times W \log_2(1 + S/N), \tag{109}$$

where S/N is the SNR of each channel. This fundamental limit may not be achieved because of linear and nonlinear impairments in the MDM transmission system.

7.2a. Capacity Limits for MDM due to Linear Impairments

The first linear impairment is modal dispersion and mode coupling. If the memory length is longer than the MGD spread, then theoretically, modal dispersion and mode coupling will not impact channel capacity. However, the MGD spread itself is random, and when it exceeds the memory length of the equalizer, the system will be out of service. The outage probability can be calculated using the cCPF of group delay spread in Fig. 11.

The second impairment is loss. Given the transfer matrix, the average loss of the MDM system is given by [193]

$$\mathrm{L} = \frac{1}{D_s} tr\{\bar{\bar{\boldsymbol{H}}}^{\dagger} \cdot \bar{\bar{\boldsymbol{H}}}\} = \frac{1}{D_s} \sum_{i=1}^{D_s} \lambda_i, \tag{110}$$

where $\lambda_i = e^{-g_i}$ are the eigenvalues of the $\bar{\bar{\boldsymbol{H}}}^{\dagger} \cdot \bar{\bar{\boldsymbol{H}}}$, which are in general not equal. The loss can come from not only fiber but also splices [194] and other components. The average loss can be compensated using the various amplification techniques described in Section 6. The penalty in this case is the noise introduced by the amplification process that reduces SNR. MDL in general reduced the capacity of SDM systems. Theoretically, the best approach to achieve maximum capacity in the presence of MDL is to transmit more power (at higher spectral efficiency) for the superposition of modes corresponding to the eigenvector $\bar{\bar{\boldsymbol{H}}}^{\dagger} \cdot \bar{\bar{\boldsymbol{H}}}$ [195] with the largest eigenvalue. Practically, this requires that the transmitter be in command of the transfer matrix, also known as channel state information, which is not possible for long-haul transmission systems. In such a case, the transmitter sends independent information in each mode with equal power, resulting in a channel capacity of

$$C = \sum_{i=1}^{D_s} W \log_2\left(1 + \lambda_i \frac{S_0}{N_0}\right), \tag{111}$$

where S_0 is the total signal power in all mode channels and N_0 is noise power per mode channel [196]. Since the transfer matrix is random, the channel capacity is also random. For systems with small MDL, the statistics of g_i is exactly the same as the MGD τ_i. The average capacity can be obtained from the pdf of g_i. It should be pointed out that the frequency correlation bandwidth of g_i is much smaller than W, the channel frequency bandwidth [58,196]. This tends to lessen the effect of MDL.

In addition, unique opportunities in source and channel coding may exist because of the multidimensionality in SDM [197–202].

7.3. Capacity Limits for MDM due to Nonlinear Impairments

At this point, the nonlinear capacity limits for MDM have not been rigorously established [203,204]. Because the number of independent channels can increase dramatically, up to 2 orders of magnitude, it may appear that MDM systems would suffer many nonlinear penalties. Preliminary research indicates that the per-mode nonlinear capacity limit in SDM systems may even exceed that of SMF for the reasons below.

First, the area of FMF or MMF is larger than that of SMF. The total nonlinear phase shift scales with power and fiber area according to

$$\phi_{\mathrm{NL}} \propto \frac{\sum P_m}{A_{\mathrm{eff}}}. \tag{112}$$

Assuming that the transmission power in each mode P_m is the same as in the case of single-mode transmission, the total nonlinear phase shift of MDM is the same as single-mode transmission because the area of fiber scales linearly with the number of modes if the relative index difference is unchanged, canceling the effect of increased power.

Second, not all of the nonlinear phase shift in Eq. (112) is effective in producing nonlinear impairments [205–208]. In the case of a fiber with two mode groups [209–211], it has been shown that four-wave mixing is not effective due to the

lack of phase-matching conditions for waves in different mode groups and cross-phase modulation is not effective due to walk-off for waves in different mode groups.

Third, linear mode coupling also plays an important role. It has been found that linear coupling lessens the effect of nonlinear distortion due to averaging effects in a distributed fashion [212] or discrete fashion [62,213–215].

To rigorously establish the nonlinear capacity for MDM, the nonlinear effects must be precisely modeled. To do so, the linear coupling matrix of Eq. (31) should be expanded as a Taylor series in frequency offsets first, and then, after inverse Fourier transform and adding the Kerr nonlinear effect, one obtains the generalized nonlinear Schrödinger equation:

$$\frac{\partial \bar{A}}{\partial z} = i\bar{\bar{\mathrm{B}}}_0 \cdot \bar{A} - \bar{\bar{\mathrm{B}}}_1 \cdot \frac{\overline{\partial A}}{\partial t} - i\bar{\bar{\mathrm{B}}}_2 \cdot \frac{\partial^2 \bar{A}}{\partial t^2} + i\gamma \sum_{jklm} C_{jk\mathrm{lm}} A_k^* A_l A_m e_j, \tag{113}$$

where

$$C_{jklm} = A_0[2D_{jklm}^{(1)} + D_{jklm}^{(2)}]/3, \tag{114a}$$

$$D_{jklm}^{(1)} = \frac{\int (\psi_j^* \cdot \psi_m)(\psi_k^* \cdot \psi_l)\mathrm{d}x\mathrm{d}y}{N_j N_k N_l N_m}, \tag{114b}$$

$$D_{jklm}^{(2)} = \frac{\int (\psi_j^* \cdot \psi_k^*)(\psi_m \cdot \psi_l)\mathrm{d}x\mathrm{d}y}{N_j N_k N_l N_m}, \tag{114c}$$

$$N_m^2 = \int |\psi_m|^2 n(x,y)\mathrm{d}x\mathrm{d}y, \tag{114d}$$

where we have used the subscript $jklm$ to represent different modes and $n(x,y)$ is the fiber index distribution. Because the correlation length of polarization coupling is of the order of tens of meters and degenerate mode coupling is of the order of hundreds of meters, numerical solution of Eq. (113) will be very computationally heavy.

In the limit when the modes are strongly coupled, the length scale for modes to completely exchange among each other is much shorter than the length scale for significant nonlinear effects. So nonlinear interactions are averaged over all possible states of mode, and therefore, based on symmetry and dimensionality considerations, the nonlinear term in Eq. (113) must have the form

$$\sum_{jklm} C_{jklm} A_k^* A_l A_m e_j = \Gamma |\bar{A}|^2 \bar{A}. \tag{115}$$

This form of the nonlinear term in Eq. (115) was obtained using an averaging method that assumes that the linear coupling matrix in Eq. (113) is a random Gaussian matrix [216]. The derivation of the effective nonlinear coefficient Γ is a summary of [217]. Multiplying both sides by $\bar{A}$ and averaging over the orientation of $\bar{A}$ yields

$$\Gamma = \sum_{jklm} C_{jklm} \langle A_k^* A_l A_m A_j^* \rangle / |\bar{A}|^4. \tag{116}$$

Since $\bar{A}$ can be considered a constant modulus vector whose orientation is uniformly distributed, we can model this by assuming that each component of $\bar{A}$ is a statistically independent complex Gaussian variable with zero mean and unit variance for both the real and imaginary parts. The results of statistical averaging gives

$$\Gamma = \sum_{jklm} C_{jklm} \frac{\delta_{jm}\delta_{kl} + \delta_{jl}\delta_{km}}{2N(2N+1)}. \tag{117}$$

This leads to the generalized Manakov equation:

$$\frac{\partial \bar{A}}{\partial z} = i\bar{\bar{B}}_0 \cdot \bar{A} - \bar{\bar{B}}_1 \cdot \frac{\partial \bar{A}}{\partial t} - i\bar{\bar{B}}_2 \cdot \frac{\partial^2 \bar{A}}{\partial z^2} + i\gamma\Gamma|\bar{A}|^2\bar{A}. \tag{118}$$

The generalized Manakov equation (Eq. (118)] can be transformed into coupled generalized Manakov equations when linear coupling between mode groups can be neglected [218]. The fundamental tools described above lay the foundation necessary for the establishment of the rigorous nonlinear capacity for MDM.

7.4. Deployment Strategy for MDM

While it appears that SDM is future proof in terms of capacity in the next 10 to 20 years, there seems to be a problem with backward compatibility, hindering the prospect of SDM for commercialization. Current optical communication systems use single-mode transmitters and receivers and SMF. MDM, by definition, cannot use SMF. The challenge is to implement SDM transmission, a potentially disruptive technology, in an evolutionary fashion, without ripping out existing SMF all at once. The answer lies in using single-mode transmission in FMFs as an intermediate step.

FMFs can be used not only for MDM but also for single-mode transmission. Moreover, single-mode transmission in FMFs provides better performance than in SMFs, because of their large effective area and thus lower nonlinearities [13,219,220].

Single-mode transmission in weakly coupled FMF with enhanced nonlinearity tolerance has been demonstrated experimentally [220]. Therefore, MDM can be implemented in an evolutionary fashion as follows. When capacity is exhausted in existing routes or in greenfield applications, install FMFs and use backward compatible single-mode transmission with improved performance. These FMFs contain "dark modes" (as opposed to dark fiber) for future capacity expansion. When single-mode capacity is exhausted, each dark mode can be turned on, on a pay-as-you-go basis.

Because MDM prefers fibers with strong mode coupling, the likely intermediate step is to realize single-mode operation in strongly coupled FMFs, together with multimode EDFAs and multimode receivers. Since there is only one data stream, DSP for this single-input–multiple-output system (SIMO) should be much simpler than for the MIMO MDM system [221]. Hence, the required single processing capability will be well within the reach of future commercial DSP circuits.

8. SDM Networking

Optical networking involving SDM can be divided into mode-selective and non-mode-selective categories. The differentiation is whether spatial modes are used as a degree of freedom for switching purposes. For long-haul networks, mode coupling is not only unavoidable but also may be a tool for mitigating mode crosstalk, modal dispersion, and MDL. Therefore, mode-selective switching is not possible and all the modes on the same wavelength must be switched together. It is convenient for these mode-multiplexed signals to be grouped together as a spatially assembled superchannel [222] (as opposed to a spectral superchannel [223]). We call such a network an SDM-compatible optical network. Mode-selective SDM networking is feasible only when modes do not couple in the transmission channel, which is possible for short-reach data center networks and on-chip waveguide interconnect networks.

8.1. SDM-Compatible Networking

So far, most research work in this area is related to components for SDM-compatible networks including wavelength-selective switches (WSS) [224–226] and (reconfigurable) optical add/drop multiplexers [(R)OADMs] [227–231]. WSS and (R)OADM configurations based on guided-wave devices for single-mode operation, such as those based on fiber Bragg gratings and waveguide switches, cannot be easily extended for SDM-compatible networking where all spatial modes on the same wavelength must be switched together. This is because the guided-wave devices themselves are mode dependent. On the other hand, WSS and (R)OADM configurations based on free-space optics can be easily extended for multimode operation. Key devices for separating wavelength in free-spaced-based WSSs and (R)OADMs, such as optical bandpass filters and diffraction gratings, are sensitive not only to wavelength but also to incident angle and thus the input spatial mode content. So the key to extending single mode to multimode WSSs and (R)OADMs is to ensure that the bandpass filters and diffraction gratings do not disperse high-order modes at any WDM channel into its neighboring channels.

In fact, this is not difficult to do. When fiber modes exit the fiber facet, they propagate in free space as superpositions of eigenmodes in free space. The number of free-space eigenmodes should be the same as the number of fiber modes. We can use the circularly symmetric Laguerre–Gaussian (LG) modes,

$$E_{pl}(r,\phi) = \sqrt{\frac{2p!}{\pi(p+|l|)!}}\frac{1}{w_0}\left[\frac{r\sqrt{2}}{w_0}\right]^{|l|}\exp\left(\frac{2r^2}{w_0^2}\right)L_p^{|l|}\left(\frac{2r^2}{w_0^2}\right)e^{il\phi}, \tag{119}$$

as the basis set in free space, where p is the radial index, l is the OAM number, $L_p^{|l|}$ is the Laguerre polynomial, and w_0 is the waist of the fundamental mode (Gaussian mode). The mth-order ($m = 2p + |l| + 1$) LG mode has a waist and divergence angle,

$$w_m = \sqrt{m}w_0, \tag{120a}$$

$$\theta_m = \sqrt{m}\theta_0, \tag{120b}$$

where θ_0 is the divergence of the fundamental Gaussian mode ($p = l = 0, m = 1$) and $w_m\theta_m = mw_0\theta_0 = m\lambda/\pi$. Therefore, the divergence of the fiber output beam scales as the square root of the total number of modes in the fiber if the fundamental mode size does not change, which agrees with the experiment in [228]. However, if we assume that MMFs are made by increasing the core radius while maintaining the numerical aperture or relative index difference to be the same, the fundamental mode size will increase by $\sqrt{m}$ and the corresponding fundamental mode divergence will decrease by $\sqrt{m}$. Therefore, only minor adjustment is needed to convert single-mode free-spaced based WSSs and (R)OADMs to SDM-compatible free-spaced based WSSs and (R)OADMs.

8.2. Mode-Selective Networking

In principle, wavelength and space are orthogonal degrees of freedom that can be separated and routed independently. However, mode crosstalk destroys orthogonality among spatial modes. Therefore, mode-selective networking seems to be incompatible with reality. This is definitely true for long-haul optical networks. However, it has been shown that crosstalk among different mode groups can be suppressed to negligible levels in fibers with large effective index difference between mode groups [13,232]. So it is possible for short-reach networks, such as data center networks, to avoid coupling among mode groups and using mode groups as degrees of freedom for switching. In addition, on the chip level, waveguide modes do not have crosstalk. Preliminary research on reconfigurable add/drop multiplexers for spatial modes [230], spatial mode-based converters [233], and elastic multidimensional spatial and spectral optical networking [234–236] has begun. There have also been research activities aimed at mode-selective networking on-chip [237–244]. One of the potential advantages of mode-selective networking over wavelength-selective networking is that mode conversion is a linear process [107,233] while wavelength conversion is not.

Techniques for mode demultiplexing in the optical domain have been proposed as described in Section 6. But mode-selective networking requires separation of all wavelength-mode degrees of freedom, and many wavelength demultiplexing devices use some form of diffraction that explicitly couples wavelength and modes. This raises an interesting question of mode–wavelength interference. Fortunately, almost all mode-division (de)multiplexers based on mode coupling using directional couplers described in Section 6.2 and references therein are wavelength insensitive. This is because, unlike the case of free-space propagation where wavelength dispersion is stronger than modal dispersion, in the guided-wave structure, modal dispersion is conversely stronger than wavelength dispersion. So all mode–wavelength degrees of freedom can be separated by mode-division demultiplexing followed by wavelength-division demultiplexing. On the other hand, mode (de)multiplexers based on directional couplers and self-aligning beam couplers can be designed to operate without fundamentally any loss. Similarly, all mode–wavelength degrees of freedom can be combined in the reverse order: WDM followed by MDM. The mode–wavelength degrees of freedom, once separated, can be routed using a space-division switch with large enough dimension, as shown in Fig. 23. However, because coupling between degenerate modes is unavoidable in circular optical fiber even over short distances of propagation, mode–wavelength switching would be easier to implement with switching granularity at the level of a mode group for a fiber

Figure 23

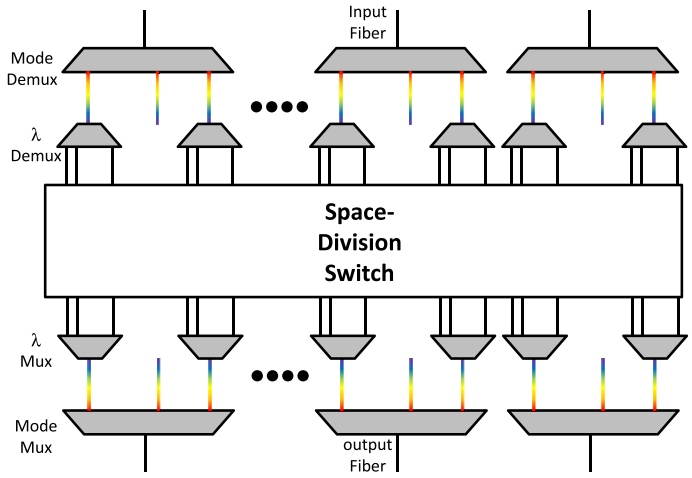

Schematic of a mode–wavelength switch.

network. In this scenario, signals contained in modes within the same mode group always travel together.

The description of Fig. 23 omits some implementation details that are necessary for correct switching and routing, for example, the use of mode converters and wavelength converters before and after the space-division switch.

8.3. SDM-Enabled Access Networks

Modes as networking resources can also be very useful in access networks. One of the major limitations of passive optical networks (PONs) for access application is the combining loss for upstream traffic if all single-mode elements are used. Figure 24 [245] shows the downstream and upstream traffic configuration at the optical line terminal (OLT) in an optical access network that avoids combining loss by taking advantage of spatial modes. In comparison, if the M:1 combiner is replaced by a device similar to the PL where the output fiber is multimode, then combining loss can be eliminated altogether. This approach could be more advantageous than WDM PON because no wavelength-locked transmitters are required at each and every optical network unit (ONU). The connecting fiber between the M:1 mode coupler and the receiver needs to be multimode, requiring the receiver to be compatible with such fibers. Since

Figure 24

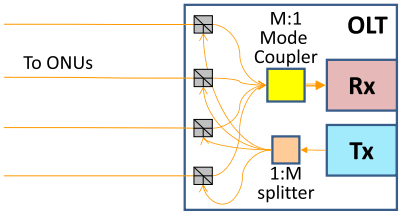

Schematic of a PON receiver in OLT where a lossless M:1 mode coupler is used in place of a traditional M:1 single-mode combiner, which has a loss of 1/M.

the splitting ratio in a PON can be as high as 1024, mode as a resource will certainly find more application for PON access networks [246].

9. Conclusions and Outlook

SDM is a new technology after the successful research, development, and deployment of digital coherent optical communication. It has been an exciting area of research that has produced fundamental breakthroughs and rapid progress in experimental demonstrations. Whether this excitement translates into commercialization remains to be seen.

From a transmission perspective, multiple mode channels in a MMF are logically the same as multiple SMFs in a fiber bundle. Whether SDM or fiber bundles win out will be determined by the cost per bit for transmission. It should be pointed out that cost savings from large-scale transmitter and receiver integration [247–250], although spurred in part because of SDM, is beneficial to both SDM and the fiber bundle approach, and therefore provides no differentiation. The following are a few aspects that might provide SDM with cost savings over the fiber bundle approach:

- Reduced cabling cost. To maintain robustness and deployability, each optical fiber cable will be limited in the number of fiber strands, especially for undersea systems. When the transmission capacity requirement exceeds that provided by a SMF bundle in one cable, SDM fibers will cost less for cabling in terms of materials, fabrication, and deployment. The degree of cost saving in cabling will be proportional to the factor over which the transmission capacity requirement exceeds a SMF cable. Using SDM, transmission capacity increases linearly with power consumption while transmission capacity using higher-order modulation formats in the limited number of fibers increases logarithmic with power consumption. Reduced power consumption not only decreases the electrical part of the cabling costs but also may lend SDM as the only solution to expand transmission capacity per cable due to power delivery considerations in the undersea environment.
- Reduce amplifier cost. Multiple mode channels can be amplified in a single FM-EDFA or Raman amplifier, which offers a higher level of integration compared to a multicore EDFA. Because the fiber bundle approach is compatible only with multicore EDFAs, SDM can have potential cost savings over the fiber bundle approach with respect to amplifier technology.

In addition, because of the large effective area of few-mode or multimode fibers, the nonlinear Shannon limit per mode for SDM may be higher than that of SMF, which can also be translated to reduced cost per bit.

On the other hand, SDM needs more DSP power. Nevertheless, because of historical trends in the progress of DSP and the fact that additional DSP for SDM is required only at the receiver, it can be expected that DSP will not introduce significant fractional cost increases to SDM long-haul transmission.

The landscape for optical networking involving SDM is wide open since SDM transmission technology is not yet mature. As aggregate network traffic increases, optical switching granularity will also increase as in the past, from wavelength to superchannel (multiple wavelength) and beyond. When the

switching granularity is increased to beyond the SMF capacity (~100 Tb/s), SDM seems to be the natural aggregation method to ensure that the switching granularity remains below single-fiber transmission capacity, thus reducing the required port count for optical switches. It should be pointed out, however, that multiple SMFs can be "aggregated" into a MCF and switched together. So SDM networking, in some sense, is independent of SDM transmission. This is also the case in access network where the spatial degree of freedom can be used to reduce combining loss.

In summary, SDM is a new frontier for optical fiber communication research. It is similar to wireless MIMO but offers two distinctions in the guided nature and nonlinearity in channel propagation. Because it is a nascent field of research, there is still much unexplored territory, involving both optics and electronics. The lessons learned in SDM research will not only determine the fate of SDM itself but also likely have broad impact on other areas of science and engineering involving optical spatial modes.

Appendix A: List of Symbols

Roman Symbols

A_{pq}	Complex amplitude of the electric field of light of the LP_{pq} mode in the time domain
$\boldsymbol{A}_{pq}$	Complex amplitude of the electric field of light of the LP_{pq} mode in the frequency domain
A_{eff}	Effective area of fiber
a	Radius of the core of step-index fibers
$\underline{a}_{1,2}(m)$	Symbols after hard-decision
$\bar{\bar{\boldsymbol{B}}}(\omega, z)$	Hermitian matrix $\frac{1}{2M}(\beta_0 \boldsymbol{I} + \bar{\beta} \cdot \underline{\underline{\boldsymbol{\sigma}}})$
B	Baud rate
C	Channel capacity
$C_{\text{TDE,FDE}}$	Computational complexity (required number of complex multiplications) per symbol per mode
$\bar{\bar{C}}_i$	Linear coupling matrix
$\bar{\bar{C}}_S$	Input–output coupling matrix of a mode (de)mutiplexer
$c_{k,l}$	Matrix elements of $\bar{\bar{C}}_S$
$c_{mn,i}$	Coupling matrix element
c	Speed of light in vacuum
D	Dispersion coefficient (ps/nm/km)
D_s	Total degrees of freedom for SDM
$d(k)$	Training symbol
d	Core-to-core distance in a multicore fiber
$E_{x,y}$	Transverse electric field of LP modes
$\bar{\boldsymbol{E}}_{i,b}$	bth error block for the ith mode
$F^{-1}\{\cdot\}, F\{\cdot\}$	(Inverse) Fourier transform
$f(z)$	Function describing random fluctuation of bending and twisting in the longitudinal direction
$f_{n,m}$	Overlap integral between the normalized intensity profiles of the nth signal and mth pump in Raman amplifiers
$\bar{\bar{\boldsymbol{G}}}$	Group delay operator in the frequency domain
$G_m^{\pm}$	Mode-dependent exponential gain due to the copropagating pump (+) and counterpropagating pump (−)
g_i	Natural log of the ith eigenvalues of loss operator $\bar{\bar{\boldsymbol{L}}}$
$H_{x,y}$	Transverse magnetic field of LP modes
$H_k(\cdot)$	Hermite polynomial
$\bar{\bar{\boldsymbol{H}}}$	Channel matrix in the frequency domain
$\boldsymbol{h}_i(\omega, z)$	Channel matrix elements in the frequency domain
$\bar{\bar{H}}$	Channel matrix in the time domain
h	Plank constant
h_{mn}	Channel matrix elements in the time domain
$h_{cd}(t)$	Impulse response of the chromatic dispersion of the LP_{01} mode of a fiber
$h_{pq}(z)$	Local power coupling coefficient between cores p and q
$\langle h_{pq} \rangle$	Average power coupling coefficient between cores p and q
$\boldsymbol{I}$	Identity matrix
I_{pq}	Intensity envelope of the LP_{pq} mode
$\bar{\boldsymbol{J}}(\omega, z)$	Generalized Jones vector in the frequency domain

(Table continued)

Continued

$\bar{J}$	Generalized Jones vector in the time domain
$J_p(\cdot)$	Bessel function of the first kind of order p
K	Spatial frequency of a wave or number of fiber sections with length slightly greater than the correlation length but much smaller than the total transmission distance
K_{pq}	Average value of coupling coefficients κ_{pq} and κ_{qp}
k_0	Propagation constant of light in vacuum
k_r	Radial component of the propagation constant $(k^2 n_1^2 - \beta^2)^{1/2}$
$\mathcal{L}$	Loss due to mode coupling
$\bar{\bar{\boldsymbol{L}}}$	Loss operator in the frequency domain
L	Length of the fiber
L_i	Longitudinal location of ith coupling event
$L_p^{\lvert l\rvert}$	Laguerre polynomial of order $\lvert l\rvert$
l_c	Coherence length
$\bar{\bar{\boldsymbol{M}}}$	Coupling matrix of a coupled multicore fiber
M	Total number of spatial modes supported by the multimode fiber
m	Degenerate mode number or symbol index label
$N_0(r,\phi)$	Total Er ion doping density
$\underline{N_0}$	Noise power per mode
$N_1(r,\phi,z)$	Er ion densities in ground state
$N_2(r,\phi,z)$	Er ion densities in excited state
N_B	Block length in the overlap-save method
N_{CP}	Length of cyclic prefix
N_{FFT}	Length of FFT
N_{Tap}, N_f	Number of taps (also called tap length or memory) of the filter
n	Refractive index of the actual fibers
n_{ideal}	Refractive index of the ideal fibers
n_1	Refractive index of the core of step-index fibers
n_2	Refractive index of the cladding of step-index fibers
n_{eff}	Effective index of one core in a multicore fiber
Δn_{eff}	Effective index difference between two cores
$\bar{\bar{\boldsymbol{P}}}_i$	Linear propagation matrix in the frequency domain
$\bar{\bar{P}}_i$	Linear propagation matrix in the time domain
$P_k(z)$	Power of the kth beam
p	Azimuthal mode number
$p_d(\tau)$	Probability density function of the eigenvalues of $\bar{\bar{\boldsymbol{G}}}$
q	Number of zero crossings of the mode profile along radial direction
$\bar{\bar{\boldsymbol{R}}}(L,z)$	Rotation matrix for the fiber extending from z to L
$R(\xi)$	Autocorrelation function of longitudinally varying coupling coefficient $\kappa(z)$
R_s	Sampling rate (samples/symbol)
R_b	Bend radius
R_{pk}	Bending radius resulting in peak crosstalk
r	Radial position in cylindrical coordinate
r_τ	Power spectral density of $R(\xi)$
$\vec{r}_{p,q}$	Position vector of cores p and q of the straight fiber
S/N	Signal-to-noise ratio
S_0	Total signal power in all modes
$s(t,r,\theta)$	MDM signals in the fiber
$s_l(x,y)$	Normalized complex optical fields of the lth spot
$\bar{\bar{\boldsymbol{T}}}(\omega,z)$	Hermitian matrix $\frac{1}{2M}(\tau_0 \boldsymbol{I} + \bar{\tau}\cdot\underline{\underline{\boldsymbol{\sigma}}})$
t	Time
$\bar{\bar{\boldsymbol{U}}}(\omega)$	Right-singular unitary matrix
$\bar{\boldsymbol{u}}_m$	Column vectors of $\bar{\bar{\boldsymbol{U}}}(\omega)$
u_k	Direction integer (1, forward; −1, backward)
V	Normalized frequency $((2\pi/\lambda)a\sqrt{n_1^2 - n_2^2})$
$\bar{\bar{\boldsymbol{V}}}(\omega)$	Left-singular unitary matrix
$\bar{\boldsymbol{v}}_m$	Column vectors of $\bar{\bar{\boldsymbol{V}}}(\omega)$
v_g	Group velocity
$\overline{\overline{W(t)}}$	Inverted channel matrix
$\overline{w_{mn}(k)}$	Inverted channel filters
$\overline{\boldsymbol{W}_{ij}^{(b)}}$	Frequency-domain filters for bth block
W	Spectral bandwidth of the channel
w_0	Waist of the fundamental mode (Gaussian mode)
ΔX_{pq}	Average crosstalk increment in power within a small segment
x	Horizontal coordinate (m)
$\overline{x(t)}$	Input signal vector
$\overline{\hat{x}(k)}$	Symbol after equalization
$\overline{y(t)}$	Output signal vector
y	Vertical coordinate (m)
$\bar{\boldsymbol{Y}}_{i,b}$	The bth signal block in the ith mode
z	Longitudinal coordinate (m)

(Table continued)

Continued

$\hat{z}$	Unit vector in the longitudinal direction
Greek Symbols	
α	Intrinsic loss coefficient of the erbium-doped fiber (EDF)
α_n	Power coefficient of the graded-index (GI) profile
$\bar{\beta}$	Generalized Stokes vector describing local coupling of fiber modes
β	Propagation constant (m^{-1})
β_{pq}	Propagation constant of the LP_{pq} mode (m^{-1})
$\beta_{p,q}$	Propagation constants of cores p and q
$\Delta\beta$	Difference between propagation constants of two modes
χ	Twist rate of a multicore fiber
$\Gamma_k(r,\phi)$	Normalized intensity profile of kth beam
γ	Fiber nonlinear coefficient
Δ	Relative index difference $(n_1 - n_2)/n_1$
δ	Dirac function
ε_0	Permittivity of free space (F/m)
$\Delta\varepsilon(x,y,z)$	Perturbation of the permittivity of a fiber
$\Delta\boldsymbol{\varepsilon}_r(x,y,K)$	Fourier transform of $\Delta\varepsilon(x,y,z)$ in the longitudinal direction
ε_i	Coupling strength associated with the ith coupling combination
$\varepsilon_{(1,2)}(m)$	Error signals
$\bar{\eta}$	Generalized Stokes vector corresponding to the channel matrix $\bar{\bar{\boldsymbol{H}}}$
η_i	$\boldsymbol{h}_{1,2}\exp(-i\Delta\beta z)$
η_{CP}	Cyclic prefix efficiency
θ	Azimuthal position in cylindrical coordinate
θ_m	Divergence angle of the mth-order Laguerre–Gaussian mode
θ_{pq}	Angle between position vectors of core p and core q
κ	Coupling coefficient
κ_{pq}	Coupling coefficient from core p to another core q
$\bar{\bar{\Lambda}}(\omega)$	Diagonal matrix of singular values of matrix $\bar{\bar{\boldsymbol{H}}}(\omega)$
λ	Wavelength (nanometers)
λ_i	ith eigenvalues of loss operator $\bar{\bar{\boldsymbol{L}}}$
$\Delta\lambda$	Bandwidth of the signal
μ	Convergence step size
ν_k	Optical frequency of kth beam
$\Delta\nu_k$	Amplified spontaneous emission (ASE) bandwidth of an erbium-doped fiber amplifier (EDFA)
ρ	Arbitrary phase
$\underline{\boldsymbol{\sigma}}$	Vector of matrices $\bar{\bar{\boldsymbol{\sigma}}}_j$
$\bar{\bar{\boldsymbol{\sigma}}}_j$	Pauli matrices
σ_{ak}	Absorption cross section of Er ions at ν_k
σ_{ek}	Emission cross section of Er ions at ν_k
$\bar{\tau}$	Modal dispersion vector
τ	Group delay
τ_i	Time delay associated with the ith coupling combination
τ_{MGD}	Total modal group delay (MGD) of the entire link
τ_{CD}	Chromatic dispersion spreading
$\Delta\tau$	Differential modal group delay (DMGD)
$\boldsymbol{\Phi}(\omega,z)$	Phase of field in frequency domain
$\hat{\phi}(m)$	Estimated laser phase fluctuations
ϕ_{NL}	Total nonlinear phase shift
ψ_{pq}	Normalized mode profile of mode LP_{pq}
Ω	Angular frequency offset
ω	Angular frequency

Acknowledgments

The authors would like to thank K.-P. Ho and J. M. Kahn for allowing us to use Fig. 10 and E. Ip for Fig. 22. We would like to thank Cristian Antonelli for helpful discussions and for preparing Fig. 11. We would like to acknowledge support from AT&T Lab, Futurewei, and NEC Labs. This research was supported in part by the National Basic Research Programme of China (973) Project #2014CB340100 and NSFC Project (61307085).

References

1. T. Li, "The impact of optical amplifiers on long-distance lightwave telecommunications," Proc. IEEE **81**, 1568–1579 (1993).

2. G. Li, "Recent advances in coherent optical communication," Adv. Opt. Photon. **1**, 279–307 (2009).
3. D. Richardson, J. Fini, and L. Nelson, "Space-division multiplexing in optical fibres," Nat. Photonics **7**, 354–362 (2013).
4. P. J. Winzer, "Optical networking beyond WDM," IEEE Photon. J. **4**, 647–651 (2012).
5. P. J. Winzer, "Spatial multiplexing: the next frontier in network capacity scaling," in *39th European Conference and Exhibition on Optical Communication (ECOC)* (2013), pp. 372–374.
6. D. Gloge, "Weakly guiding fibers," Appl. Opt. **10**, 2252–2258 (1971).
7. S. Berdagué and P. Facq, "Mode division multiplexing in optical fibers," Appl. Opt. **21**, 1950–1955 (1982).
8. C. Antonelli, A. Mecozzi, M. Shtaif, and P. J. Winzer, "Stokes-space analysis of modal dispersion in fibers with multiple mode transmission," Opt. Express **20**, 11718–11733 (2012).
9. C. Antonelli, A. Mecozzi, M. Shtaif, and P. J. Winzer, "Random coupling between groups of degenerate fiber modes in mode multiplexed transmission," Opt. Express **21**, 9484–9490 (2013).
10. L. Palmieri, "Coupling mechanism in multimode fibers," Proc. SPIE **9009**, 90090G (2013).
11. K. Okamoto, *Fundamentals of Optical Waveguides* (Academic, 2005).
12. R. Olshansky, "Mode coupling effects in graded-index optical fibers," Appl. Opt. **14**, 935–945 (1975).
13. F. Yaman, N. Bai, B. Zhu, T. Wang, and G. Li, "Long distance transmission in few-mode fibers," Opt. Express **18**, 13250–13257 (2010).
14. X. Chen, J. He, A. Li, J. Ye, and W. Shieh, "Characterization of dynamic evolution of channel matrix in two-mode fibers," in *Optical Fiber Communication Conference*, OSA Tech. Digest (online) (Optical Society of America, 2013), paper OM2C.3.
15. S. Randel, R. Ryf, A. Sierra, P. J. Winzer, A. H. Gnauck, C. A. Bolle, R.-J. Essiambre, D. W. Peckham, A. McCurdy, and R. Lingle, "6 × 56-Gb/s mode-division multiplexed transmission over 33-km few-mode fiber enabled by 6 × 6 MIMO equalization," Opt. Express **19**, 16697–16707 (2011).
16. S. Randel, P. J. Winzer, M. Montoliu, and R. Ryf, "Complexity analysis of adaptive frequency-domain equalization for MIMO-SDM transmission," in *39th European Conference and Exhibition on Optical Communication (ECOC)* (2013), pp. 801–803.
17. N. Bai and G. Li, "Adaptive frequency-domain equalization for mode-division multiplexed transmission," IEEE Photon. Technol. Lett. **24**, 1918–1921 (2012).
18. X. Zhou, J. Wang, Y. Weng, and Z. Pan, "A fast convergence frequency domain least mean square algorithm for compensation of differential mode group delay in few mode fibers," in *Optical Fiber Communication Conference*, OSA Tech. Digest (online) (Optical Society of America, 2013), paper OM2C.4.
19. A. Viterbi, "Nonlinear estimation of PSK-modulated carrier phase with application to burst digital transmission," IEEE Trans. Inf. Theory **29**, 543–551 (1983).
20. S. Zhang, P. Y. Kam, J. Chen, and C. Yu, "Decision-aided maximum likelihood detection in coherent optical phase-shift-keying system," Opt. Express **17**, 703–715 (2009).

21. M. Kuschnerov, M. Chouayakh, K. Piyawanno, B. Spinnler, E. De Man, P. Kainzmaier, M. S. Alfiad, A. Napoli, and B. Lankl, "Data-aided versus blind single-carrier coherent receivers," IEEE Photon. J. **2**, 387–403 (2010).
22. N. Bai, E. Ip, M.-J. Li, T. Wang, and G. Li, "Long-distance mode-division multiplexed transmission using normalized adaptive frequency-domain equalization," in *Photonics Society Summer Topical Meeting Series*, July 8–10, 2013 (IEEE, 2013), pp. 135–136.
23. S. Haykin, *Adaptive Filter Theory* (Prentice-Hall, 2001).
24. S. O. Arik, D. Askarov, and J. M. Kahn, "Adaptive frequency-domain equalization in mode-division multiplexing systems," J. Lightwave Technol. **32**, 1841–1852 (2014).
25. M. S. Faruk and K. Kikuchi, "Adaptive frequency-domain equalization in digital coherent optical receivers," Opt. Express **19**, 12789–12798 (2011).
26. S. O. Arik, D. Askarov, and J. M. Kahn, "Effect of mode coupling on signal processing complexity in mode-division multiplexing," J. Lightwave Technol. **31**, 423–431 (2013).
27. B. Inan, S. L. Jansen, B. Spinnler, F. Ferreira, D. Van den Borne, M. Kuschnerov, A. Lobato, S. Adhikari, V. A. J. M. Sleiffer, and N. Hanik, "DSP requirements for MIMO spatial multiplexed receivers," in *IEEE Photonics Society Summer Topical Meeting Series* (IEEE, 2012), pp. 187–188.
28. B. Inan, Y. Jung, V. Sleiffer, M. Kuschnerov, L. Gruner-Nielsen, S. Adhikari, S. L. Jansen, D. J. Richardson, S.-U. Alam, B. Spinnler, and N. Hanik, "Low computational complexity mode division multiplexed OFDM transmission over 130 km of few mode fiber," in *Optical Fiber Communication Conference*, OSA Tech. Digest (online) (Optical Society of America, 2013), paper OW4F.4.
29. B. Inan, B. Spinnler, F. Ferreira, D. van den Borne, S. Adhikari, N. Hanik, and S. L. Jansen, "Complexity analysis for higher order few mode fiber DSP equalizers," in *38th European Conference and Exhibition on Optical Communications (ECOC)*, OSA Tech. Digest (online) (Optical Society of America, 2012), paper Th.2.D.5.
30. B. Inan, B. Spinnler, F. Ferreira, D. van den Borne, A. Lobato, S. Adhikari, V. A. Sleiffer, M. Kuschnerov, N. Hanik, and S. L. Jansen, "DSP complexity of mode-division multiplexed receivers," Opt. Express **20**, 10859–10869 (2012).
31. N. Bai, E. Ip, Y.-K. Huang, E. Mateo, F. Yaman, M.-J. Li, S. Bickham, S. Ten, J. Liñares, C. Montero, V. Moreno, X. Prieto, V. Tse, K. M. Chung, A. P. T. Lau, H.-Y. Tam, C. Lu, Y. Luo, G.-D. Peng, G. Li, and T. Wang, "Mode-division multiplexed transmission with inline few-mode fiber amplifier," Opt. Express **20**, 2668–2680 (2012).
32. N. Bai, E. Ip, M.-J. Li, T. Wang, and G. Li, "Experimental demonstration of adaptive frequency-domain equalization for mode-division multiplexed transmission," in *Optical Fiber Communication Conference/National Fiber Optic Engineers Conference*, OSA Tech. Digest (Optical Society of America, 2013), paper OM2C.5.
33. T. Sakamoto, T. Mori, T. Yamamoto, and S. Tomita, "Differential mode delay managed transmission line for WDM-MIMO system using multi-step index fiber," J. Lightwave Technol. **30**, 2783–2787 (2012).
34. L. Gruner-Nielsen, S. Yi, J. W. Nicholson, D. Jakobsen, K. G. Jespersen, R. Lingle, and B. Palsdottir, "Few mode transmission fiber with low DGD, low mode coupling, and low loss," J. Lightwave Technol. **30**, 3693–3698 (2012).

35. R. Ryf, S. Randel, A. H. Gnauck, C. Bolle, A. Sierra, S. Mumtaz, M. Esmaeelpour, E. C. Burrows, R.-J. Essiambre, P. J. Winzer, D. W. Peckham, A. H. McCurdy, and R. Lingle, "Mode-division multiplexing over 96 km of few-mode fiber using coherent 6 × 6 MIMO processing," J. Lightwave Technol. **30**, 521–531 (2012).
36. W. Streifer and C. N. Kurtz, "Scalar analysis of radially inhomogeneous guiding media," J. Opt. Soc. Am. **57**, 779–786 (1967).
37. D. Gloge and E. A. J. Marcatili, "Multimode theory of graded-core fibers," Bell Syst. Tech. J. **52**, 1563–1578 (1973).
38. H. Kubota, H. Takara, T. Nakagawa, M. Matsui, and T. Morioka, "Inter-modal group velocity dispersion of few-mode fiber," IEICE Electron. Express **7**, 1552–1556 (2010).
39. F. Ferreira, D. Fonseca, and H. Silva, "Design of few-mode fibers with arbitrary and flattened differential mode delay," IEEE Photon. Technol. Lett. **25**, 438–441 (2013).
40. F. M. Ferreira, D. Fonseca, and H. J. A. da Silva, "Design of few-mode fibers with M-modes and low differential mode delay," J. Lightwave Technol. **32**, 353–360 (2014).
41. K. Sato, R. Maruyama, N. Kuwaki, S. Matsuo, and M. Ohashi, "Optimized graded index two-mode optical fiber with low DMD, large A_{eff} and low bending loss," Opt. Express **21**, 16231–16238 (2013).
42. D. Askarov and J. M. Kahn, "Design of transmission fibers and doped fiber amplifiers for mode-division multiplexing," IEEE Photon. Technol. Lett. **24**, 1945–1948 (2012).
43. T. Sakamoto, T. Mori, T. Yamamoto, L. Ma, N. Hanzawa, S. Aozasa, K. Tsujikawa, and S. Tomita, "Transmission over large-core few-mode photonic crystal fiber using distance-independent modal dispersion compensation technique," Opt. Express **19**, B478–B485 (2011).
44. F. Yaman, E. Mateo, and T. Wang, "Impact of modal crosstalk and multipath interference on few-mode fiber transmission," in *Optical Fiber Communication Conference*, OSA Tech. Digest (Optical Society of America, 2012), paper OTu1D.2.
45. N. Bai and G. Li, "Equalizer tap length requirement for mode group delay-compensated fiber link with weakly random mode coupling," Opt. Express **22**, 4247–4255 (2014).
46. C. D. Poole and R. E. Wagner, "Phenomenological approach to polarisation dispersion in long single-mode fibres," Electron. Lett. **22**, 1029–1030 (1986).
47. S. Fan and J. M. Kahn, "Principal modes in multimode waveguides," Opt. Lett. **30**, 135–137 (2005).
48. M. B. Shemirani and J. M. Kahn, "Higher-order modal dispersion in graded-index multimode fiber," J. Lightwave Technol. **27**, 5461–5468 (2009).
49. C. D. Poole, "Statistical treatment of polarization dispersion in single-mode fiber," Opt. Lett. **13**, 687–689 (1988).
50. K. Kitayama, S. Seikai, and N. Uchida, "Impulse response prediction based on experimental mode coupling coefficient in a 10-km long graded-index fiber," IEEE J. Quantum Electron. **16**, 356–362 (1980).
51. K.-P. Ho and J. M. Kahn, "Linear propagation effects in mode-division multiplexing systems," J. Lightwave Technol. **32**, 614–628 (2014).
52. K. Ho and J. Kahn, "Mode coupling and its impact on spatially multiplexed systems," in *Optical Fiber Telecommunications VI* (Elsevier, 2013), pp. 491–568.

53. K.-P. Ho and J. M. Kahn, "Delay-spread distribution for multimode fiber with strong mode coupling," IEEE Photon. Technol. Lett. **24**, 1906–1909 (2012).
54. K.-P. Ho and J. M. Kahn, "Statistics of group delays in multimode fiber with strong mode coupling," J. Lightwave Technol. **29**, 3119–3128 (2011).
55. M. L. Mehta, *Random Matrices* (Academic, 2004).
56. C. A. Tracy and H. Widom, "Level-spacing distributions and the Airy kernel," Phys. Lett. B **305**, 115–118 (1993).
57. K.-P. Ho, "Exact model for mode-dependent gains and losses in multimode fiber," J. Lightwave Technol. **30**, 3603–3609 (2012).
58. K.-P. Ho and J. M. Kahn, "Mode-dependent loss and gain: statistics and effect on mode-division multiplexing," Opt. Express **19**, 16612–16635 (2011).
59. A. Lobato, F. Ferreira, M. Kuschnerov, D. van den Borne, S. L. Jansen, A. Napoli, B. Spinnler, and B. Lankl, "Impact of mode coupling on the mode-dependent loss tolerance in few-mode fiber transmission," Opt. Express **20**, 29776–29783 (2012).
60. A. Andrusier, M. Shtaif, C. Antonelli, and A. Mecozzi, "Assessing the effects of mode-dependent loss in space-division multiplexed systems," J. Lightwave Technol. **32**, 1317–1322 (2014).
61. J. P. Gordon and H. Kogelnik, "PMD fundamentals: polarization mode dispersion in optical fibers," Proc. Natl. Acad. Sci. **97**, 4541–4550 (2000).
62. S. Warm and K. Petermann, "Capacity increase in spliced mode-muliplexed transmission systems by using mode mixers," in *IEEE Photonics Society Summer Topical Meeting Series* (IEEE, 2012), pp. 201–202.
63. F. Ferreira, D. Fonseca, A. Lobato, B. Inan, and H. Silva, "Reach improvement of mode division multiplexed systems using fiber splices," IEEE Photon. Technol. Lett. **25**, 1091–1094 (2013).
64. A. Li, C. Xi, A. Al Amin, and W. Shieh, "Mode converters and couplers for few-mode transmission," in *IEEE Photonics Society Summer Topical Meeting Series* (IEEE, 2012), pp. 197–198.
65. R. Ryf, R. J. Essiambre, S. Randel, M. A. Mestre, C. Schmidt, and P. J. Winzer, "Impulse response analysis of coupled-core 3-core fibers," in *European Conference and Exhibition on Optical Communication*, OSA Tech. Digest (online) (Optical Society of America, 2012), paper Mo.1.F.4.
66. C. Xia, N. Bai, R. Amezcua-Correa, E. Antonio-Lopez, A. Schulzgen, M. Richardson, X. Zhou, and G. Li, "Supermodes in strongly-coupled multicore fibers," in *Optical Fiber Communication Conference*, OSA Tech. Digest (Optical Society of America, 2013), paper OTh3K.
67. C. Xia, N. Bai, I. Ozdur, X. Zhou, and G. Li, "Supermodes for optical transmission," Opt. Express **19**, 16653–16664 (2011).
68. L. Ming-Jun, B. Hoover, V. N. Nazarov, and D. L. Butler, "Multicore fiber for optical interconnect applications," in *17th Opto-Electronics and Communications Conference (OECC)* (IEEE, 2012), pp. 564–565.
69. B. Zhu, T. Taunay, M. Yan, J. Fini, M. Fishteyn, E. Monberg, and F. Dimarcello, "Seven-core multicore fiber transmissions for passive optical network," Opt. Express **18**, 11117–11122 (2010).
70. V. Francois and F. Laramee, "Multicore fiber optimization for application to chip-to-chip optical interconnects," J. Lightwave Technol. **31**, 4022–4028 (2013).
71. M. A. Taubenblatt, "Space division multiplexing in data communications and high performance computing," in *IEEE Photonics Society Summer Topical Meeting Series* (IEEE, 2012), pp. 195–196.

72. C. Xia, R. Amezcua-Correa, N. Bai, E. Antonio-Lopez, D. M. Arrioja, A. Schulzgen, M. Richardson, J. Liñares, C. Montero, E. Mateo, X. Zhou, and G. Li, "Hole-assisted few-mode multicore fiber for high-density space-division multiplexing," IEEE Photon. Technol. Lett. **24**, 1914–1917 (2012).
73. Y. Kokubun and M. Koshiba, "Novel multi-core fibers for mode division multiplexing: proposal and design principle," IEICE Electron. Express **6**, 522–528 (2009).
74. K. Takenaga, Y. Sasaki, N. Guan, S. Matsuo, M. Kasahara, K. Saitoh, and M. Koshiba, "Large effective-area few-mode multicore fiber," IEEE Photon. Technol. Lett. **24**, 1941–1944 (2012).
75. Y. Sasaki, K. Takenaga, G. Ning, S. Matsuo, K. Saitoh, and M. Koshiba, "Large-effective-area uncoupled few-mode multi-core fiber," in *European Conference and Exhibition on Optical Communication*, OSA Tech. Digest (online) (Optical Society of America, 2012), paper Tu.1.F.3.
76. K. Takenaga, S. Matsuo, K. Saitoh, and M. Koshiba, "Multicore fiber with ring structure," in *IEEE Photonics Society Summer Topical Meeting Series* (IEEE, 2013), pp. 72–73.
77. J. M. Fini, B. Zhu, T. F. Taunay, M. F. Yan, and K. S. Abedin, "Statistical models of multicore fiber crosstalk including time delays," J. Lightwave Technol. **30**, 2003–2010 (2012).
78. J. M. Fini, B. Zhu, T. F. Taunay, M. F. Yan, and K. S. Abedin, "Crosstalk in multicore fibers with randomness: gradual drift vs. short-length variations," Opt. Express **20**, 949–959 (2012).
79. T. Hayashi, T. Sasaki, E. Sasaoka, K. Saitoh, and M. Koshiba, "Physical interpretation of intercore crosstalk in multicore fiber: effects of macrobend, structure fluctuation, and microbend," Opt. Express **21**, 5401–5412 (2013).
80. M. Koshiba, K. Saitoh, K. Takenaga, and S. Matsuo, "Analytical expression of average power-coupling coefficients for estimating intercore crosstalk in multicore fibers," IEEE Photon. J. **4**, 1987–1995 (2012).
81. K. Saitoh, M. Koshiba, K. Takenaga, and S. Matsuo, "Crosstalk and core density in uncoupled multicore fibers," IEEE Photon. Technol. Lett. **24**, 1898–1901 (2012).
82. K. Saitoh and S. Matsuo, "Multicore fibers for large capacity transmission," Nanophotonics **2**, 441–454 (2013).
83. K. Imamura, K. Mukasa, and T. Yagi, "Investigation on multi-core fibers with large Aeff and low micro bending loss," in *Optical Fiber Communication Conference*, OSA Tech. Digest (CD) (Optical Society of America, 2010), paper OWK6.
84. T. Sakamoto, K. Saitoh, N. Hanzawa, K. Tsujikawa, M. Lin, M. Koshiba, and F. Yamamoto, "Crosstalk suppressed hole-assisted 6-core fiber with cladding diameter of 125 μm," in *39th European Conference and Exhibition on Optical Communication (ECOC)* (2013), pp. 7–9.
85. X. Cen, R. Amezcua-Correa, B. Neng, E. Antonio-Lopez, D. May-Arrioja, A. Schulzgen, M. Richardson, J. Linares, C. Montero, E. Mateo, Z. Xiang, and L. Guifang, "Low-crosstalk few-mode multi-core fiber for high-mode-density space-division multiplexing," in *38th European Conference and Exhibition on Optical Communications (ECOC)*, OSA Tech. Digest (online) (Optical Society of America, 2012), paper Mo.1.F.5.
86. X. Cen, R. Amezcua-Correa, B. Neng, E. Antonio-Lopez, D. May-Arriojo, A. Schulzgen, M. Richardson, J. Linares, C. Montero, E. Mateo, Z. Xiang, and L. Guifang, "Hole-assisted few-mode multi-core fiber for high-density

space-division multiplexing," in *IEEE Photonics Society Summer Topical Meeting Series* (IEEE, 2012), pp. 206–207.
87. Z. Lin, G. Ren, S. Zheng, and S. Jian, "Wide-band dual-mode operation of multi-core fibers with air-hole structure," Opt. Laser Technol. **51**, 11–16 (2013).
88. T. Watanabe and Y. Kokubun, "Over 300 channels uncoupled few-mode multi-core fiber for space division multiplexing," in *Optical Fiber Communication Conference*, OSA Tech. Digest (online) (Optical Society of America, 2014), paper Th2A.50.
89. T. Watanabe and Y. Kokubun, "Ultra-large number of transmission channels in space division multiplexing using few-mode multi-core fiber with optimized air-hole-assisted double-cladding structure," Opt. Express **22**, 8309–8319 (2014).
90. T. Hayashi, T. Taru, O. Shimakawa, T. Sasaki, and E. Sasaoka, "Design and fabrication of ultra-low crosstalk and low-loss multi-core fiber," Opt. Express **19**, 16576–16592 (2011).
91. R. G. H. van Uden, R. Amezcua-Correa, E. Antonio-Lopez, F. M. Huijskens, G. Li, A. Schulzgen, H. de Waardt, and C. Okonkwo, "1 km hole-assisted few-mode multi-core fiber 32QAM WDM transmission," in *European Conference and Exhibition on Optical Communication (ECOC)* (2014), paper Mo 3.3.4.
92. M. Yoshida, T. Hirooka, M. Nakazawa, K. Imamura, R. Sugizaki, and T. Yagi, "Detailed comparison between mode couplings along multi-core fibers and structural irregularities using a synchronous multi-channel OTDR system with a high dynamic range," Opt. Express **21**, 29157–29164 (2013).
93. T. Jiajing, K. Saitoh, M. Koshiba, K. Takenaga, and S. Matsuo, "Optimized design method for bend-insensitive heterogeneous trench-assisted multi-core fiber with ultra-low crosstalk and high core density," J. Lightwave Technol. **31**, 2590–2598 (2013).
94. J. Tu, K. Saitoh, K. Takenaga, and S. Matsuo, "Heterogeneous trench-assisted few-mode multi-core fiber with low differential mode delay," Opt. Express **22**, 4329–4341 (2014).
95. D. Menashe, M. Tur, and Y. Danziger, "Interferometric technique for measuring dispersion of high order modes in optical fibres," Electron. Lett. **37**, 1439–1440 (2001).
96. S. Ramachandran and P. Gregg, "Looking inside a fiber: measuring mode content and properties," in *IEEE Photonics Society Summer Topical Meeting Series* (IEEE, 2013), p. 88.
97. S. Ramachandran, J. M. Fini, M. Mermelstein, J. W. Nicholson, S. Ghalmi, and M. F. Yan, "Ultra-large effective-area, higher-order mode fibers: a new strategy for high-power lasers," Laser Photon. Rev. **2**, 429–448 (2008).
98. S. Golowich, N. Bozinovic, P. Kristensen, and S. Ramachandran, "Complex mode amplitude measurement for a six-mode optical fiber," Opt. Express **21**, 4931–4944 (2013).
99. J. Jasapara and A. D. Yablon, "Spectrogram approach to S2 fiber mode analysis to distinguish between dispersion and distributed scattering," Opt. Lett. **37**, 3906–3908 (2012).
100. Y. Abe, K. Shikama, S. Yanagi, and T. Takahashi, "Physical-contact-type fan-out device for multicore fibre," Electron. Lett. **49**, 711–712 (2013).
101. W. Klaus, J. Sakaguchi, B. J. Puttnam, Y. Awaji, N. Wada, T. Kobayashi, and M. Watanabe, "Free-space coupling optics for multicore fibers," IEEE Photon. Technol. Lett. **24**, 1902–1905 (2012).

102. R. Nagase, "How to connect multicore and multimode fibers," in *Optical Fiber Communication Conference*, OSA Tech. Digest (online) (Optical Society of America, 2014), paper Tu3D.2.
103. N. Psaila, "Couplers for multicore fibers and 3D waveguide technology," in *Optical Fiber Communication Conference*, OSA Tech. Digest (online) (Optical Society of America, 2014), paper M3 K.3.
104. Y. Amma, Y. Arakawa, A. Takahashi, K. Takenaga, and S. Matsuo, "Low-loss fusion splice technique for multicore fiber with a large cladding diameter," in *IEEE Photonics Society Summer Topical Meeting Series* (IEEE, 2013), pp. 74–75.
105. Y. Tottori, H. Tsuboya, T. Kobayashi, and M. Watanabe, "Integrated optical connection module for 7-core multi-core fiber and 7 single mode fibers," in *IEEE Photonics Society Summer Topical Meeting Series* (IEEE, 2013), pp. 82–83.
106. W. Zheng, "Automated alignment and splicing for multicore fibers," in *Optical Fiber Communication Conference*, OSA Tech. Digest (online) (Optical Society of America, 2013), paper OM3I.4.
107. I. Giles, A. Obeysekara, R. Chen, D. Giles, F. Poletti, and D. Richardson, "Fiber LPG mode converters and mode selection technique for multimode SDM," IEEE Photon. Technol. Lett. **24**, 1922–1925 (2012).
108. M. Heinrich, M.-A. Miri, S. Stutzer, R. El-Ganainy, S. Nolte, A. Szameit, and D. N. Christodoulides, "Supersymmetric mode converters," arXiv:1401.5734 (2014).
109. D. A. B. Miller, "All linear optical devices are mode converters," Opt. Express **20**, 23985–23993 (2012).
110. C. Montero-Orille, V. Moreno, X. Prieto-Blanco, E. F. Mateo, E. Ip, J. Crespo, and J. Liñares, "Ion-exchanged glass binary phase plates for mode-division multiplexing," Appl. Opt. **52**, 2332–2339 (2013).
111. M. Salsi, C. Koebele, D. Sperti, P. Tran, H. Mardoyan, P. Brindel, S. Bigo, A. Boutin, F. Verluise, P. Sillard, M. Astruc, L. Provost, and G. Charlet, "Mode-division multiplexing of 2 100 Gb/s channels using an LCOS-based spatial modulator," J. Lightwave Technol. **30**, 618–623 (2012).
112. R. Ryf, C. A. Bolle, and J. von Hoyningen-Huene, "Optical coupling components for spatial multiplexing in multi-mode," in *37th European Conference and Exposition on Optical Communications*, OSA Tech. Digest (CD) (Optical Society of America, 2011), paper Th.12.B.1.
113. R. Ryf, N. K. Fontaine, and R. J. Essiambre, "Spot-based mode couplers for mode-multiplexed transmission in few-mode fiber," IEEE Photon. Technol. Lett. **24**, 1973–1976 (2012).
114. J. Carpenter and T. D. Wilkinson, "All optical mode-multiplexing using holography and multimode fiber couplers," J. Lightwave Technol. **30**, 1978–1984 (2012).
115. D. Flamm, C. Schulze, D. Naidoo, S. Schroter, A. Forbes, and M. Duparre, "All-digital holographic tool for mode excitation and analysis in optical fibers," J. Lightwave Technol. **31**, 1023–1032 (2013).
116. J. Carpenter and T. D. Wilkinson, "Holographic offset launch for dynamic optimization and characterization of multimode fiber bandwidth," J. Lightwave Technol. **30**, 1437–1443 (2012).
117. Y. Wakayama, A. Okamoto, K. Kawabata, A. Tomita, and K. Sato, "Mode demultiplexer using angularly multiplexed volume holograms," Opt. Express **21**, 12920–12933 (2013).

118. K. Aoki, A. Okamoto, Y. Wakayama, A. Tomita, and S. Honma, "Selective multimode excitation using volume holographic mode multiplexer," Opt. Lett. **38**, 769–771 (2013).
119. C. Haoshuo, V. Sleiffer, F. Huijskens, R. van Uden, C. Okonkwo, P. Leoni, M. Kuschnerov, L. Gruner-Nielsen, S. Yi, H. de Waardt, and T. Koonen, "Employing prism-based three-spot mode couplers for high capacity MDM/WDM transmission," IEEE Photon. Technol. Lett. **25**, 2474–2477 (2013).
120. R. Ryf, N. K. Fontaine, and R. Essiambre, "Spot-based mode coupler for mode-multiplexed transmission in few-mode fiber," in *IEEE Photonics Society Summer Topical Meeting Series* (IEEE, 2012), pp. 199–200.
121. N. K. Fontaine, R. Ryf, J. Bland-Hawthorn, and S. G. Leon-Saval, "Geometric requirements for photonic lanterns in space division multiplexing," Opt. Express **20**, 27123–27132 (2012).
122. I. Spaleniak, S. Gross, N. Jovanovic, R. J. Williams, J. S. Lawrence, M. J. Ireland, and M. J. Withford, "Multiband processing of multimode light: combining 3D photonic lanterns with waveguide Bragg gratings," Laser Photon. Rev. **8**, L1–L5 (2014).
123. J. Carpenter, S. G. Leon-Saval, J. R. Salazar-Gil, J. Bland-Hawthorn, G. Baxter, L. Stewart, S. Frisken, M. l. A. F. Roelens, B. J. Eggleton, and J. Schroder, "1×11 few-mode fiber wavelength selective switch using photonic lanterns," Opt. Express **22**, 2216–2221 (2014).
124. S. G. Leon-Saval, N. K. Fontaine, J. R. Salazar-Gil, B. Ercan, R. Ryf, and J. Bland-Hawthorn, "Mode-selective photonic lanterns for space-division multiplexing," Opt. Express **22**, 1036–1044 (2014).
125. S. Yerolatsitis, I. Gris-Sánchez, and T. A. Birks, "Adiabatically-tapered fiber mode multiplexers," Opt. Express **22**, 608–617 (2014).
126. N. Riesen and J. D. Love, "Weakly-guiding mode-selective fiber couplers," IEEE J. Quantum Electron. **48**, 941–945 (2012).
127. N. Riesen and J. D. Love, "Ultra-broadband tapered mode-selective couplers for few-mode optical fiber networks," IEEE Photon. Technol. Lett. **25**, 2501–2504 (2013).
128. N. Riesen and J. D. Love, "Tapered velocity mode-selective couplers," J. Lightwave Technol. **31**, 2163–2169 (2013).
129. N. Riesen, J. D. Love, and J. W. Arkwright, "Few-mode elliptical-core fiber data transmission," IEEE Photon. Technol. Lett. **24**, 344–346 (2012).
130. J. M. Kahn and K.-P. Ho, "Mode coupling effects in mode-division-multiplexed systems," in *IEEE Photonics Society Summer Topical Meeting Series* (IEEE, 2012), p. 203.
131. B. Huang, C. Xia, G. Matz, N. Bai, and G. Li, "Structured directional coupler pair for multiplexing of degenerate modes," in *Optical Fiber Communication Conference/National Fiber Optic Engineers Conference*, OSA Tech. Digest (online) (Optical Society of America, 2013), paper JW2A.25.
132. N. Riesen, J. D. Love, and J. W. Arkwright, "Few-core spatial-mode multiplexers/demultiplexers based on evanescent coupling," IEEE Photon. Technol. Lett. **25**, 1324–1327 (2013).
133. L. An, Y. Jia, C. Xi, and W. Shieh, "Fabrication of a low-loss fused fiber spatial-mode coupler for few-mode transmission," IEEE Photon. Technol. Lett. **25**, 1985–1988 (2013).
134. C. P. Tsekrekos and D. Syvridis, "Symmetric few-mode fiber couplers as the key component for broadband mode multiplexing," J. Lightwave Technol. **32**, 2461–2467 (2014).

135. M. Annamalai and M. Vasilyev, "Phase-sensitive multimode parametric amplification in a parabolic-index waveguide," IEEE Photon. Technol. Lett. **24**, 1949–1952 (2012).
136. N. Zhao, B. Huang, R. Amezcua-Correa, X. Li, and G. Li, "Few-mode fiber optical parametric amplifier," in *Optical Fiber Communication Conference/National Fiber Optic Engineers Conference*, OSA Tech. Digest (online) (Optical Society of America, 2013), paper OTu2D.5.
137. C. D. Stacey and R. M. Jenkins, "Demonstration of fundamental mode propagation in highly multimode fibre for high power EDFAs," in *Conference on Lasers and Electro-Optics Europe (CLEO/Europe)* (IEEE, 2005), p. 558.
138. E. Desurvire, *Erbium-Doped Fiber Amplifiers: Principles and Applications* (Wiley-Interscience, 1994).
139. M. Gong, Y. Yuan, C. Li, P. Yan, H. Zhang, and S. Liao, "Numerical modeling of transverse mode competition in strongly pumped multimode fiber lasers and amplifiers," Opt. Express **15**, 3236–3246 (2007).
140. Q. Kang, E.-L. Lim, Y. Jung, J. K. Sahu, F. Poletti, C. Baskiotis, S.-U. Alam, and D. J. Richardson, "Accurate modal gain control in a multimode erbium doped fiber amplifier incorporating ring doping and a simple LP01 pump configuration," Opt. Express **20**, 20835–20843 (2012).
141. G. Le Cocq, L. Bigot, A. Le Rouge, M. Bigot-Astruc, P. Sillard, C. Koebele, M. Salsi, and Y. Quiquempois, "Modeling and characterization of a few-mode EDFA supporting four mode groups for mode division multiplexing," Opt. Express **20**, 27051–27061 (2012).
142. N. Bai, E. Ip, T. Wang, and G. Li, "Multimode fiber amplifier with tunable modal gain using a reconfigurable multimode pump," Opt. Express **19**, 16601–16611 (2011).
143. N. Bai, E. Ip, Y. Luo, G.-D. Peng, T. Wang, and G. Li, "Experimental study on multimode fiber amplifier using modal reconfigurable pump," in *Optical Fiber Communication Conference*, OSA Tech. Digest (Optical Society of America, 2012), paper OW1D.3.
144. Y. Yung, S.-U. Alam, Z. Li, A. Dhar, D. Giles, I. Giles, J. Sahu, L. Grüner-Nielsen, F. Poletti, and D. Richardson, "First demonstration of multimode amplifier for spatial division multiplexed transmission systems," in *37th European Conference and Exposition on Optical Communications*, OSA Tech. Digest (CD) (Optical Society of America, 2011), paper Th.13.K.4.
145. M. Salsi, J. Vuong, C. Koebele, P. Genevaux, H. Mardoyan, P. Tran, S. Bigo, G. Le Cocq, L. Bigot, Y. Quiquempois, A. Le Rouge, P. Sillard, M. Bigot-Astruc, and G. Charlet, "In-line few-mode optical amplifier with erbium profile tuned to support LP01, LP11, and LP21 mode groups," in *38th European Conference and Exhibition on Optical Communications (ECOC)*, OSA Tech. Digest (online) (Optical Society of America, 2012), paper Tu.3.F.1.
146. M. Salsi, D. Peyrot, G. Charlet, S. Bigo, R. Ryf, N. K. Fontaine, M. A. Mestre, S. Randel, X. Palou, C. Bolle, B. Guan, G. Le Cocq, L. Bigot, and Y. Quiquempois, "A six-mode erbium-doped fiber amplifier," in *European Conference and Exhibition on Optical Communication*, OSA Tech. Digest (online) (Optical Society of America, 2012), paper Th.3.A.6.
147. G. Le Cocq, Y. Quiquempois, A. Le Rouge, G. Bouwmans, H. El Hamzaoui, K. Delplace, M. Bouazaoui, and L. Bigot, "Few mode

Er^{3+} doped fiber with micro-structured core for mode division multiplexing in the C-band," Opt. Express **21**, 31646–31659 (2013).
148. E. Ip, "Gain equalization for few-mode fiber amplifiers beyond two propagating mode groups," IEEE Photon. Technol. Lett. **24**, 1933–1936 (2012).
149. S. Akhtari and P. M. Krummrich, "Impact of mode beating effects in optical multi-mode amplifiers for space division multiplexing," IEEE Photon. Technol. Lett. **25**, 2482–2485 (2013).
150. E. E. L. Lim, Y. Jung, Q. Kang, T. C. May-Smith, N. H. L. Wong, R. Standish, F. Poletti, J. K. Sahu, S. Alam, and D. J. Richardson, "First demonstration of cladding pumped few-moded EDFA for mode division multiplexed transmission," in *Optical Fiber Communication Conference*, OSA Tech. Digest (online) (Optical Society of America, 2014), paper M2 J.2.
151. R. Ryf, R. Essiambre, J. von Hoyningen-Huene, and P. Winzer, "Analysis of mode-dependent gain in Raman amplified few-mode fiber," in *Optical Fiber Communication Conference*, OSA Tech. Digest (Optical Society of America, 2012), paper OW1D.2.
152. R. Ryf, A. Sierra, R.-J. Essiambre, S. Randel, A. Gnauck, C. A. Bolle, M. Esmaeelpour, P. J. Winzer, R. Delbue, P. Pupalaikis, A. Sureka, D. Peckham, A. McCurdy, and R. Lingle, "Mode-equalized distributed Raman amplification in 137-km few-mode fiber," in *37th European Conference and Exposition on Optical Communications*, OSA Tech. Digest (CD) (Optical Society of America, 2011), paper Th.13.K.5.
153. C. Antonelli, A. Mecozzi, and M. Shtaif, "Raman amplification in multimode fibers with random mode coupling," Opt. Lett. **38**, 1188–1190 (2013).
154. K. Abedin, T. Taunay, M. Fishteyn, M. Yan, B. Zhu, J. Fini, E. Monberg, F. Dimarcello, and P. Wisk, "Amplification and noise properties of an erbium-doped multicore fiber amplifier," Opt. Express **19**, 16715–16721 (2011).
155. Y. Tsuchida, K. Maeda, K. Watanabe, T. Saito, S. Matsumoto, K. Aiso, Y. Mimura, and R. Sugizaki, "Simultaneous 7-core pumped amplification in multicore EDF through fibre based fan-in/out," in *European Conference and Exhibition on Optical Communication*, OSA Tech. Digest (online) (Optical Society of America, 2012), paper Tu.4.F.2.
156. P. M. Krummrich, "Optical amplification and optical filter based signal processing for cost and energy efficient spatial multiplexing," Opt. Express **19**, 16636–16652 (2011).
157. Y. Mimura, Y. Tsuchida, K. Maeda, R. Miyabe, K. Aiso, H. Matsuura, and R. Sugizaki, "Batch multicore amplification with cladding-pumped multicore EDF," in *European Conference and Exhibition on Optical Communication*, OSA Tech. Digest (online) (Optical Society of America, 2012), paper Tu.4.F.2.
158. K. Abedin, T. Taunay, M. Fishteyn, D. DiGiovanni, V. Supradeepa, J. Fini, M. Yan, B. Zhu, E. Monberg, and F. Dimarcello, "Cladding-pumped erbium-doped multicore fiber amplifier," Opt. Express **20**, 20191–20200 (2012).
159. P. M. Krummrich, "Optical amplifiers for multi mode/multi core transmission," in *Optical Fiber Communication Conference*, OSA Tech. Digest (Optical Society of America, 2012), paper OW1D.1.
160. H. Ono, M. Yamada, K. Takenaga, S. Matsuo, Y. Abe, K. Shikama, and T. Takahashi, "Amplification method for crosstalk reduction in multi-core fibre amplifier," Electron. Lett. **49**, 138–140 (2013).

161. I. Ozdur, H. Shu, M. Bass, and G. Li, "Think outside the fiber: imaging amplifier for space-multiplexed optical transmission," IEEE Photon. J. **4**, 1316–1324 (2012).
162. K. Igarashi, T. Tsuritani, I. Morita, Y. Tsuchida, K. Maeda, M. Tadakuma, T. Saito, K. Watanabe, K. Imamura, R. Sugizaki, and M. Suzuki, "Super-Nyquist-WDM transmission over 7,326-km seven-core fiber with capacity-distance product of 1.03 Exabit/s·km," Opt. Express **22**, 1220–1228 (2014).
163. T. Kobayashi, H. Takara, A. Sano, T. Mizuno, H. Kawakami, Y. Miyamoto, K. Hiraga, Y. Abe, H. Ono, M. Wada, Y. Sasaki, I. Ishida, K. Takenaga, S. Matsuo, K. Saitoh, M. Yamada, H. Masuda, and T. Morioka, "2 × 344 Tb/s propagation-direction interleaved transmission over 1500-km MCF enhanced by multicarrier full electric-field digital back-propagation," in *39th European Conference and Exhibition on Optical Communication (ECOC)* (2013).
164. H. Takahashi, T. Tsuritani, E. L. T. de Gabory, T. Ito, W. R. Peng, K. Igarashi, K. Takeshima, Y. Kawaguchi, I. Morita, Y. Tsuchida, Y. Mimura, K. Maeda, T. Saito, K. Watanabe, K. Imamura, R. Sugizaki, and M. Suzuki, "First demonstration of MC-EDFA-repeatered SDM transmission of 40 × 128-Gbit/s PDM-QPSK signals per core over 6,160-km 7-core MCF," Opt. Express **21**, 789–795 (2013).
165. A. H. Gnauck, S. Chandrasekhar, X. Liu, S. Randel, S. Corteselli, T. Taunay, B. Zhu, and M. Fishteyn, "WDM transmission of 603-Gb/s superchannels over 845 km of 7-core fiber with 42.2 b/s/Hz spectral efficiency," in *European Conference and Exhibition on Optical Communication*, OSA Tech. Digest (online) (Optical Society of America, 2012), paper Th.2.C.2.
166. J. Sakaguchi, B. J. Puttnam, W. Klaus, Y. Awaji, N. Wada, A. Kanno, T. Kawanishi, K. Imamura, H. Inaba, K. Mukasa, R. Sugizaki, T. Kobayashi, and M. Watanabe, "305 Tb/s space division multiplexed transmission using homogeneous 19-core fiber," J. Lightwave Technol. **31**, 554–562 (2013).
167. S. Chandrasekhar, A. Gnauck, X. Liu, P. Winzer, Y. Pan, E. C. Burrows, B. Zhu, T. Taunay, M. Fishteyn, M. Yan, J. M. Fini, E. Monberg, and F. Dimarcello, "WDM/SDM transmission of 10 × 128-Gb/s PDM-QPSK over 2688-km 7-core fiber with a per-fiber net aggregate spectral-efficiency distance product of 40,320 km. b/s/Hz," in *European Conference and Exposition on Optical Communications*, OSA Tech. Digest (CD) (Optical Society of America, 2011), paper Th.13.C.4.
168. X. Liu, S. Chandrasekhar, X. Chen, P. Winzer, Y. Pan, B. Zhu, T. Taunay, M. Fishteyn, M. Yan, J. M. Fini, E. Monberg, and F. Dimarcello, "1.12-Tb/s 32-QAM-OFDM superchannel with 8.6-b/s/Hz intrachannel spectral efficiency and space-division multiplexing with 60-b/s/Hz aggregate spectral efficiency," in *37th European Conference and Exposition on Optical Communications*, OSA Tech. Digest (CD) (Optical Society of America, 2011), paper Th.13.B.1.
169. R. Ryf, A. Sierra, R. Essiambre, A. Gnauck, S. Randel, M. Esmaeelpour, S. Mumtaz, P. J. Winzer, R. Delbue, P. Pupalaikis, A. Sureka, T. Hayashi, T. Taru, and T. Sasaki, "Coherent 1200-km 6 × 6 MIMO mode-multiplexed transmission over 3-core microstructured fiber," in *37th European Conference and Exposition on Optical Communications*, OSA Tech. Digest (CD) (Optical Society of America, 2011), paper Th.13.C.1.

170. B. Zhu, T. Taunay, M. Fishteyn, X. Liu, S. Chandrasekhar, M. Yan, J. Fini, E. Monberg, and F. Dimarcello, "112-Tb/s space-division multiplexed DWDM transmission with 14-b/s/Hz aggregate spectral efficiency over a 76.8-km seven-core fiber," Opt. Express **19**, 16665–16671 (2011).
171. B. Zhu, T. Taunay, M. Fishteyn, X. Liu, S. Chandrasekhar, M. Yan, J. Fini, E. Monberg, and F. Dimarcello, "Space-, wavelength-, polarization-division multiplexed transmission of 56-Tb/s over a 76.8-km seven-core fiber," in *Optical Fiber Communication Conference/National Fiber Optic Engineers Conference*, OSA Tech. Digest (CD) (Optical Society of America, 2011), paper PDPB7.
172. J. Sakaguchi, Y. Awaji, N. Wada, A. Kanno, T. Kawanishi, T. Hayashi, T. Taru, T. Kobayashi, and M. Watanabe, "109-Tb/s (7 × 97 × 172-Gb/s SDM/WDM/PDM) QPSK transmission through 16.8-km homogeneous multi-core fiber," in *Optical Fiber Communication Conference/National Fiber Optic Engineers Conference*, OSA Tech. Digest (CD) (Optical Society of America, 2011), paper PDPB6.
173. D. Qian, E. Ip, M.-F. Huang, M.-J. Li, A. Dogariu, S. Zhang, Y. Shao, Y.-K. Huang, Y. Zhang, X. Cheng, Y. Tian, P. Ji, A. Collier, Y. Geng, J. Linares, C. Montero, V. Moreno, X. Prieto, and T. Wang, "1.05 Pb/s transmission with 109 b/s/Hz spectral efficiency using hybrid single- and few-mode cores," in *Frontiers in Optics 2012/Laser Science XXVIII*, OSA Tech. Digest (online) (Optical Society of America, 2012), paper FW6C.3.
174. R. Ryf, N. K. Fontaine, H. Chen, B. Guan, S. Randel, N. Sauer, S. J. B. Yoo, A. Koonen, R. Delbue, P. Pupalaikis, A. Sureka, R. Shubochkin, Y. Sun, and R. Lingle, "23 Tbit/s transmission over 17-km conventional 50 μm graded-index multimode fiber," in *Optical Fiber Communication Conference: Postdeadline Papers* (Optical Society of America, 2014), paper Th5B.1.
175. R. Ryf, S. Randel, N. K. Fontaine, M. Montoliu, E. Burrows, S. Chandrasekhar, A. H. Gnauck, C. Xie, R. Essiambre, P. Winzer, R. Delbue, P. Pupalaikis, A. Sureka, Y. Sun, L. Gruner-Nielsen, R. V. Jensen, and R. Lingle, "32-bit/s/Hz spectral efficiency WDM transmission over 177-km few-mode fiber," in *Optical Fiber Communication Conference/National Fiber Optic Engineers Conference 2013*, OSA Tech. Digest (online) (Optical Society of America, 2013), paper PDP5A.1.
176. Y. Jung, V. Sleiffer, N. Baddela, M. Petrovich, J. R. Hayes, N. Wheeler, D. Gray, E. R. Numkam Fokoua, J. Wooler, N. Wong, F. Parmigiani, S. Alam, J. Surof, M. Kuschnerov, V. Veljanovski, H. de Waardt, F. Poletti, and D. J. Richardson, "First demonstration of a broadband 37-cell hollow core photonic bandgap fiber and its application to high capacity mode division multiplexing," in *Optical Fiber Communication Conference/National Fiber Optic Engineers Conference*, OSA Tech. Digest (online) (Optical Society of America, 2013), paper PDP5A.3.
177. R. Ryf, N. K. Fontaine, M. A. Mestre, S. Randel, X. Palou, C. Bolle, A. H. Gnauck, S. Chandrasekhar, X. Liu, B. Guan, R. Essiambre, P. J. Winzer, S. Leon-Saval, J. Bland-Hawthorn, R. Delbue, P. Pupalaikis, A. Sureka, Y. Sun, L. Grüner-Nielsen, R. V. Jensen, and R. Lingle, "12 × 12 MIMO transmission over 130-km few-mode fiber," in *Frontiers in Optics 2012/Laser Science XXVIII*, OSA Tech. Digest (online) (Optical Society of America, 2012), paper FW6C.4.

178. V. Sleiffer, Y. Jung, V. Veljanovski, R. van Uden, M. Kuschnerov, Q. Kang, L. Grüner-Nielsen, Y. Sun, D. Richardson, S. Alam, F. Poletti, J. Sahu, A. Dhar, H. Chen, B. Inan, T. Koonen, B. Corbett, R. Winfield, A. Ellis, and H. de Waardt, "73.7 Tb/s (96 × 3 × 256-Gb/s) mode-division-multiplexed DP-16QAM transmission with inline MM-EDFA," in *European Conference and Exhibition on Optical Communication (ECOC)* (Optical Society of America, 2012), paper Th.3.C.4.
179. R. Ryf, M. Mestre, S. Randel, C. Schmidt, A. Gnauck, R. Essiambre, P. Winzer, R. Delbue, P. Pupalaikis, A. Sureka, Y. Sun, X. Jiang, D. W. Peckham, A. McCurdy, and R. Lingle, "Mode-multiplexed transmission over a 209-km DGD-compensated hybrid few-mode fiber span," IEEE Photon. Technol. Lett. **24**, 1965–1968 (2012).
180. S. Randel, R. Ryf, A. Gnauck, M. A. Mestre, C. Schmidt, R. Essiambre, P. Winzer, R. Delbue, P. Pupalaikis, A. Sureka, Y. Sun, X. Jiang, and R. Lingle, "Mode-multiplexed 6 × 20-GBd QPSK transmission over 1200-km DGD-compensated few-mode fiber," in *National Fiber Optic Engineers Conference*, OSA Tech. Digest (Optical Society of America, 2012), paper PDP5C.5.
181. E. Ip, N. Bai, Y. Huang, E. Mateo, F. Yaman, M. Li, S. Bickham, S. Ten, Y. Luo, G. Peng, G. Li, T. Wang, J. Linares, C. Montero, and V. Moreno, "6×6 MIMO transmission over 50 + 25 + 10 km heterogeneous spans of few-mode fiber with inline erbium-doped fiber amplifier," in *Optical Fiber Communication Conference*, OSA Tech. Digest (Optical Society of America, 2012), paper OTu2C.4.
182. C. Koebele, M. Salsi, L. Milord, R. Ryf, C. A. Bolle, P. Sillard, S. Bigo, and G. Charlet, "40 km transmission of five mode division multiplexed data streams at 100 Gb/s with low MIMO-DSP complexity," in *37th European Conference and Exposition on Optical Communications*, OSA Tech. Digest (CD) (Optical Society of America, 2011), paper Th.13.C.3.
183. E. Ip, N. Bai, Y.-K. Huang, E. Mateo, F. Yaman, S. Bickham, H.-Y. Tam, C. Lu, M.-J. Li, S. Ten, A. P. T. Lau, V. Tse, G.-D. Peng, C. Montero, X. Prieto, and G. Li, "88 × 3 × 112-Gb/s WDM transmission over 50-km of three-mode fiber with inline multimode fiber amplifier," in *37th European Conference and Exposition on Optical Communications*, OSA Tech. Digest (CD) (Optical Society of America, 2011), paper Th.13.C.2.
184. R. Ryf, S. Randel, A. H. Gnauck, C. Bolle, R. Essiambre, P. J. Winzer, D. W. Peckham, A. McCurdy, and R. Lingle, "Space-division multiplexing over 10 km of three-mode fiber using coherent 6 × 6 MIMO processing," in *Optical Fiber Communication Conference/National Fiber Optic Engineers Conference*, OSA Tech. Digest (CD) (Optical Society of America, 2011), paper PDPB10.
185. M. Salsi, C. Koebele, D. Sperti, P. Tran, P. Brindel, H. Mardoyan, S. Bigo, A. Boutin, F. Verluise, P. Sillard, M. Bigot-Astruc, L. Provost, F. Cerou, and G. Charlet, "Transmission at 2 × 100 Gb/s, over two modes of 40km-long prototype few-mode fiber, using LCOS based mode multiplexer and demultiplexer," in *Optical Fiber Communication Conference/National Fiber Optic Engineers Conference*, OSA Tech. Digest (CD) (Optical Society of America, 2011), paper PDPB9.
186. A. Li, A. Al Amin, X. Chen, and W. Shieh, "Reception of mode and polarization multiplexed 107-Gb/s CO-OFDM signal over a two-mode fiber," in

Optical Fiber Communication Conference/National Fiber Optic Engineers Conference, OSA Tech. Digest (CD) (Optical Society of America, 2011), paper PDPB8.
187. H. Takara, A. Sano, T. Kobayashi, H. Kubota, H. Kawakami, A. Matsuura, Y. Miyamoto, Y. Abe, H. Ono, K. Shikama, Y. Goto, K. Tsujikawa, Y. Sasaki, I. Ishida, K. Takenaga, S. Matsuo, K. Saitoh, M. Koshiba, and T. Morioka, "1.01-Pb/s (12 SDM/222 WDM/456 Gb/s) crosstalk-managed transmission with 91.4-b/s/Hz aggregate spectral efficiency," in *European Conference and Exhibition on Optical Communication*, OSA Tech. Digest (online) (Optical Society of America, 2012), paper Th.3.C.1.
188. K. Igarashi, T. Tsuritani, I. Morita, Y. Tsuchida, K. Maeda, M. Tadakuma, T. Saito, K. Watanabe, K. Imamura, R. Sugizaki, and M. Suzuki, "1.03-Exabit/skm super-Nyquist-WDM transmission over 7,326-km seven-core fiber," in *39th European Conference and Exhibition on Optical Communication (ECOC)* (2013).
189. R. Ryf, R. Essiambre, A. Gnauck, S. Randel, M. A. Mestre, C. Schmidt, P. Winzer, R. Delbue, P. Pupalaikis, A. Sureka, T. Hayashi, T. Taru, and T. Sasaki, "Space-division multiplexed transmission over 4200 km 3-core microstructured fiber," in *Optical Fiber Communication Conference*, OSA Tech. Digest (Optical Society of America, 2012), paper PDP5C.2.
190. E. Ip, M.-J. Li, C. Montero, and Y. Yano, "6×28-Gbaud few-mode recirculating loop transmission with gain-equalized inline few-mode fiber amplifier," in *Optical Fiber Communication Conference/National Fiber Optic Engineers Conference*, OSA Tech. Digest (online) (Optical Society of America, 2013), paper OW4F.3.
191. E. Ip, M.-J. Li, Y.-K. Huang, A. Tanaka, E. Mateo, W. Wood, J. Hu, Y. Yano, and K. Koreshkov, "146λ × 6 × 19-Gbaud wavelength-and mode-division multiplexed transmission over 10 × 50-km spans of few-mode fiber with a gain-equalized few-mode EDFA," in *Optical Fiber Communication Conference/National Fiber Optic Engineers Conference*, OSA Tech. Digest (online) (Optical Society of America, 2013), paper PDP5A.2.
192. T. Mizuno, T. Kobayashi, H. Takara, A. Sano, H. Kawakami, T. Nakagawa, Y. Miyamoto, Y. Abe, T. Goh, M. Oguma, T. Sakamoto, Y. Sasaki, I. Ishida, K. Takenaga, S. Matsuo, K. Saitoh, and T. Morioka, "12-core × 3-mode dense space division multiplexed transmission over 40 km employing multi-carrier signals with parallel MIMO equalization," in *Optical Fiber Communication Conference: Postdeadline Papers* (Optical Society of America, 2014), paper Th5B.2.
193. P. J. Winzer and G. J. Foschini, "Outage calculations for spatially multiplexed fiber links," in *Optical Fiber Communication Conference/National Fiber Optic Engineers Conference*, OSA Tech. Digest (CD) (Optical Society of America, 2011), paper OThO5.
194. S. Warm and K. Petermann, "Splice loss requirements in multi-mode fiber mode-division-multiplex transmission links," Opt. Express **21**, 519–532 (2013).
195. D. Rafique, S. Sygletos, and A. D. Ellis, "Impact of power allocation strategies in long-haul few-mode fiber transmission systems," Opt. Express **21**, 10801–10809 (2013).
196. P. J. Winzer and G. J. Foschini, "MIMO capacities and outage probabilities in spatially multiplexed optical transport systems," Opt. Express **19**, 16680–16696 (2011).

197. I. B. Djordjevic, "Energy-efficient spatial-domain-based hybrid multidimensional coded-modulations enabling multi-Tb/s optical transport," Opt. Express **19**, 16708–16714 (2011).
198. I. B. Djordjevic, "Spatial-domain-based hybrid multidimensional coded-modulation schemes enabling multi-Tb/s optical transport," J. Lightwave Technol. **30**, 3888–3901 (2012).
199. I. B. Djordjevic, M. Arabaci, L. Xu, and T. Wang, "Spatial-domain-based multidimensional modulation for multi-Tb/s serial optical transmission," Opt. Express **19**, 6845–6857 (2011).
200. I. B. Djordjevic, T. Liu, and T. Wang, "On the adaptive software-defined LDPC-coded multidimensional spatial-MIMO multiband generalized OFDM enabling beyond 10-Tb/s optical transport," IEEE Photon. J. **5**, 7200207 (2013).
201. I. B. Djordjevic, T. Liu, L. Xu, and T. Wang, "On the multidimensional signal constellation design for few-mode-fiber-based high-speed optical transmission," IEEE Photon. J. **4**, 1325–1332 (2012).
202. I. B. Djordjevic, L. Xu, and T. Wang, "Multidimensional hybrid modulations for ultrahigh-speed optical transport," IEEE Photon. J. **3**, 1030–1038 (2011).
203. A. D. Ellis, N. Mac Suibhne, F. C. G. Gunning, and S. Sygletos, "Expressions for the nonlinear transmission performance of multi-mode optical fiber," Opt. Express **21**, 22834–22846 (2013).
204. F. Ferreira, S. Jansen, P. Monteiro, and H. Silva, "Nonlinear semi-analytical model for simulation of few-mode fiber transmission," IEEE Photon. Technol. Lett. **24**, 240–242 (2012).
205. R. Essiambre, M. A. Mestre, R. Ryf, A. H. Gnauck, R. W. Tkach, A. R. Chraplyvy, S. Yi, J. Xinli, and R. Lingle, "Experimental observation of inter-modal cross-phase modulation in few-mode fibers," IEEE Photon. Technol. Lett. **25**, 535–538 (2013).
206. R. Essiambre, M. A. Mestre, R. Ryf, A. H. Gnauck, R. W. Tkach, A. R. Chraplyvy, S. Yi, J. Xinli, and R. Lingle, "Experimental investigation of inter-modal four-wave mixing in few-mode fibers," IEEE Photon. Technol. Lett. **25**, 539–542 (2013).
207. G. Rademacher, S. Warm, and K. Petermann, "Nonlinear interference in mode multiplexed multi-mode fibers," in *IEEE Photonics Society Summer Topical Meeting Series* (IEEE, 2012), pp. 177–178.
208. G. Rademacher, S. Warm, and K. Petermann, "Analytical description of cross-modal nonlinear interaction in mode multiplexed multimode fibers," IEEE Photon. Technol. Lett. **24**, 1929–1932 (2012).
209. X. Chen, A. Li, G. Gao, and W. Shieh, "Study of fiber nonlinearity impact on the system capacity of two-mode fibers," in *Optical Fiber Communication Conference*, OSA Tech. Digest (Optical Society of America, 2012), paper JW2A.40.
210. C. Koebele, M. Salsi, G. Charlet, and S. Bigo, "Nonlinear effects in long-haul transmission over bimodal optical fibre," in *36th European Conference and Exhibition on Optical Communication (ECOC)* (2010).
211. C. Koebele, M. Salsi, G. Charlet, and S. Bigo, "Nonlinear effects in mode-division-multiplexed transmission over few-mode optical fiber," IEEE Photon. Technol. Lett. **23**, 1316–1318 (2011).

212. S. Mumtaz, R.-J. Essiambre, and G. P. Agrawal, "Reduction of nonlinear penalties due to linear coupling in multicore optical fibers," IEEE Photon. Technol. Lett. **24**, 1574–1576 (2012).
213. G. Rademacher, S. Warm, and K. Petermann, "Influence of discrete mode coupling on the nonlinear interaction in mode-multiplexed systems," IEEE Photon. Technol. Lett. **25**, 1203–1206 (2013).
214. G. Rademacher, S. Warm, and K. Petermann, "Splice induced nonlinear performance penalty in mode-division multiplexed transmission systems," in *39th European Conference and Exhibition on Optical Communication (ECOC)* (2013).
215. G. Rademacher, S. Warm, and K. Petermann, "Splice induced performance penalty in mode multiplexed few-mode fibers," in *IEEE Photonics Society Summer Topical Meeting Series* (IEEE, 2013), pp. 123–124.
216. S. Mumtaz, R. Essiambre, and G. P. Agrawal, "Nonlinear propagation in multimode and multicore fibers: generalization of the Manakov equations," J. Lightwave Technol. **31**, 398–406 (2013).
217. A. Mecozzi, C. Antonelli, and M. Shtaif, "Nonlinear propagation in multimode fibers in the strong coupling regime," Opt. Express **20**, 11673–11678 (2012).
218. A. Mecozzi, C. Antonelli, and M. Shtaif, "Coupled Manakov equations in multimode fibers with strongly coupled groups of modes," Opt. Express **20**, 23436–23441 (2012).
219. H. Louchet, A. A. Juarez, C. A. Bunge, P. M. Krummrich, A. Richter, and K. Petermann, "Capacity upgrade of legacy fiber plant using space division multiplexing and multimode/multicore EDFAs," in *37th European Conference and Exposition on Optical Communications*, OSA Tech. Digest (CD) (Optical Society of America, 2011), paper We.10.P1.74.
220. F. Yaman, N. Bai, Y. K. Huang, M. F. Huang, B. Zhu, T. Wang, and G. Li, "10 × 112 Gb/s PDM-QPSK transmission over 5032 km in few-mode fibers," Opt. Express **18**, 21342–21349 (2010).
221. N. Bai, C. Xia, and G. Li, "Adaptive frequency-domain equalization for the transmission of the fundamental mode in a few-mode fiber," Opt. Express **20**, 24010–24017 (2012).
222. A. Li, X. Chen, A. Al Amin, J. Ye, and W. Shieh, "Space-division multiplexed high-speed superchannel transmission over few-mode fiber," J. Lightwave Technol. **30**, 3953–3964 (2012).
223. S. Chandrasekhar, L. Xiang, B. Zhu, and D. W. Peckham, "Transmission of a 1.2-Tb/s 24-carrier no-guard-interval coherent OFDM superchannel over 7200-km of ultra-large-area fiber," in *35th European Conference on Optical Communication (ECOC)* (2009).
224. J. A. Carpenter, S. G. Leon-Saval, J. R. Salazar Gil, J. Bland-Hawthorn, G. Baxter, L. Stewart, S. Frisken, M. A. Roelens, B. J. Eggleton, and J. Schröder, "1×11 few-mode fiber wavelength selective switch using photonic lanterns," in *Optical Fiber Communication Conference*, OSA Tech. Digest (online) (Optical Society of America, 2014), paper Th4A.2.
225. N. K. Fontaine, R. Ryf, and D. T. Neilson, "Fiber-port-count in wavelength selective switches for space-division multiplexing," in *39th European Conference and Exhibition on Optical Communication (ECOC)* (2013), pp. 609–611.

226. N. K. Fontaine, R. Ryf, B. Guan, and D. T. Neilson, "Wavelength blocker for few-mode-fiber space-division multiplexed systems," in *Optical Fiber Communication Conference/National Fiber Optic Engineers Conference*, OSA Tech. Digest (online) (Optical Society of America, 2013), paper OTh1B.1.
227. L. E. Nelson, M. D. Feuer, K. Abedin, X. Zhou, T. F. Taunay, J. M. Fini, B. Zhu, R. Isaac, R. Harel, G. Cohen, and D. M. Marom, "Spatial superchannel routing in a two-span ROADM system for space division multiplexing," J. Lightwave Technol. **32**, 783–789 (2014).
228. C. Xi, L. An, Y. Jia, A. Al Amin, and W. Shieh, "Demonstration of few-mode compatible optical add/drop multiplexer for mode-division multiplexed superchannel," J. Lightwave Technol. **31**, 641–647 (2013).
229. M.-Y. Chen and J. Zhou, "Design of add-drop multiplexer based on multicore optical fibers for mode-division multiplexing," Opt. Express **22**, 1440–1451 (2014).
230. D. A. B. Miller, "Reconfigurable add-drop multiplexer for spatial modes," Opt. Express **21**, 20220–20229 (2013).
231. K.-P. Ho, J. M. Kahn, and J. P. Wilde, "Wavelength-selective switches for mode-division-multiplexed systems," arXiv:1401.7090 (2014).
232. P. Sillard, M. Astruc, D. Boivin, H. Maerten, and L. Provost, "Few-mode fiber for uncoupled mode-division multiplexing transmissions," in *37th European Conference and Exposition on Optical Communications*, OSA Tech. Digest (CD) (Optical Society of America, 2011), paper Tu.5. LeCervin.7.
233. C. P. Tsekrekos and D. Syvridis, "All-fiber broadband mode converter for future wavelength and mode division multiplexing systems," IEEE Photon. Technol. Lett. **24**, 1638–1641 (2012).
234. M. Cvijetic, I. B. Djordjevic, and N. Cvijetic, "Dynamic multidimensional optical networking based on spatial and spectral processing," Opt. Express **20**, 9144–9150 (2012).
235. N. Amaya, M. Irfan, G. Zervas, R. Nejabati, D. Simeonidou, J. Sakaguchi, W. Klaus, B. J. Puttnam, T. Miyazawa, Y. Awaji, N. Wada, and I. Henning, "Fully-elastic multi-granular network with space/frequency/time switching using multi-core fibres and programmable optical nodes," Opt. Express **21**, 8865–8872 (2013).
236. N. Amaya, S. Yan, M. Channegowda, B. R. Rofoee, Y. Shu, M. Rashidi, Y. Ou, G. Zervas, R. Nejabati, D. Simeonidou, B. J. Puttnam, W. Klaus, J. Sakaguchi, T. Miyazawa, Y. Awaji, H. Harai, and N. Wada, "First demonstration of software defined networking (SDN) over space division multiplexing (SDM) optical networks," in *39th European Conference and Exhibition on Optical Communication (ECOC)* (2013).
237. S. Bagheri and W. M. J. Green, "Silicon-on-insulator mode-selective add-drop unit for on-chip mode-division multiplexing," in *6th IEEE International Conference on Group IV Photonics (GFP)* (IEEE, 2009), pp. 166–168.
238. C. P. Chen, J. B. Driscoll, N. Ophir, R. R. Grote, R. M. Osgood, and K. Bergman, "First demonstration of polarization-multiplexing combined with on-chip mode-division-multiplexing," in *Optical Fiber Communication Conference*, OSA Tech. Digest (online) (Optical Society of America, 2014), paper Th4A.3.

239. D. Dai, J. Wang, and S. He, "Silicon multimode photonic integrated devices for on-chip mode-division-multiplexed optical interconnects," (invited review) Prog. Electromagn. Res. **143**, 773–819 (2013).
240. D. Dai, J. Wang, and Y. Shi, "Silicon mode (de)multiplexer enabling high capacity photonic networks-on-chip with a single-wavelength-carrier light," Opt. Lett. **38**, 1422–1424 (2013).
241. Y. Ding, J. Xu, F. Da Ros, B. Huang, H. Ou, and C. Peucheret, "On-chip two-mode division multiplexing using tapered directional coupler-based mode multiplexer and demultiplexer," Opt. Express **21**, 10376–10382 (2013).
242. J. B. Driscoll, R. R. Grote, B. Souhan, J. I. Dadap, M. Lu, and R. M. Osgood, "Asymmetric Y junctions in silicon waveguides for on-chip mode-division multiplexing," Opt. Lett. **38**, 1854–1856 (2013).
243. L.-W. Luo, N. Ophir, C. P. Chen, L. H. Gabrielli, C. B. Poitras, K. Bergmen, and M. Lipson, "WDM-compatible mode-division multiplexing on a silicon chip," Nat. Commun. **5**, 3069 (2014).
244. J. Wang, S. He, and D. Dai, "On-chip silicon 8-channel hybrid (de)multiplexer enabling simultaneous mode- and polarization-division-multiplexing," Laser Photon. Rev. **8**, L18–L22 (2014).
245. C. Ning, L. Zhenxing, and F. J. Effenberger, "Large splitting and long reach passive optical networks with mode coupling receivers," in *36th European Conference and Exhibition on Optical Communication (ECOC)* (2010).
246. C. Xia, N. Chand, A. M. Velázquez-Benítez, X. Liu, J. E. A. Lopez, H. Wen, B. Zhu, F. Effenberger, R. Amezcua-Correa, and G. Li, "Demonstration of world's first few-mode GPON," in *European Conference and Exhibition on Optical Communication (ECOC)* (2014), paper PD.1.5.
247. C. R. Doerr, "Silicon photonics for space-division multiplexing," in *IEEE Photonics Society Summer Topical Meeting Series* (IEEE, 2012), pp. 242–243.
248. A. J. Koonen, C. Haoshuo, H. P. A. Van den Boom, and O. Raz, "Silicon photonic integrated mode multiplexer and demultiplexer," IEEE Photon. Technol. Lett. **24**, 1961–1964 (2012).
249. T. Pinguet, P. M. De Dobbelaere, D. Foltz, S. Gloeckner, S. Hovey, L. Yi, M. Mack, G. Masini, A. Mekis, M. Peterson, S. Sahni, J. Schramm, M. Sharp, D. Song, B. P. Welch, K. Yokoyama, and Y. Shuhuan, "Silicon photonics multicore transceivers," in *IEEE Photonics Society Summer Topical Meeting Series* (IEEE, 2012), pp. 238–239.
250. D. Yunhong, O. Haiyan, X. Jing, and C. Peucheret, "Silicon photonic integrated circuit mode multiplexer," IEEE Photon. Technol. Lett. **25**, 648–651 (2013).

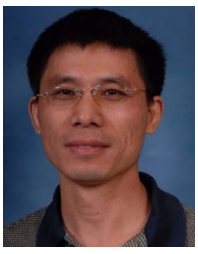

Guifang Li received his Ph.D. degree from The University of Wisconsin at Madison. He was the director of the NSF IGERT program in Optical Communications and Networking at UCF. He is the recipient of the NSF CAREER award and the Office of Naval Research Young Investigator award. Dr. Li is a Fellow of IEEE, The Optical Society (OSA), and SPIE. Dr. Li is a Deputy Editor for Optics Express (OSA), Overseas Editor-in-Chief of Frontiers of Optoelectronics, and an Associate Editor for Photonics Technology Letters (IEEE/IPS) and the Chinese Optics Letters.

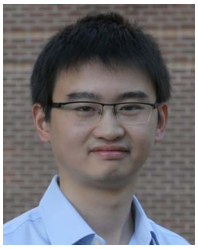

Neng Bai received his B.E. degree in Electrical Engineering from Tianjin University, China, in 2008 and Ph.D. degree from CREOL, The University of Central Florida in 2013. Currently, he is a Senior Hardware Development Engineer at Infinera Corp. From 2008 to 2013, he worked with Dr. Guifang Li in the Optical Fiber Communications Group at CREOL. His Ph.D. research mainly focused on mode-division multiplexed (MDM) systems. He was a research intern at NEC laboratories America from 2010 to 2011, working on few-mode EDFA and MDM transmission experiments. Dr. Bai is the author or co-author of 11 journal papers, 14 conference proceedings and 5 pending patents. He was a recipient of the 2012 SPIE Scholarship in Optics and Photonics and the 2013 CREOL Student of Year.

Ningbo Zhao received his Ph.D. degree in physics from the University of Science and Technology of China in 2008, with a thesis on quantum information. In 2008, he joined the College of Precision Instrument and Opto-electronics Engineering, Tianjin University, China. His research interests include quantum and nonlinear phenomena in optical fibers and optical communications.

Cen Xia received her B.S. degree in optical engineering from Zhejiang University, China, in 2009 and is currently pursuing her Ph.D. degree at CREOL, The University of Central Florida. Her research interests include space division multiplexing and fiber design and characterization. She has published 11 journal and conference papers and received best student paper award (first prize) in the 2014 Asia Communications and Photonics Conference.